The Design and Synthesis of Multidentate N–Heterocyclic Carbenes as Metathesis Catalyst Ligands

A thesis submitted in fulfilment of the requirements for the degree of

MASTER OF SCIENCE

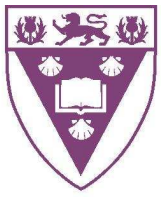

RHODES UNIVERSITY

Grahamstown • 6140 • South Africa

Byron John Truscott

2010

Abstract

This study has focused on the design and preparation of bi– and tridentate N–Heterocyclic Carbene (NHC) ligands in order to investigate the effect of a multidentate approach to the formation, stability and catalytic activity of coordination complexes.

Chapters 1 – 3 provide background information of relevant catalysis, carbene and coordination chemistry, followed by previous work performed within our research group. In Chapter 4 attention is given to the synthetic aspects of the research conducted, comprising two distinct approaches to the preparation of unsymmetrical saturated and unsaturated NHCs. Firstly, an investigation of the saturated NHC ligands yielded three novel, unsymmetrical pro–ligands, *viz.*, two halopropyl imidazolinium salts and a bidentate hydroxypropyl imidazolinium salt. Secondly, eight imidazolium salts have been generated, including a hydroxypropyl analogue and novel decyl and tridentate malonyl derivatives. These compounds were prepared using microwave–assisted methodology for the alkylation of *N*–mesitylimidazole – an approach that drastically reduced reaction times (from 8 hours – 7 days to *ca.* 0.5 – 2 hours) and facilitated isolation of the imidazolium salts. Many of the compounds prepared in this study are novel and were fully characterized using HRMS and 1– and 2–D NMR analysis.

Coordination studies using a selection of the prepared pro–ligands afforded an alkoxy–NHC silver derivative and four novel Ru–complexes, *viz.*, Grubbs II–type Ru–complexes containing:– chloropropyl imidazolinylidene; propenyl imidazolylidene; and bidentate alkoxypropyl imidazolylidene ligands. Furthermore, a well–defined benzyl mesitylimidazolylidene Ru–complex has been isolated, which exhibited good stability in air. DFT–level geometry–optimization studies, using the Accelrys DMol^3 package have given valuable insights into the likely geometries of the prepared and putative catalysts.

.

Acknowledgements

I would like to express my profound gratitude to Prof. Perry Kaye, without whom, this study would not have been possible. His wisdom and guidance, particularly in mechanistic approaches, and his unwavering support and encouragement were invaluable throughout this study.

Thank you to Dr. Rosa Klein for her co–supervision and assistance, particularly with organometallic concepts and related chemistry. Her guidance and support were invaluable.

Many thanks to Dr. Kevin Lobb for his patience and assistance with molecular modelling; to Andre Adrian for the making of specialized glassware that was essential in the complexation studies and to Prof. Mike Davies–Coleman for all his support and advice. I am very grateful to Sunny and Matthew for their help with proof–reading and moral support in the final stages of the report.

Additionally, I would like to thank Prof. Mannie Vosloo and his students at North–West University, particularly Carlijn Huismans for their assistance and for giving up their time to teach me vital “air–free” techniques – skills that played an important role in this project and to Dr. Wolfgang Meyer for all of his advice and assistance as a mentor during this project.

Without the financial support of Sasol I would not have been able to reach this point in my education – so thank you to them for all that they have done.

Lastly – thank you to my loving parents and brother for always believing in me and for supporting me in everything that I have done; and to Jessica for all her love and support.

Unless stated otherwise in the text, this thesis is my own original work. It has not been submitted for a degree at any other university.

Byron Truscott

Table of Contents

Pg

Introduction

Discussion

Experimental

List of Abbreviations

aq.	aqueous
ATR	attenuated total reflection
BuLi	butyllithium
CM	cross metathesis
conc.	concentration
COSY	^{1}H–^{1}H shift–correlated spectroscopy
d	doublet
DCM	dichloromethane
DEPT	distortionless enhancement by polarization transfer
DFT	density functional theory
DMSO	dimethyl sulfoxide
EtOH	ethanol
h	hours
HMBC	heteronuclear multiple bond coherence
HRMS	high–resolution mass spectrometry
HSQC	heteronuclear spin quantum correlation
IR	infrared
KHMDS	potassium hexamethyldisilazide
MeOH	methanol
Mes	mesityl
min.	minutes
mol	moles
mmol	millimoles
MS	mass spectrometry
NMR	nuclear magnetic resonance
NHC	nitrogen–containing heterocyclic carbene
PCy_3	tricyclohexyl phosphine
ppm	parts per million
q	quartet
R	alkyl group
RCM	ring–closing metathesis
ROM	ring–opening metathesis
ROMP	ring–opening metathesis polymerization
s	singlet
satd.	saturated
t	triplet
THF	tetrahydrofuran
TLC	thin layer chromatography

List of Figures

Pg

List of Schemes

Pg

List of Tables

Pg

Introduction

1. CATALYSIS IN INDUSTRY

A catalyst is described as "a substance or mixture of substances which increases the rate of a reaction by providing an alternative, faster route, without modifying the thermodynamics of the reaction, and with the catalyst remaining mostly unmodified upon completion of the reaction."[1]

Research in the field of catalysis was reported as early as the beginning of the 19th century, with Davy[2] and Doebereiner,[3] independently describing the combustion of alcohol in the presence of platinum and the combustion of hydrogen on palladium and iridium[4] and on platinum.[5] The concept of catalysis was first proposed by Berzelius and Emmet[6] and "catalysis" was coined by Berzelius as he described catalysts as "materials that facilitate the execution of reactions without seemingly taking part in the said reactions."[6, 7] Later in the 19th century, Ostwald's quantitative measurements of reaction rates led him to the discovery that catalysts do indeed accelerate reactions and in 1894 he concluded that "catalysis may not modify the thermodynamics of the reacting system,"[7] but that the catalyst may have an effect on the kinetics of the reaction. In reporting this theory, Ostwald introduced a very important characteristic of catalysis, namely that of kinetic selectivity.[6, 7] In 1912 Langmuir introduced the concept of chemisorption (cited by Frennet)[7] and, as a result, catalysis began to receive significant scientific attention. However, it was not until the 1960's that the catalytic surface and structure were considered and the relationship between the catalytic surface and catalytic activity became apparent. At about the same time, vacuum techniques were being developed, which enabled the study of metal surfaces using physical methods and Tamaru indicated that the most important surface properties were probably those of the catalyst whilst in its active state (cited by Frennet).[7]

The impending world oil crisis was first appreciated in the 1970's and marked the beginning of the search for alternative fuels and better utilization of fossil reserves. Processes such as the conversion of heavy fractions, that had previously been discarded, into lighter products led to the development of catalytic cracking and during the latter part of the 20th century,

catalysis began to play an increasingly important role in the refining and petrochemical industries. Most catalytic processes were heterogeneous and involved acid, metal, sulphur, and bifunctional catalysts. Processes such as catalytic cracking, reforming, hydrotreating, isomerisation of short paraffins, and the oligomerization of olefins received a great deal of attention and have advanced considerably with solid and organometallic catalysts in particular showing much development since the 1980's.[8] However, the application of homogeneous catalysis in the production of more valuable fuel stocks, such as the light olefins, ethylene and propylene has increased steadily at 2.2 and 2.9% per annum respectively since the last quarter of the 20th century.[8]

Catalysis is employed in many areas of synthetic chemistry. For example, it is vital in the preparation of fine chemicals, chemical intermediates, polymers and active compounds; in the catalytic cracking and hydrotreatments involved in refining; and in technologies employed in the control of pollutants such as NO, CO and hydrocarbons in gaseous emissions. Catalytic processes are so widely employed in the chemical industry that in 2003 it was reported that between 80 and 90% of everyday use products had been exposed to one or other form of catalysis during their production.[1]

1.1. Properties of an industrial catalyst

A catalyst may be described in terms of particular properties, such as activity, selectivity, stability, lifetime, recovery, toxicity and cost. These properties determine the efficiency of a catalyst. The activity is expressed as:– rate ("moles of product per volume of catalyst per hour");[1] as turnover number, expressed as "moles of product per mole of catalyst or active site";[1] or as conversion in "moles of transformed reactant per mole of inlet reactant."[1] It is clear that higher activity leads to higher productivity as well as the employment of milder reaction conditions.[1] Catalytic selectivity, be it chemo–, stereo– or regioselectivity, is expressed as "moles of desired product per moles of converted reactant"[1] and has direct consequences for separation, purification, reagent quantities and equivalence, waste treatment and the costs involved therein.[1] In addition, selectivity bears a direct relationship to energy demand of a particular transformation.[8] Recovery and regeneration of a spent catalyst influences the catalyst's overall lifetime (either in years or quantity of product per mass of catalyst) and will affect the cost of catalyst replacement and disposal. Environmental

concerns are also important and the safe handling and disposal of catalysts, reaction by–products and solvent media need to be considered.[1]

1.2. Catalyst Classification

Catalysis can be classified according to function, such as pyrolysis; catalytic combustion; porphyrin catalysis; or according to constitution, such as Pd catalysts or organocatalysts. The more conventional general classification of catalysis is based on solubility and describes catalytic processes as either heterogeneous or homogeneous.[6]

1.2.1. Heterogeneous catalysis

A heterogeneous processes is defined as one in which the catalyst, reactants and products are not all in the same phase. The catalyst is usually an inorganic solid, while the reactants and products are typically in the liquid or vapour phase. There are advantages associated with having the catalyst in a different phase to the reactants and products, the most important of which are the simplicity of separation and control of corrosion and problems associated with liquid waste treatments. Heterogeneous processes do however have limitations including mass transfer and temperature control, as well as the need for high mechanical and erosion resistance.[1]

1.2.2. Homogeneous catalysis

Homogeneous catalysis is defined as a process in which the catalyst is in the same phase as the reactants and products, normally dissolved in a solvent. The catalyst may be an acid, base, salt or organometallic compound. It is important to mention that there is a difference between true homogeneous catalysts and soluble or metal–particle catalysts. While true homogeneous catalysts have only a single type of active site, metal particles have several types of active sites, which may vary according to particle–size, preparation and catalytic conditions, which may affect selectivity, catalytic lifetime, activity and sensitivity to catalyst poisons.[9]

Homogeneous catalysts are capable of higher activity and/or selectivity compared to heterogeneous catalysts in many transformations, which makes the former option particularly attractive. There are, however certain disadvantages associated with the use of homogeneous catalysts. Firstly, organic solvents are normally utilized as reaction media, with negative implications for the environment in terms of volatile organic compounds (VOC's) and the treatment thereof. It is possible that a large percentage of organic solvents could be replaced by supercritical solvents, such as liquid carbon dioxide; such solvents would offer advantages in extraction and reaction conditions and in minimizing negative environmental impact. Secondly, there are difficulties associated with the separation of a homogeneous catalyst from the reaction products, which is being addressed to some extent by the use of microporous membranes to immobilise catalysts in the reaction medium.[10]

1.3. Current and future trends in catalysis

In the past, catalyst research and development has focused on activity and optimization of the turnover rates. However, the focus is now shifting towards the development of greater selectivity and the elimination of unwanted by–products,[6] to:– enable cleaner manufacturing processes; eliminate the need for waste disposal; and provide green catalytic industrial processes.[6]

Advancements in combinatorial chemistry, molecular modelling, high–performance analytical techniques and more efficient data collection and correlation are playing increasingly important roles in the development of catalysis, while the replacement of fossil fuels by alternative energy sources will call for crucial technological and scientific breakthroughs.[8]

In the fine chemicals sector, enantioselective catalysis by supported metals is a major challenge,[11] while soluble transition metal catalysts have important applications in the manufacture of bulk commodities and specialty products. Industrial competition and the demand for selective, efficient and environmentally friendly processes continue to drive catalyst research.[12]

2. TRANSITION METAL COMPLEXES AND CATALYSIS

Two of the reaction types that have had the most influence on C–C bond–creation and thus on synthetic development in the last twenty–five years are the palladium–catalyzed cross–coupling reaction and the metathesis reactions of olefins, enynes and alkynes with the latter being considered the most influential series of transformations in organic synthesis.[13]

2.1. Olefin metathesis

Olefin metathesis refers to a set of reactions involving rearrangement of carbon–carbon double bonds. Metathesis comes from the Greek word meaning "change of position" or "transposition."[14] It is used in coupling, cleaving, ring–closing, ring–opening and polymerizing olefinic substrates[14] as summarized in Scheme 2.1.

Cross metathesis refers to the intermolecular rearrangement of C=C bonds; *eg.* $C^1=C^2$ and $C^3=C^4$ can be converted to $C^1=C^3$ and $C^2=C^4$. Ring–closing metathesis involves the reaction of two terminal alkenes to form a cyclic olefin, while in ring–opening metathesis, a cyclic olefin reacts with a linear olefin to give an acyclic diene as shown in Scheme 2.1[15]

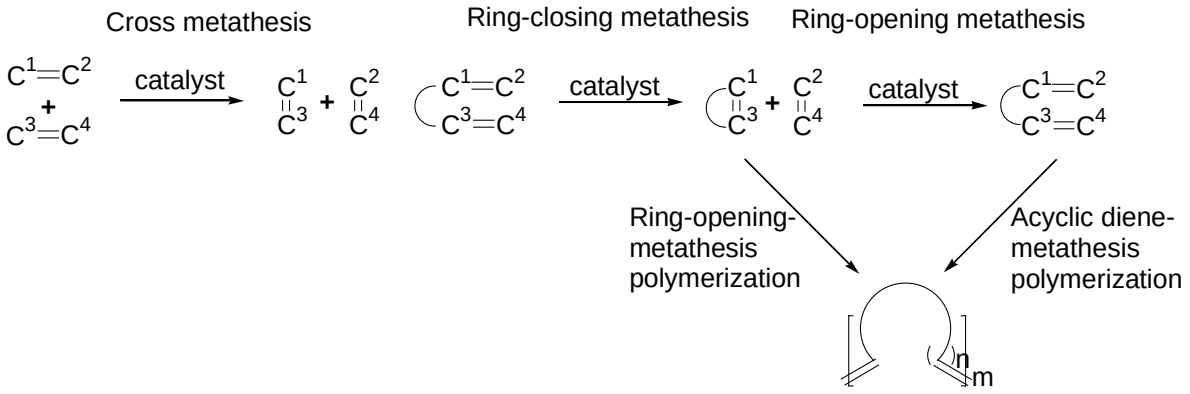

Scheme 2.1 Commonly used olefin metathesis transformations.[13, 15]

2.1.1. Metathesis reactions and their applications

Metathesis was first reported in 1931, when propene was converted to ethylene and 2–butene at high temperature.[16] The first catalyzed metathesis reaction to be reported involved ethylene disproportionation in the presence of molybdenum or tungsten.[16] In 1971 Chauvin published what became known as the 'Chauvin mechanism',[16, 17] which is now generally accepted as the mechanism of olefin metathesis. The mechanism comprises a series of [2+2] cycloadditions and cycloreversions, involving olefinic molecules, metal–carbenes and metallacyclobutane intermediates as shown in Scheme 2.2.[18] It was through this molecular level understanding that the field of metathesis began to evolve.[19]

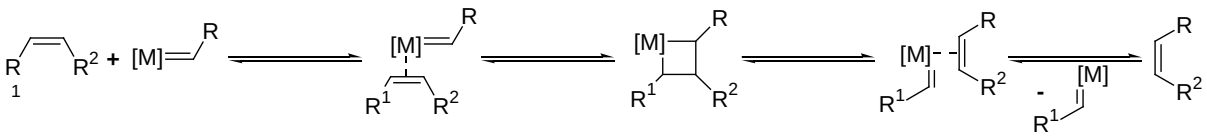

Scheme 2.2 A simplified version of Chauvin's mechanism (1971), illustrating catalyzed olefin metathesis.[17, 20]

Catalytic olefin metathesis, through the reorganization of C=C and the creation of new C–C bonds, is used to transform simple substrates into more complex and valuable products. By affording alternative, more efficient synthetic routes, olefin metathesis has significantly enriched the fields of organic synthesis and polymer and materials science, thus enabling the preparation of valuable targets that did not previously exist or were in quantities too small to study.[15, 16] Olefin metathesis has provided alternative synthetic routes to many important compounds, including, for example:– the anticancer epothilones;[21, 22] fluvirucin B_1;[23, 24] the cytotoxic agent, bistramide A;[24] and baconipyrone C,[25] a siphonaniid metabolite isolated from a false limpet. The commercial preparation of BILN 2061 ZW,[15, 26] a potent anti–hepatitis C drug involves a vital catalytic ring–closing metathesis step while, in the synthesis of cylindrocyclophane, a cytotoxic agent,[27] cross metathesis and subsequent ring–closing metathesis are implemented in the preparation of essential precursors.[15]

The industrial preparation of organic feedstocks and polymers has also been greatly affected by the advent of catalytic metathesis. Many polymers can be prepared by ROMP processes under mild conditions, including polyoctenamer (Vestenamer), polynorbornene (Norsorex)

and the most widely utilized, polydicyclopentadiene.[15, 28] Metathesis has even been investigated in the generation of renewable monomer feedstock, as in the cross metathesis of methyl oleate and ethylene to form 1–decene and methyl 9–decenoate.[29]

2.1.1.1. Ring–closing metathesis (RCM)

The general mechanism of RCM is shown in Scheme 2.3. As with all metathesis transformations, the reaction is initiated by the generation of the active catalyst and coordination of an olefin moiety in the substrate **1** with the metal. Cross–metathesis between the activated metal–carbene or –alkylidene and the coordinated olefin moiety generates the metallacyclobutane **2**. Following pathway b (Scheme 2.3), the M–CH_2 and the C_1–C_2 bonds are broken to give **3** with the metal as part of the new substrate. Rearrangement within the substrate gives a second metallacyclobutane, which disintegrates to give the cyclic product **5** and a metal–carbene, M=C^3, which is coordinated with another substrate, propagating the process.[15]

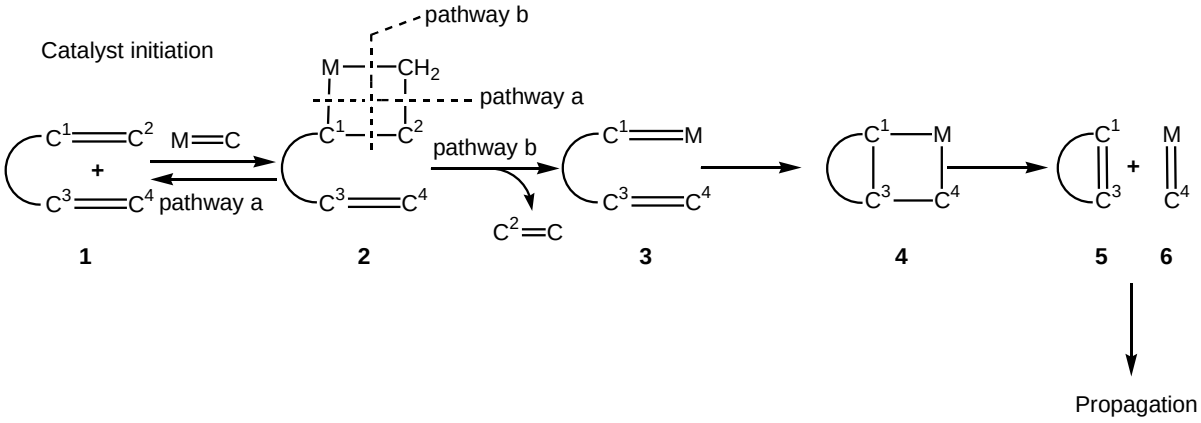

Scheme 2.3 The general mechanism of ring–closing olefin metathesis (RCM) (M=C is an activated carbene catalyst).[15]

Scheme 2.4 illustrates the RCM involved in the total synthesis of the natural product, Fluvirucin B_1,[23] whereby the linear precursor **7** is converted to the 14–membered lactam ring **8** by a Molybdenum catalyst. The undesirable formation of the dimer **9** is due to cross

metathesis of two molecules of **7** and the key to the success of this transformation lies in the reversible nature of olefin metathesis. The Molybdenum catalyst is able to convert the dimer **9** back to the substrate **7**, whereas the cyclic product **8** is much more hindered and not easily dismantled by a ring–opening process. Clearly, the desired transformation is dependent on the correct balance between cross–metathesis, RCM and possible disassembly of the macrocycle by ring–opening metathesis. In two further steps, the lactam **8** is converted to fluvirucin B_1,[23] with ethylene as the by–product.

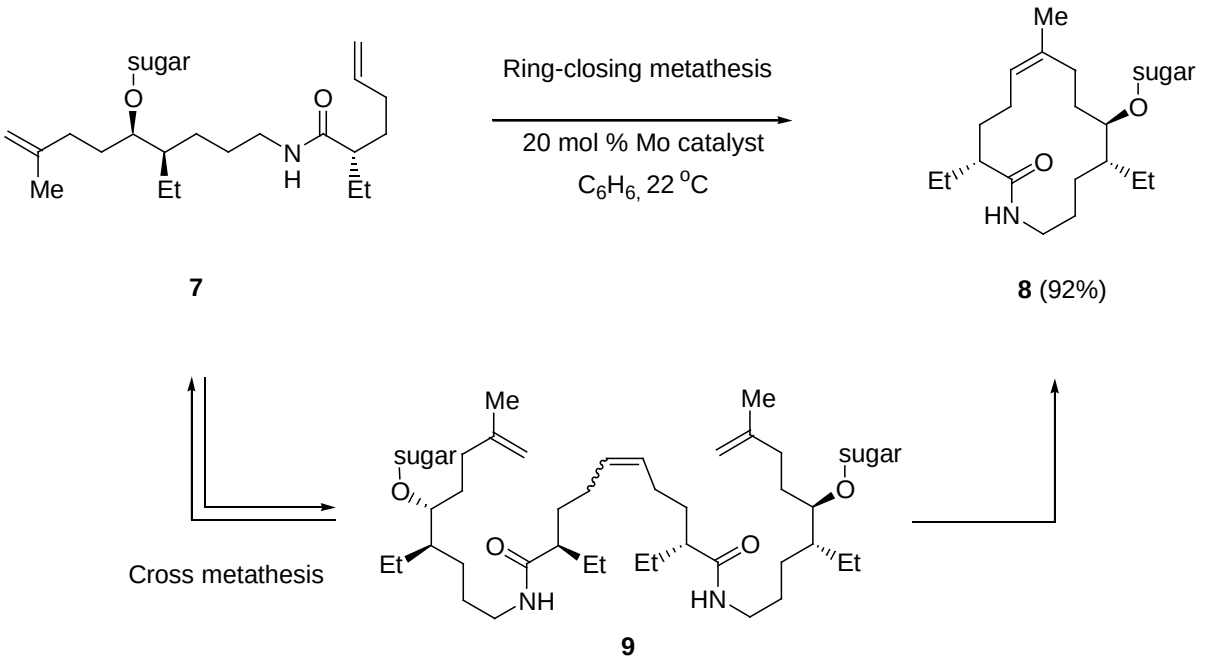

7 **8** (92%) **9**

Scheme 2.4 Metathesis involved in the total synthesis of fluviricin B_1.[23, 15]

2.1.1.2. Ring–opening/cross metathesis and ring–opening metathesis polymerization (ROCM and ROMP)

The general mechanism of ring–opening metathesis is given in Scheme 2.5 and involves the generation of metallacyclobutane **11**, which subsequently collapses to give an acyclic intermediate **12**. Reaction with an added acyclic olefin generates a second metallacyclobutane **13**, which ruptures to yield the ring–opened product and the active catalyst, which permits propogation of the sequence. The conversion of intermediate **12** to **14** is a cross–metathesis process and, hence, the sequence is known as 'ring–opening/cross metathesis'. A situation may occur in which the cyclic olefin is more reactive than the cross–partner (C_3=C_4) or the

cross–partner is absent. In this case, intermediate **12** will react with another molecule of substrate **10** and the new M=C will transform another molecule of **10** and so on, to eventually form a polymeric product **16**. This process is known as ring–opening metathesis polymerization (ROMP). If the cross–partner is more reactive than the cyclic olefin then the major product will result from the homo–coupling of the linear substrate (C_3=C_4). It is therefore critical that the catalyst reacts with the substrates and the cross–partner in the correct order to achieve high yields – a requirement that poses significant challenges in catalyst design.[15]

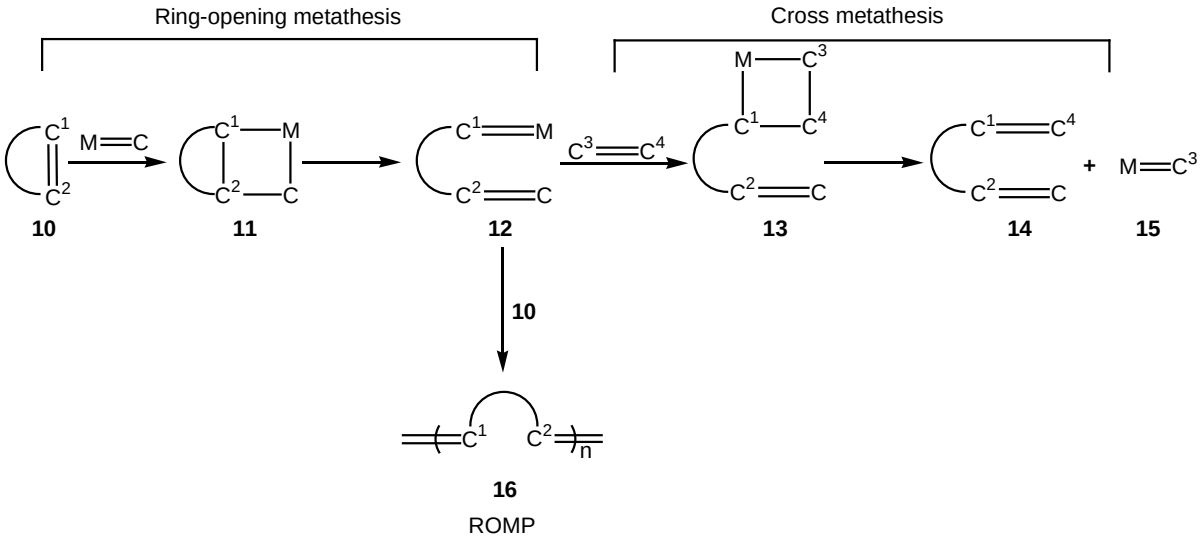

Scheme 2.5 The general mechanism for ring–opening/cross metathesis (ROCM) and possible ring–opening metathesis polymerisation (ROMP).[15,16]

A good example of ring–opening/cross metathesis is provided in the total synthesis of bistramide A (Scheme 2.6).[15, 24] The cyclopropene substrate **17** undergoes ROCM, coupling with the acyclic olefin **17** to give intermediate **19**; a second cross–metathesis involving the alkene gives the precursor for the final product, bistramide A – the tandem metathesis reactions effectively 'stitching' together three molecules.[15, 24]

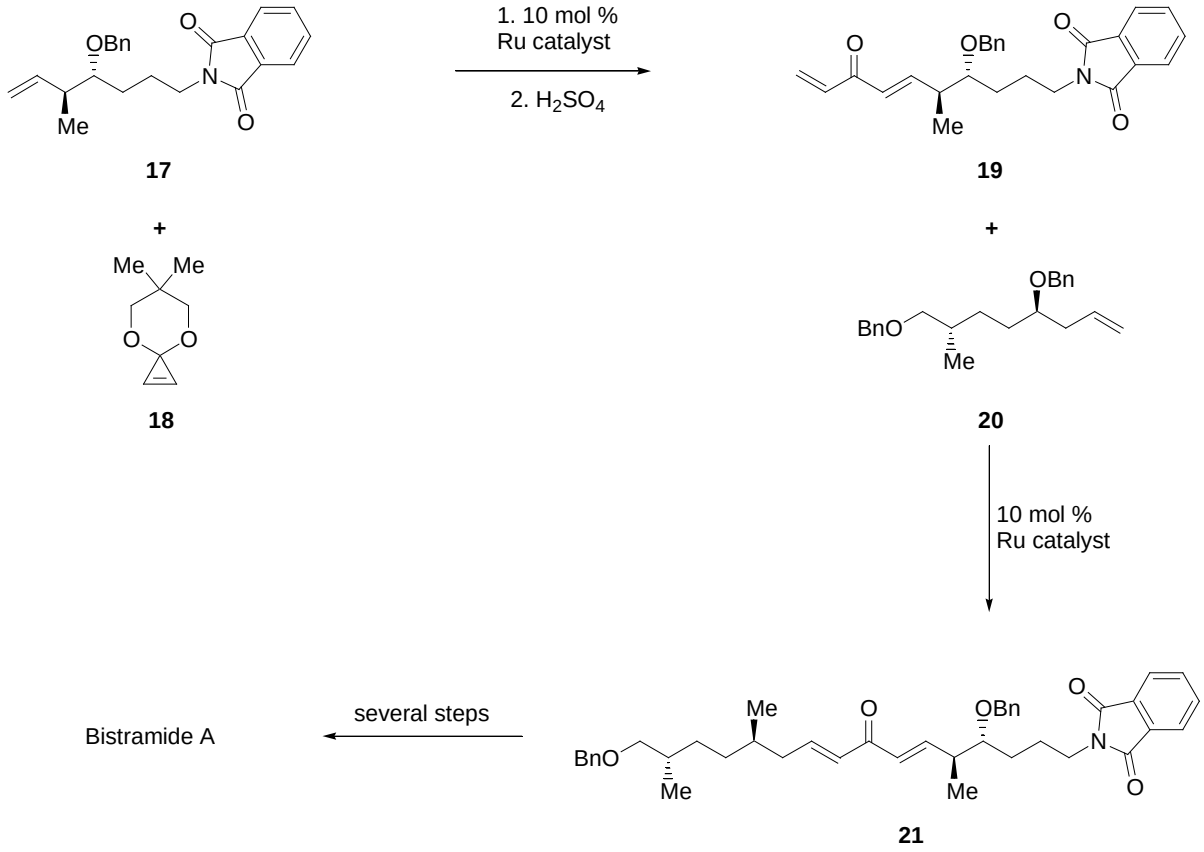

Scheme 2.6 Tandem metathesis processes involved in the total synthesis of bistramide A.[15, 24]

2.1.2. Metathesis catalysts

The Chauvin mechanism implicated a metal–carbene in the initiation of the metathesis reaction that led to the development of metal carbene catalysts. In 1974, the first metal–alkylidene complex [Ta=CHBu^t(CH_2Bu^t)$_3$] was isolated by Schrock[19] and his subsequent research (1980) supported the Chauvin mechanism. This was followed shortly after by preparation of the first unimolecular metathesis catalyst.[16, 30] Schrock's studies continued, with the preparation of tantalum–alkylidene complexes and a family of very active tungsten– and molybdenum–alkylidene complexes of the general formula [M(=CHCMe$_2$Ph)(=N–Ar)(OR$_2$] – the first commercial catalyst being the molybdenum complex **22** (Figure 2.1).[16, 31, 32]

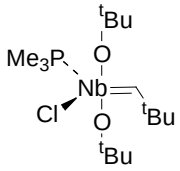

First unimolecular metal-alkylidene metathesis catalyst, Schrock 1980

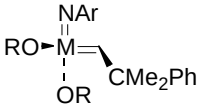

Schrock's family of metathesis catalysts, 1990
M = Mo of W

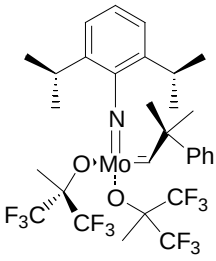

22
The first commercially successful metathesis catalyst, prototype of Schrock's catalyst family

Figure 2.1 A selection of Schrock's unimolecular metathesis catalysts.[16, 30–32]

2.1.2.1. Ruthenium metathesis catalysts

In an effort to exploit the metathesis reaction, Grubbs concentrated on developing functional–group tolerant catalysts and isolated the first ruthenium catalyst **23** (Figure 2.2) in 1988,[16, 33] followed by the first well–defined, air–stable ruthenium–carbene **24.**[16, 34, 35] Although the catalytic activity of the complex **24** was limited, its structural definition and stability provided a platform for modification and, three years later, Grubbs reported the well–defined Ru–catalyst **25**, which was closely related to the earlier vinylidene–complex **24**. Catalyst **25** was subsequently commercialised and became known as the "first–generation" Grubbs catalyst.[36] Grubbs–type catalysts typically consist of:– a ruthenium centre coordinated to five ligands; two neutral, electron–donating species, especially trialkylphosphines or triarylphosphines; two monoanionic halide ligands – normally chlorine; and an alkylidene moiety. The first–generation Grubbs catalyst **25** demonstrated good functional–group tolerance and insensitivity to air and water, thus affording favourable handling properties. Furthermore, the catalyst proved to be effective in:– ring–opening polymerizations;[34] ring–closing metathesis to prepare disubstituted olefins;[37] ethenolysis;[38] cross–metathesis of terminal olefins;[39] and enyne metathesis to prepare 1,3–dienes.[14, 40] Catalyst **25** is still used in processes such as the ethenolysis of bio–renewable seed oil feedstock[29] and in the production of macrocyclic hepatitis C drugs.[26]

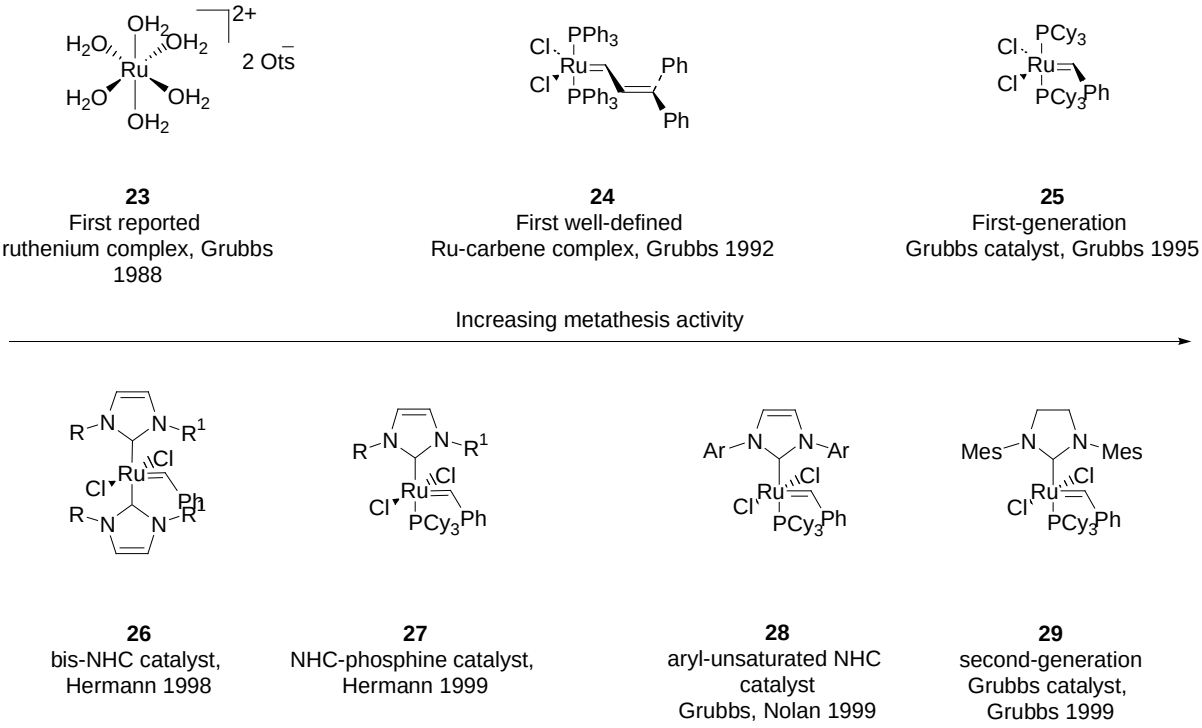

23
First reported ruthenium complex, Grubbs 1988

24
First well-defined Ru-carbene complex, Grubbs 1992

25
First-generation Grubbs catalyst, Grubbs 1995

26
bis-NHC catalyst, Hermann 1998

27
NHC-phosphine catalyst, Hermann 1999

28
aryl-unsaturated NHC catalyst Grubbs, Nolan 1999

29
second-generation Grubbs catalyst, Grubbs 1999

Figure 2.2 The evolution of ruthenium metathesis catalysts (Mes = mesityl).[14, 16]

However, the first–generation catalyst **25** suffered from low activity compared to the Schrock complexes which, although very sensitive, were still more active than the ruthenium catalysts. Through mechanistic studies aimed at understanding the structure and activity profile of the Ru–catalysts, it was discovered that the five–coordinate complex was a catalytic precursor and that the metathesis transformation was initiated by the dissociation of a phosphine ligand, generating a reactive 14–electron metal intermediate. This discovery explained why the more bulky tricyclohexylphosphine ligand was more effective than triphenylphosphine, and Grubbs[43] addressed the short–comings of his first–generation catalyst by increasing the lability of the phosphine ligand and, hence, accelerating the dissociation step. This approach led, ultimately to the replacement of one of the phosphines by the bulkier, more powerful electron donating *N*–heterocyclic moiety in the very successful second–generation Grubbs catalyst **29**.[14]

However, the first *N*–Heterocyclic Carbene (NHC)–containing metathesis catalysts were reported by Hermann and co–workers in 1998.[41] The bis–NHC ruthenium benzylidene species **26** contained unsaturated NHCs with either chiral or achiral alkyl substituents on the nitrogens, and were prepared with the intention of tuning catalytic properties and achieving

asymmetric transformations.[41] These bis–NHC catalysts offered little or no improvement in reactivity in ROMP or RCM, but the first mixed NHC–phosphine catalyst **27** was reported by Hermann and co–workers in 1999.[14, 41]

In the same year, catalysts containing aryl–substituted unsaturated NHCs were independently reported by Grubbs[42, 43] and Nolan.[44] This catalyst **28** was more active and stable than the first–generation Grubbs catalyst[42, 44, 45] and, soon afterwards, Grubbs *et al.*[43] reported that using dimesityl imidazolidin–2–ylidene (SIMes) as a phosphine substitute furnished the catalyst which became known as the "second–generation" Grubbs catalyst. Catalyst **29** super ceded the activity of catalyst **28** in most metathesis transformations, while retaining excellent functional–group tolerance and insensitivity to air and water.[14] Soon the catalyst **29** proved superior to its predecessors in most metathesis transformations, including:– the RCM of sterically demanding olefins;[43,46] macrocyclizations;[47] and the difficult CM of olefins containing α,β–unsaturated carbonyls.[14, 48]

Following these developments, the 2005 Nobel Prize in Chemistry was awarded to Yves Chauvin, Robert H. Grubbs and Richard R. Schrock for their contributions in the area of metathesis.[14, 49, 50,51] The understanding of the metathesis mechanism proposed by Chauvin was responsible for many of the subsequent developments[17, 49, 52] and, while Schrock prepared the first well–defined and active unimolecular catalysts, Grubbs developed active catalysts that showed wide functional group tolerance and insensitivity to atmospheric conditions.[14, 50, 53]

A library of metathesis catalysts has since evolved for the production of fine chemicals, pharmaceuticals and materials. With a greater understanding of the mechanistic aspects of metathesis reactions, catalysts can be tailored for specific transformations and, while there is no single catalyst that is superior in all metathesis procedures, each one possesses characteristic strengths.[14]

2.1.2.1.1. Mechanistic studies of ruthenium metathesis catalysts

Mechanistic investigations of olefin metathesis have proven the involvement of metallacyclobutane intermediates as indicated by the Chauvin mechanism.[54] Metathesis initiation typically involves the loss of a phosphine ligand from the original 16–electron complex (the precatalyst **29**) to give an active 14–electron species **30** (Scheme 2.7) which

may either rebind to a phosphine or coordinate an olefinic substrate to form a ruthenacyclobutane **32**. Fragmention of the ruthenacyclobutane **32** affords the new olefinic product **34**.[54, 55]

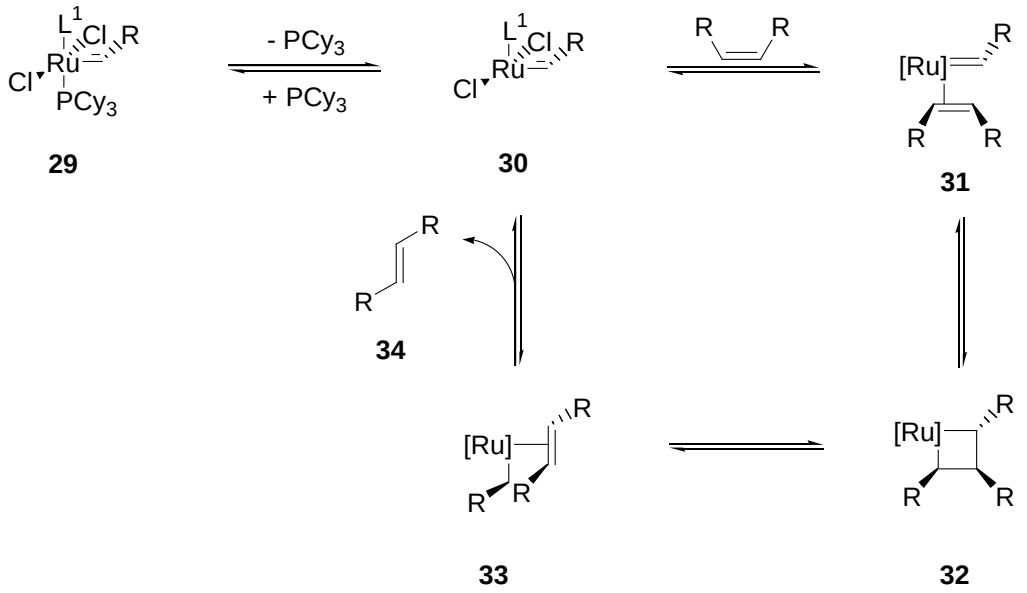

Scheme 2.7 Proposed mechanistic sequence for the metathesis of a *cis*–olefin to its *trans*–isomer using a second–generation ruthenium catalyst.[14]

Mechanistic studies have also indicated that the second–generation Grubbs catalyst actually has slower initiation rates compared to the first–generation catalyst, but that the superior ability of the Grubbs II catalyst **29** to coordinate an olefinic substrate in the presence of free phosphine is largely responsible for its improved activity.[14]

2.1.2.1.2. Phosphine–free metathesis catalysts

In 1999, Hoveyda and co–workers[56] reported the *in situ* formation of an Ru–chelate complex during the transformation of styrenyl ether to chromene. The complex was isolated and characterised as the extremely robust ruthenium complex **35** – now commonly referred to as the first–generation Hoveyda–Grubbs catalyst. The chelate complex **35** showed high activity in the RCM of terminal olefin–containing dienes and could be recovered in high yields *via* chromatographic methods and reused in subsequent transformations.[56] Following this work, Hoveyda and co–workers[57] turned their attention to alternative ligands in an effort to increase

catalytic activity. Substitution of the PCy_3 moiety in the Grubbs II complex **29** with a chelating benzylidene ligand facilitated the preparation of the phosphine–free, recyclable Ru–catalyst **36**.[57] The activity of this "second–generation" Hoveyda–Grubbs catalyst **36** was comparable with that of the Grubbs II catalyst **29** but their substrate specificities differed somewhat and **36** proved useful in the metathesis of electron–deficient substrates like acrylonitrile and various fluorinated alkenes. Other complexes have subsequently been developed by varying the chelating benzylidene ether ligand to create faster initiating complexes than the parent Hoveyda–Grubbs systems.[14]

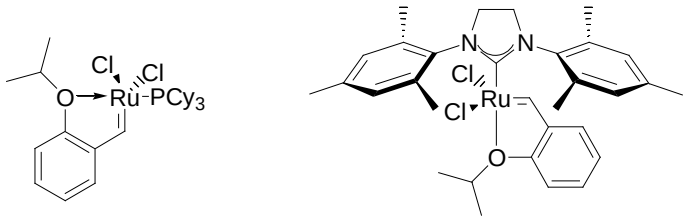

35
Hoveyda-Grubbs
first-generation

36
Hoveyda-Grubbs
second-generation

Figure 2.3 First–[56] and second–generation (phosphine–free) Hoveyda–Grubbs catalysts.[57]

2.2. Ligand effects on metal complexes and ligand design

2.2.1. Carbenes as neutral donor ligands

Carbenes have become very important as spectator ligands on transition–metal centres, and the advances in carbene chemistry are largely due to the isolation of stable carbenes.[58] The term 'carbene' refers to a 6–electron, divalent carbon centre which may either be linear or bent. The linear, sp–hybridised carbene is in the triplet state, with each of the two unpaired electrons occupying the degenerate and mutually orthogonal 2*p*–orbitals. The bent carbene, on the other hand, is sp^2–hybridised with the degeneracy of the p–orbitals lifted; such carbenes may be either singlet or triplet in nature, with the multiplicity depending on the α–substituents.[59] In the singlet state there is a lone pair and a low–energy unoccupied orbital on the same atom. While the properties of carbenes depend largely on their structure and on the

nature of nearby functional groups, they are highly reactive, especially in double bond addition and single bond insertion reactions.[59, 60]

Both the stability and philicity of a carbene are important in describing whether it is predominantly electrophilic or nucleophilic in character. A classification of the reactivity surface of singlet state carbenes, based on the differences in reactivity of insertion into methane, acetonitrile and isobutane C–H bonds has been calculated by means of DFT *in silico* methods.[61] In this study, 19 alkyl carbenes were compared in terms of stability/reactivity, which was plotted against philicity on a two–dimensional scale and NHCs emerged as the most stable and nucleophilic carbenes.[61]

2.2.1.1. Nitrogen–containing heterocyclic carbene compounds (NHCs)

NHCs are well known carbenes and can be prepared from three–, four–, six–, and even seven–membered heterocycles, although the most frequently used NHCs are the five–membered imidazol–2–ylidines **37**, imidazolin–2–ylidines **38**, benzimidazol–2–ylidines **39** and triazol–2–ylidines **40.**[62]

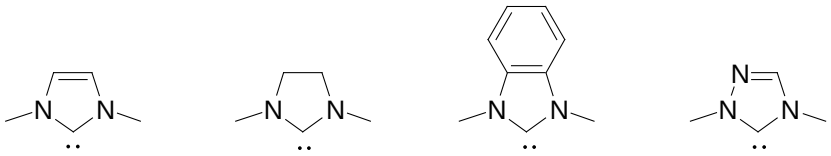

Figure 2.4 Common five–membered NHCs.[62]

Scientific interest in NHCs was first documented in 1962 by Wanzlick, who published an article entitled "Aspects of Nucleophilic Carbene Chemistry,"[63] while the first metal–NHCs to be isolated were by Wanzlick and Öfele in 1968 (Scheme 2.8)[16, 64-67] In both cases, preparation of the metal–NHC involved the deprotonation of an imidazolium salt precursor **41** and **43** to afford imidazol–2–ylidene complexes **42** and **44** respectively; the methodology was later extended by Lappert to include complexes bearing imidazolin–2–ylidines.[68]

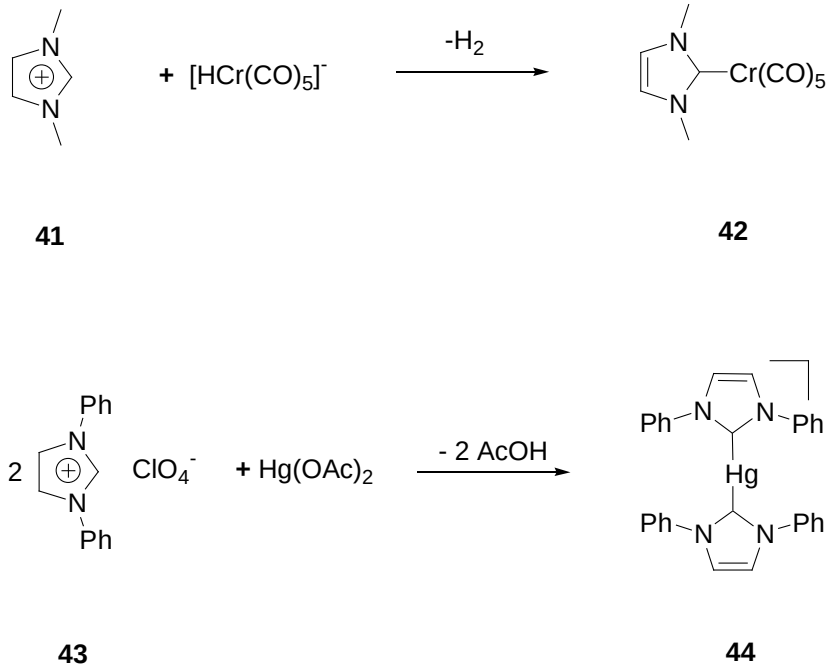

Scheme 2.8 Preparation of the first metal–NHC complexes by Öfele (**41** → **42**) and Wanzlick (**43** → **44**).[16, 64, 65]

In 1991 Arduengo *et al.*[69] crystallized the first free carbene **45** from 1,3–bis(adamantly) imidazolium chloride; this was followed by the isolation of the *p*–tolyl– and mesityl–substituted analogues (**46** and **47**, Figure 2.5) a year later.[70,71] The availability of free carbenes facilitated the preparation of metal–NHC complexes directly, many of which have been used in C–C and C–N cross–couplings and the metathesis reactions.[15, 16, 60, 72]

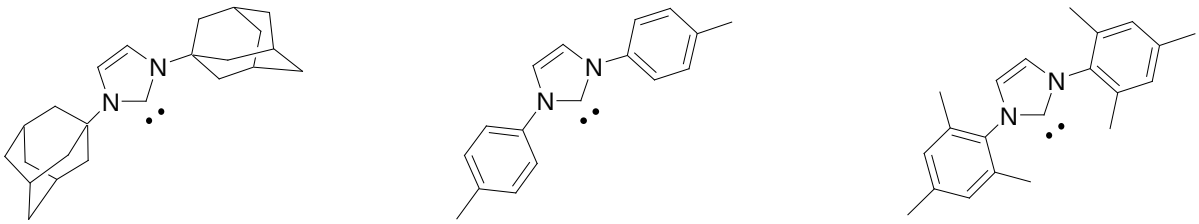

Figure 2.5 Arduengo's imidazol–2–ylidenes, the first stable free NHCs.[69, 71]

NHCs such as those illustrated in Figure 2.5 are inherently bent due to their cyclic structure, with the two nitrogens rendering the 2*p*–orbitals of the carbene carbon unequal in energy. The difference in energy between the previously degenerate orbitals enhances the thermodynamic stability and nucleophilicity of the carbene with singlet carbenes displaying particularly large differences in energy between the HOMO and the LUMO.[73] The carbene's α–substituents (amines) have two important effects on the ground–state multiplicity of the carbene, *viz.*, inductive and mesomeric effects. σ–Electron–withdrawing substituents stabilize the σ–non–bonding orbital by increasing its s–character, while the p_π–orbital remains unaltered; the result is a large gap between the σ– and p_π–orbitals of the carbene carbon, thus favouring the singlet state.[59, 66]

The vacant p–orbital is destabilized by the mesomeric effect of π–donating groups (*i.e.* :NR_2). The amino lone pairs interact with the p_π–orbital, resulting in a 'polarised four–electron three–centre π–system'[66] with some multiple bond character at the carbene carbon and hence the existence of a zwitterionic type structure with the negative charge at the carbon.[66] This mesomeric/inductive relationship between σ–withdrawing and π–donating *N*–substituents ensures electroneutrality at the carbene centre and renders the singlet state dominant.[59]

NHCs have proven to be very useful as neutral two–electron donor ligands in organometallic chemistry and are increasingly replacing the traditional phosphine ligands on metal centres. Although NHCs and phosphines differ quite markedly in their steric and electronic properties, they both possess a non–bonding singlet lone pair and may act as Lewis base donors to a metal.[59] NHCs are powerful σ–donor nucleophiles with low π–acidity, and are comparable to heteroatom–donating ligands rather than the classical Fischer or Schrock carbenes. They typically form long metal–carbon bonds with high dissociation energies that are chemically and thermodynamically more inert to cleavage than the metal–phosphorous bonds observed with phosphine ligands.[74] This unusual metal–NHC bonding character is a result of the high energy of the p_π–orbital of the carbenic carbon, resulting in an essentially pure σ–bond between the metal and the ligand.[66] Moreover, NHC ligands convey electronic properties to the metal centre that may differ quite markedly from those with phosphine or other traditional neutral ligands.[75] These electronic properties may enhance the reactivity and/or stability of the complex, as is the case with the second–generation Grubbs catalyst and the palladium catalysts used for C–C and C–N coupling reactions.[43, 76, 77] NHC–metal

complexes are generally less sensitive to moisture, heat and air than their phosphine counterparts,[62] and, thus, may allow for synthetic transformations under more adverse conditions.[78] Mechanistic studies of ruthenium carbene complexes have also revealed that the auxiliary ligands may have particular effects on the rate of initiation and propagation in various olefin metathesis reactions.[79, 80]

Of particular interest is the ease with which catalyst activity and efficiency can be altered by making structural changes to the ligand, both at the nitrogen sites and on the carbon backbone, tailoring steric and electronic properties to fit specific reactions.[37, 43, 53, 77, 81, 82]

Maj *et al.*[83] have reported that catalysts bearing various dialkyl–substituted NHCs showed no activity in the polymerization of cyclooctene, whereas aryl–substituted ligand complexes were active so long as all of the available *ortho*–positions were blocked by alkyl groups, thereby avoiding *ortho*–metallation and any alteration of the coordination sphere.[83] A library of biphenyl imidazolium salts were prepared (Figure 2.6) as ligand precursors, with the biphenyl substituents (R^1 and R^2) having different electron–withdrawing or donating ability and varying steric bulk. Altering the substituents (R^1 and R^2) was found to have no effect on catalyst activity since the substituents lay outside of the metal coordination sphere, confirming that structural changes need to be effected within the coordination sphere to have any influence.[83] This conclusion is supported by the results of a study by Stylianides *et al.*[84] involving NHCs with vacant *ortho*–sites on either one or both phenyl rings; it was observed that complexes of these ligands with palladium underwent facile cyclometallation, confirming the need to block the *ortho*–sites of the ligand.[84]

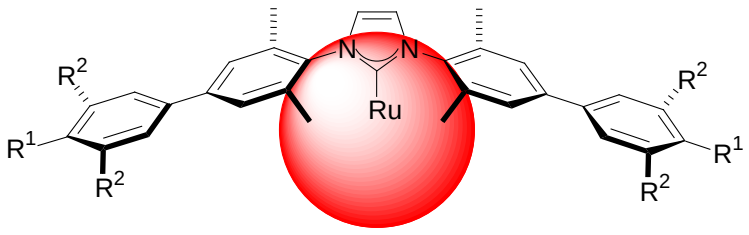

48

Figure 2.6 The coordination sphere (red) of a ruthenium centre bearing a NHC ligand with biphenyl substituents.[83]

In contrast to these findings, a study by Grubbs and co–workers[85] aimed at preparing catalysts capable of RCM to form tetra–substituted cyclic olefins, led to the preparation of complexes with mono–*ortho* substituted aryl NHCs (Figure 2.7). It was observed that the catalysts **49** and **50** were much more efficient in sterically demanding reactions, probably owing to the fact that the NHCs with mono–*ortho*–substituted aryl rings formed complexes with significantly less steric crowding within the coordination sphere, thus allowing the catalytic site to coordinate much larger olefin substrates.[85]

49 **50**

R = Me; Et; *i*Pr

Figure 2.7 Mono–*ortho* substituted NHC Ru–complexes.[85]

According to Ritter *et al.*[86] NHCs possessing *ortho*–halides show an increased activity. Ritter prepared NHCs possessing fluorine atoms at all of the *ortho*–positions and upon complexation and testing of the complex **51** (Figure 2.8), observed a change in reactivity. A halide–ruthenium interaction was considered responsible for reducing the activation energy of the rate–limiting phosphine dissociation, thereby accelerating catalyst initiation and enhancing the efficiency of the catalyst.[86]

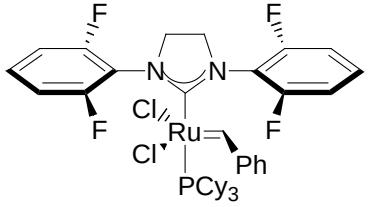

51

Figure 2.8 Ruthenium complex bearing *ortho*–flourinated NHC.[86]

2.2.1.1.1. Second–generation metathesis catalysts with unsymmetrical NHCs

Studies involving modifications to the NHC framework are still limited, particularly those involving catalysts bearing saturated unsymmetrical NHCs (imidazolin–2–ylidines). Mol and co–workers were among the first to investigate second–generation type catalysts with unsymmetrical NHC ligands, particularly those possessing combinations of alkyl and aryl groups.[87] They prepared a mixed adamantyl/mesityl NHC Ru–complex, which proved to be a very poor catalyst, possibly owing to the steric bulk of the adamantyl group.[87] Complexes prepared by Blechert and co–workers[88] (Figure 2.9), possessing methyl or ethyl mesitylimidazolin–2–ylidine moieties, showed efficiencies comparable to the second–generation Grubbs and Hoveyda–Grubbs catalysts **29** and **36** in some reactions but behaved more poorly in others.[88] The aim of their study was to replace one mesityl group with a more σ–donating alkyl group (methyl or ethyl), thereby enhancing the σ–donating properties of the ligand and thus, influencing stereoselectivity and activity in CM and RCM.[88] Increased σ–donation was suggested as a reason for increased activity in second–generation Grubbs catalysts. It was therefore postulated that unsymmetrical ligands may be capable of altering the steric environment during metathesis and thus effecting stereocontrol in CM as well as in certain diastereoselective RCM transformations. Characterization of complexes **52** and **53 (a** and **b)** indicated shorter NHC–metal bonds and increased electron density at the metal centre, consistent with stronger σ–electron–donation. The unsymmetrical catalysts **52** and **53** displayed activities comparable to the symmetrical parent catalysts **29** and **36** in the RCM of *N,N*–diallyl–*p*–toluenesulfonamide while the methyl–substituted catalyst **52a** produced different *E:Z* selectivity in CM and both novel catalysts **52a** and **53a** showed improved selectivity in diastereoselective RCM.[88]

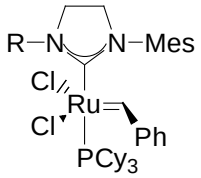

52a: R = Me
52b: R = Et

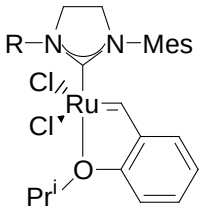

53a: R = Me
53b: R = Et

Figure 2.9 Metathesis catalysts bearing unsymmetrical, saturated NHC ligands.[88]

While NHCs are very efficient donor–ligands, suitable for coordination with a wide range of metals,[89] they are better suited to mid– and late–transition metals due to their soft character and the early transition metals exhibit significantly weaker metal–carbene bonds. Hence, significant functionalization may be required for use with early–transition metals and the use of multidentate NHC systems is expanding rapidly as a means of anchoring the ligand to the metal. Typically, anionic tethers are used to covalently attach the NHC to the metal centre, ensuring that the ligand will remain bound or in close proximity to the metal centre if dissociation occurs.[60] The anionic/NHC donor platform provides effective ligands for a range of metals across the periodic table, especially for early transition metals, stabilized by short metal–carbene bonds,[59,60] and there is some suggestion from *in silico* studies that the presence of π–electron donating ligands such as alkoxides or halides serve to stabilize the ground–state complex.[90, 91]

There are various scaffolds that can be used to prepare tethered NHCs and selected bidentate alkoxide and aryloxide ligands are shown in Figure 2.10.[60, 78, 92–96]

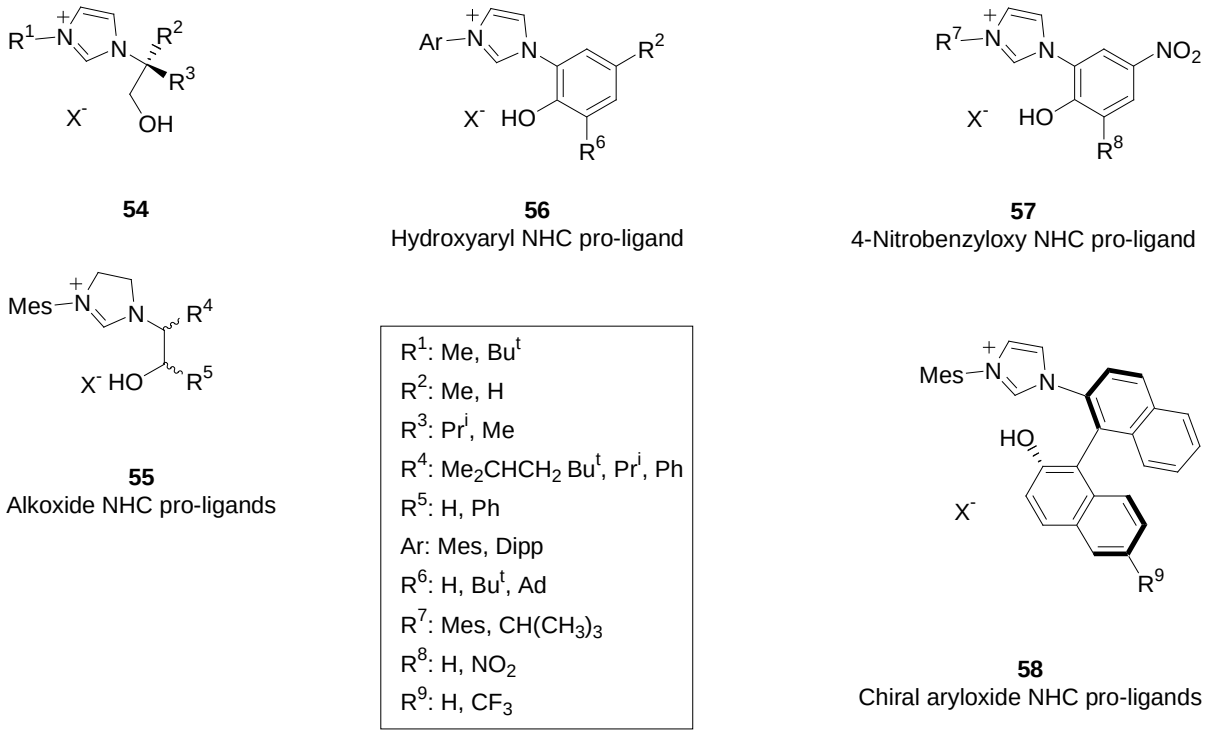

Figure 2.10 Examples of bidentate aryloxy– and alkoxy–NHC pro–ligands.[60,78,92–96]

Alkoxide NHCs such as **54** and **55** are easily accessible *via* epoxides and can be chiral in nature. Such alkoxide NHCs have been coordinated in various forms to copper, uranium and titanium.[78, 92, 93] Chiral aryloxides have been used to construct chiral catalysts such as the Ru–catalyst **59**, prepared by transmtellation of the axially chiral aminohydroxybinapthalene pro–ligand **58** with silver and Ru–catalyst **35**.[97, 98]

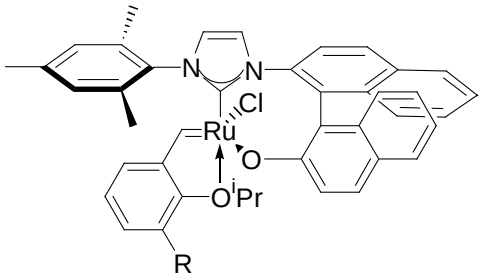

59

Figure 2.11 Chiral Hoveyda–Grubbs complex for enantioselective metathesis.[96]

Waltman and Grubbs[75] have reported the synthesis of a range of bidentate, saturated, hydroxyaryl imidazolin–2–ylidine ligands and their corresponding complexes with nickel and palladium, while Occhipinti *et al.*[94, 95] have prepared substituted analogues of the Hoveyda–Grubbs catalyst **35,** bearing the bidentate 4–nitrobenzyloxy NHC **57** *via* silver transmetallation.

Prühs *et al*.[99] have described the preparation of complexes with unsaturated imidazolylidenes bearing hydroxy–alkyl side chains of varying lengths; including the Ru–hydroxyethyl imidazol–2–ylidine **62** (Scheme 2.9). The complex **61** was prepared by coordinating a trimethylsilyloxypropyl imidazolium with Grubbs I catalyst **25** by deprotonation with a strong base. Desilylation with catalytic amounts of HCl affords the complex **62** bearing the hydroxypropyl imidazolium. In the absence of pyridine, the ligand behaves as a mono–dentate species with the hydroxyethyl chain remaining free. However, upon treatment of complex **61** with pyridine, the chloride ligands are displaced by two pyridine ligands to form a six–coordinate octahedral cationic complex **63** with the hydroxyl group coordinated to the metal and the second chloride acting as the counter anion. The complex showed unusual stability in air and was even recrystallized from ethanol but, unfortunately, proved to be devoid of activity in RCM – an observation attributed to the tightly bound pyridine ligands.[99]

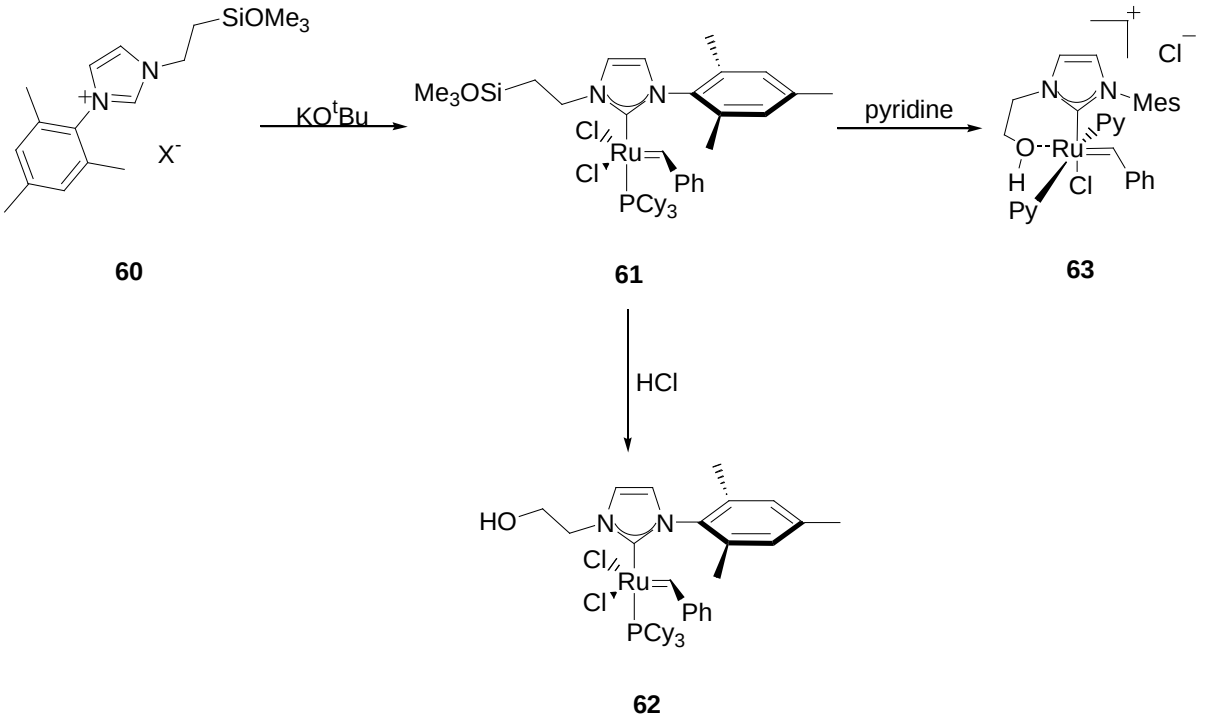

60 **61** **63**

62

Scheme 2.9 Preparation of hydroxyalkyl–functionalized ruthenium–carbene complexes.[99]

3. PREVIOUS WORK IN THE GROUP AND AIMS OF THE PRESENT INVESTIGATION

3.1. Previous work in the group

Previous work in the group was focussed on the preparation of strongly electron–donating NHCs with anionic tethers for coordination with ruthenium to form halide–free metathesis catalysts.[100–102]

Malonate systems are attractive replacement options for the chloride ligands on metal catalysts due to their potential for chelating the metal and the possibility of tethering the malonate moiety to a neutral electron donor ligand such as an NHC. The malonate functionality is known to bind to metals in three ways, specifically in a (i) unidentate; (ii) bidentate; or (iii) bis–chelating manner. Mode iii would seem unlikely, due to the preferred *trans* orientation of the anions in the square pyramidal arrangement of the ruthenium complexes discussed here.[100] Of particular interest was the bidentate binding option (ii) and the possibility of replacing both chlorides on the metal core with a single malonate group since chelation of a stable 6–membered ring within the ligand sphere could promote additional stability, structural rigidity and the alleviation of steric crowding at the substrate coordination site.

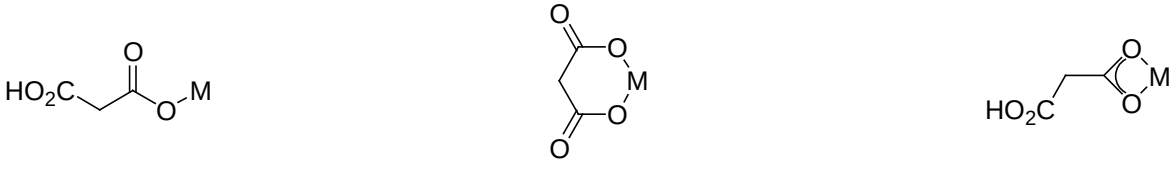

Figure 3.1 The different binding modes of the malonate dianion.[100]

Studies by Sabbagh[100] showed the importance of ligand electronic factors and the effect of the electron–donating or –withdrawing ability of the ligands on catalyst stability and activity. Modelling of the Hoveyda–Grubbs catalyst using trifluoroacetate as chloride replacements

(**64**, Figure 3.2) revealed lengthening of the Ru–O bond, relative to the Hoveyda–Grubbs II system **36**. The consequent weakening of this bond enhances the lability of the leaving group and hence, accelerates the rate of catalyst initiation. It is important to note that decomposition of the complex also involves dissociation of the leaving group and a weakening of the bond between the leaving group and the metal may affect the stability of the complex. Consequently, an appropriate balance between activity and stability is critical in the design of a useful catalyst.[100]

Preliminary theoretical analysis of the ability of a malonate functionality to bind in a bidentate manner led to the design of a tridentate system incorporating an NHC and a malonate moiety. Complexes **65** and **66** were geometry–optimised at the DFT–level by Sabbagh. Firstly, the DFT model of complex **65** revealed that the Ru–NHC bond is undisturbed and that the Ru–phenoxy bond is slightly elongated – arrangements that could be favourable for metathesis initiation.[100] It was thought that linking the malonate moiety to the NHC ligand would give a tridentate system. The resultant rigidity could potentially reduce steric crowding at the substrate co–ordination site and enhance the stability of the system through the presence of a 6–membered chelate ring. Structure **66** was calculated to possess a significantly shorter Ru–phenoxy bond than that of **65**, indicating that the coordination of a tridentate ligand system might lead to a more stable system.[100]

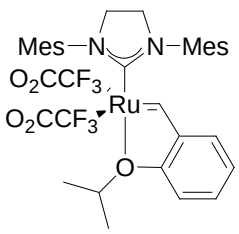

64

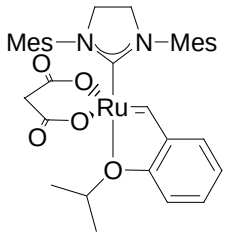

65

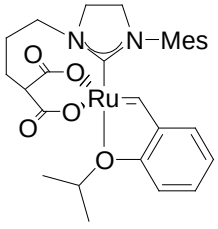

66

Figure 3.2 Putative Hoveyda–Grubbs type complexes involving triflouroacetate (**64**) and malonate groups as chloride replacements (**65** and **66**).

3.2. Aims of the present investigation

Various synthetic approaches to the tridentate ligand that would be used to prepare complex **66** were followed by both Sabbagh[100] and Millward[102] but success was somewhat limited. Millward[102] proposed to access the malonic ester imidazolinium pro–ligand *via* a functionalized *N*–propylimidazolinium and it was this approach that is explored in the current study.

The present investigation has, therefore been directed towards the development of novel multidentate NHC pro–ligands and an evaluation of potential ruthenium metathesis catalysts, and represents a progression from research conducted by previous members of the group. More specifically, we proposed to achieve the following:

(i) The preparation of bidentate NHC ligands such as **67**, which possess a heteroatom on the side chain, capable of binding the metal.

(ii) The preparation of tridentate ligands, such as **68,** by tethering a bidentate side chain with terminal heteroatoms capable of binding the metal in a 'pincer' fashion.

(iii) The preparation and evaluation of metal complexes such as **69** – **72** as multidentate analogues of the second–generation Grubbs and Hoveyda–Grubbs type pre–catalysts.

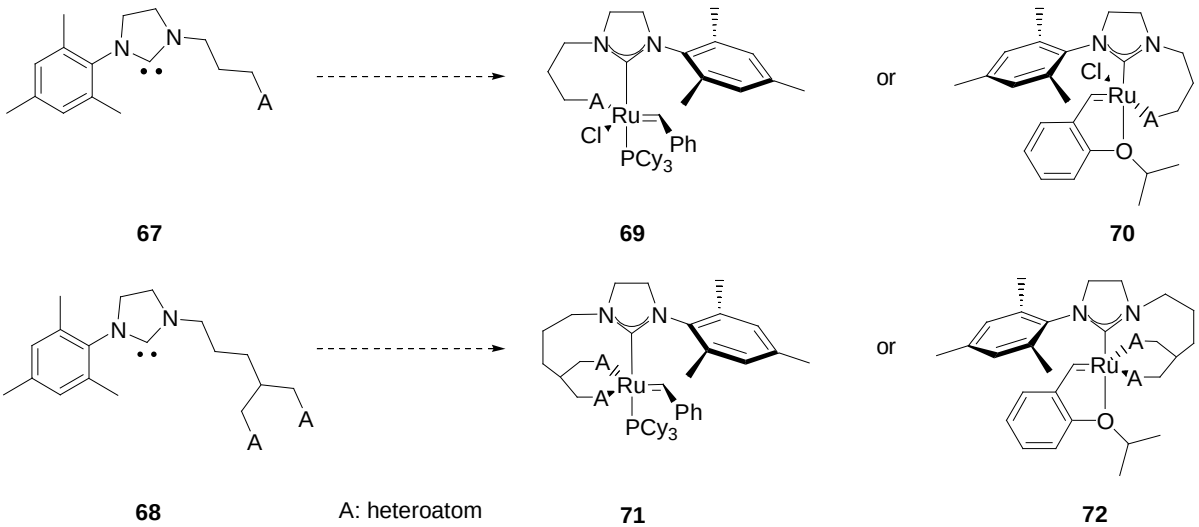

67 **69** **70**

68 **71** **72**

Figure 3.3 Proposed multidentate NHCs and possible coordination complexes thereof.

Discussion

4. RATIONAL DESIGN AND SYNTHETIC STUDY

4.1. Preparation of imidazolinium pro–ligands

Millward had suggested the possibility of using the imidazolinium salt **76** as a precursor to a tridentate pro–ligand, and we decided to explore the synthesis of this salt, utilizing procedures reported in the literture[75, 102, 103] for the preparation of symmetrical imidazolinium derivatives.

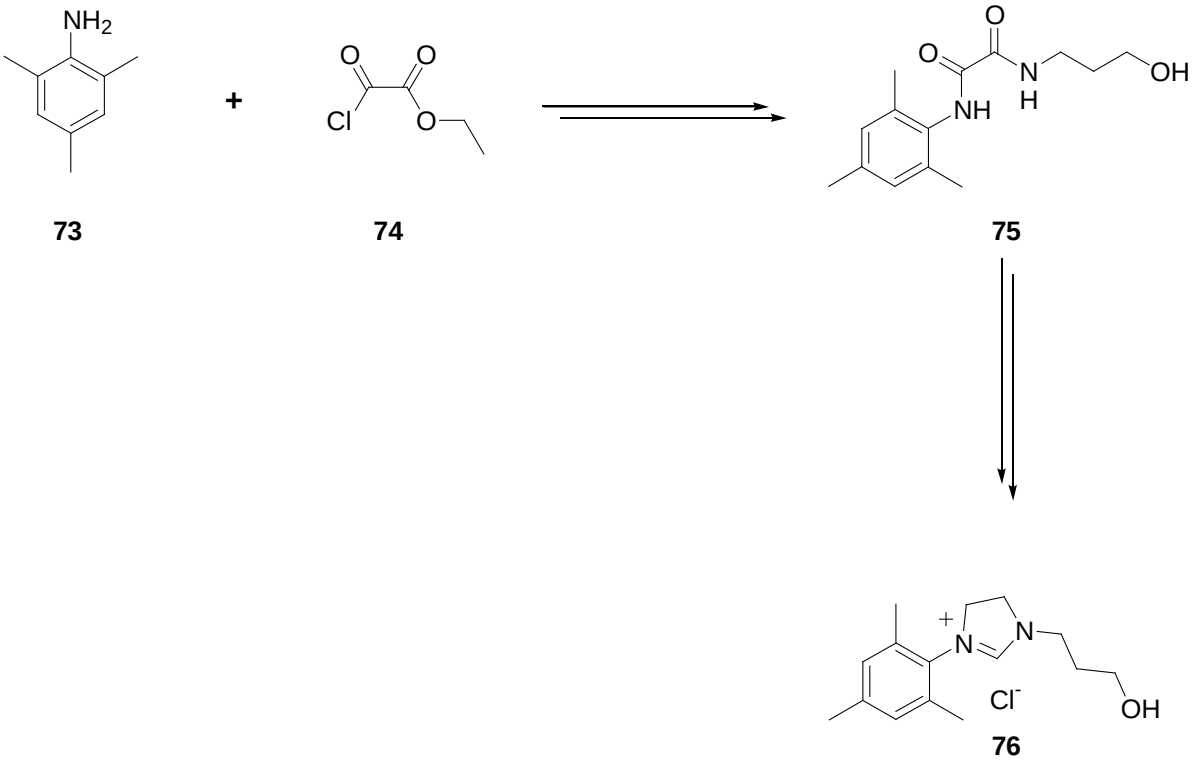

73 **74** **75** **76**

Scheme 4.1 Synthetic route proposed for the preparation of the bidentate pro–ligand **76**.

The diamide **75** was identified as a key precursor and was accessed *via* the oxanilic acid ester **77**, obtained in turn from reaction of the aryl amine **73** and ethyl chlorooxoacetate **74**,[75]

followed by a second amidation with 3–aminopropanol **78** to give the alcohol oxamide **75**. Modifications to Millward's procedure,[102] produced **75** in 85% yield from the intermediate **77** (Scheme 4.2). The structure of the product **75** was confirmed by the absence of ^{1}H NMR signals corresponding to the ethyl group and the presence of the three requisite methylene signals in the range (δ_H 1.80 – 3.69 ppm).

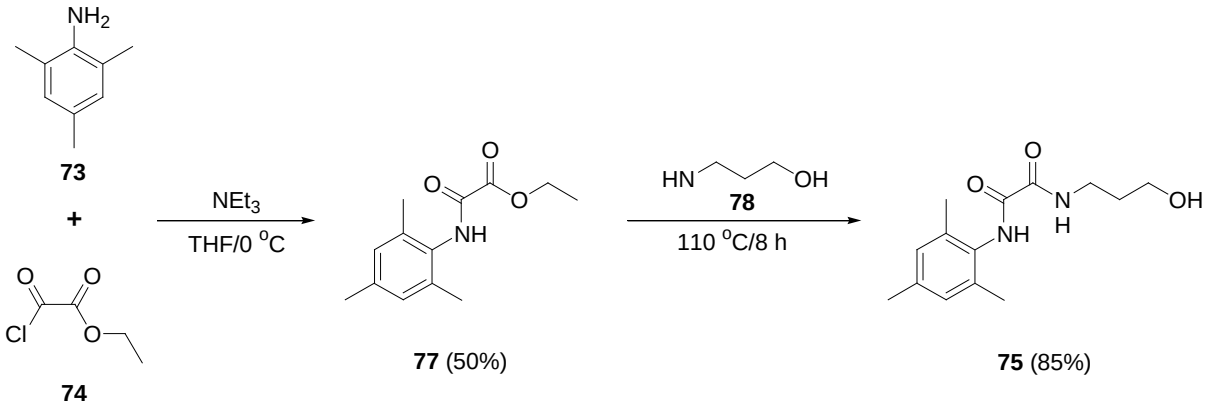

Scheme 4.2 Preparation of the alcohol oxamide **75**.

The ethylenediamide functionality of **75** then needed to be reduced to the diamine dihydrochloride salt, and this was achieved by adopting modifications to the established general procedures (Scheme 4.3). Most importantly, $LiAlH_4$[84] was used instead of the usual BH_3–THF complex,[75] since no identifiable products were detected when the diamide **75** was treated with BH_3–THF. The structure of the novel dihydrochloride salt **79** was confirmed by NMR analysis (Figure 4.1), which revealed the spectral differences between the precursor **75** and product **79**. Of particular significance is the absence of carbonyl carbon signals for the product **79** and the emergence of two new methylene proton signals (δ_H 2.82 and 3.03 ppm) corresponding to the 1– and 2–methylene groups, respectively. Additionally, DEPT 135 analysis of the product **79** indicated the presence of five methylene carbons, as shown in Figure 4.1B.

The dihydrochloride salt **79** was treated with triethyl orthoformate **80** in sufficient excess to act as both solvent and reactant and, after an hour at 135 °C, the ethanol produced during the reaction was removed *in vacuo*. The published purification procedure was modified since the

product appeared as a partially soluble oil and not a solid as reported for similar compounds.[75, 104]

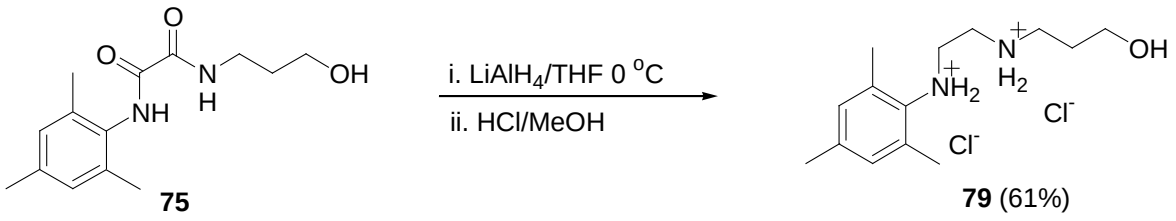

Scheme 4.3 Reduction of the diamide **75** to the dihydrochloride salt **79**

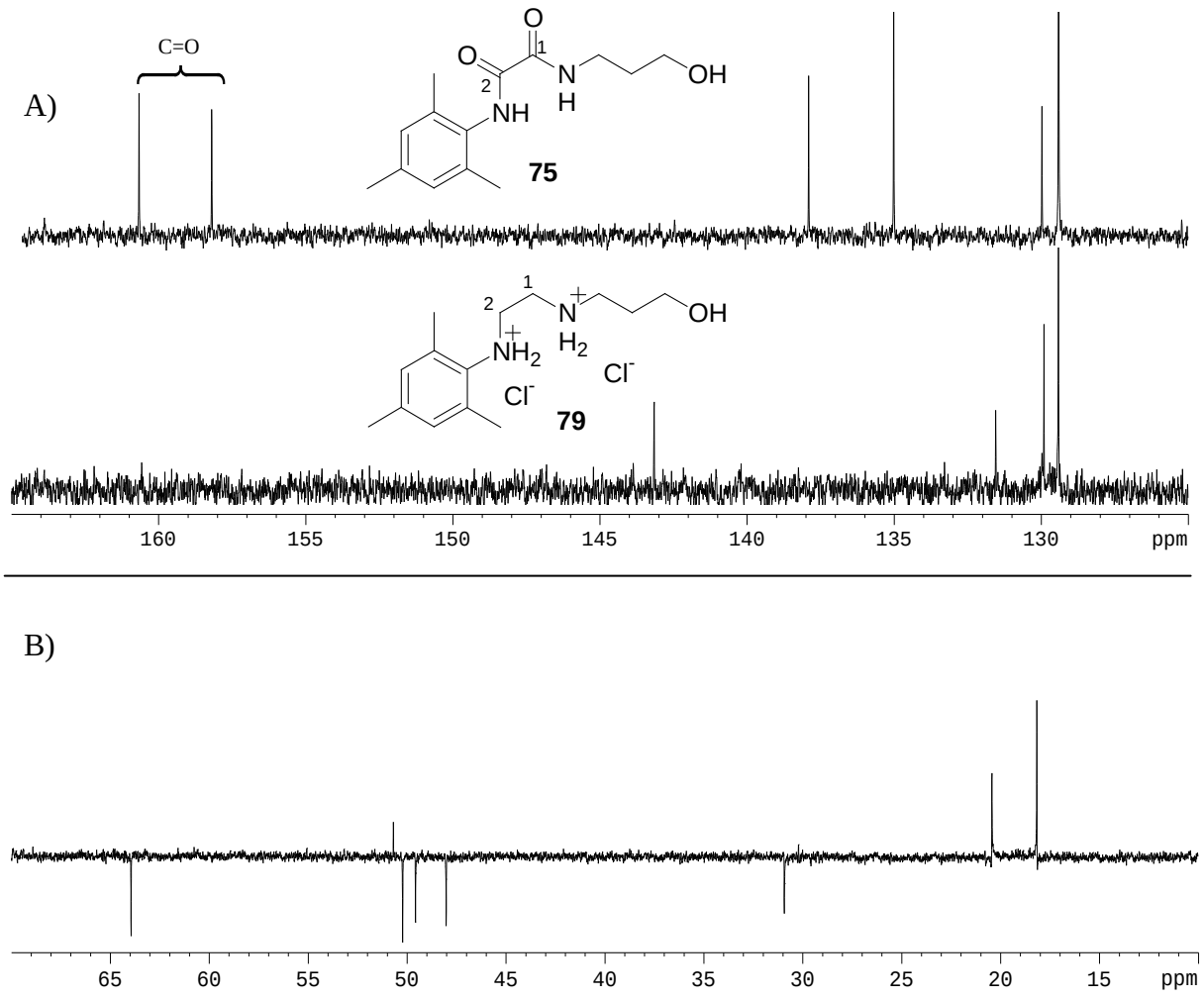

Figure 4.1 A) Partial 100 MHz ^{13}C NMR spectra ($CDCl_3$; 100 MHz) of compounds **75** and **79**, and B) partial DEPT 135 NMR spectrum of the product **79** in $CDCl_3$.

Biphasic extractions and recrystallizations were attempted using diethyl ether, chloroform, ethyl acetate, ethanol and methanol as solvents. The most successful of these techniques involved heating the material in ethyl acetate under reflux with the dropwise addition of ethanol to dissolve the oil, followed by very slow cooling to afford a brown crystalline solid in 20 % isolated yield, compared to yields of between 35 % and 85 % reported for similar compounds in the literature.[75] An alternative purification was therefore employed to improve the yield and purity; this involved preparative column chromatography using Dianion® HP–20 polystyrene beads. The product was purified by gradient elution with MeOH–H_2O in four elutions, from 100% MeOH, increasing the polarity to 90% H_2O in the final elution and resulting in the isolation of **76** as a yellow–white solid in a yield of 31%.

A low field singlet at 9.56 ppm in the 400 MHz ^{1}H NMR spectrum of compound **76** (Figure 4.2) was assigned to the deshielded 2–methine proton, the chemical shift being characteristic of an imidazolinium salt and indicating successful cyclization. Ordinarily, the 4– and 5–methylene protons would couple with each other, with each pair resonating as a triplet. However, the 4– and 5–methylene nuclei have very similar chemical shifts in this compound and exhibit higher–order coupling, resulting in the splitting pattern shown in Figure 4.3A. By running the spectrum at higher magnetic field (600 MHz), the expected first–order coupling was observed and the clear triplet signals permitted accurate measurement of the coupling constants (Figure 4.3B).

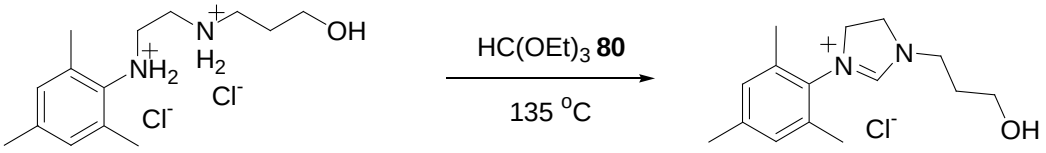

79 **76** (31%)

Scheme 4.4 Cyclization of the dihydrochloride salt **79** to afford imidazolinium salt **76**.

Shown in Figure 4.4 are the 1–D and 2–D NMR spectral data used to elucidate the structure of imidazolinium salt **76** and to confirm the ^{1}H NMR spectroscopic assignments shown in Figure 4.2. The DEPT 135 spectrum shows five methylene signals, representative of the trimethylene side–chain and the two imidazolinium backbone methylene groups. The ^{1}H NMR signal at 9.56 ppm, due to the 2–methine proton has HMBC correlations (blue peaks)

to three of the methylene ^{13}C signals, *viz.*, those representing the 1'–, 4– and 5–methylene groups as shown in the expanded region A. The expanded region B reveals the HSQC (red peaks) and HMBC correlations (blue peaks), involving four of the methylene groups and were used to assign the ^{1}H and ^{13}C NMR signals to specific methylene groups and to establish the structure of the imidazolinium ring.

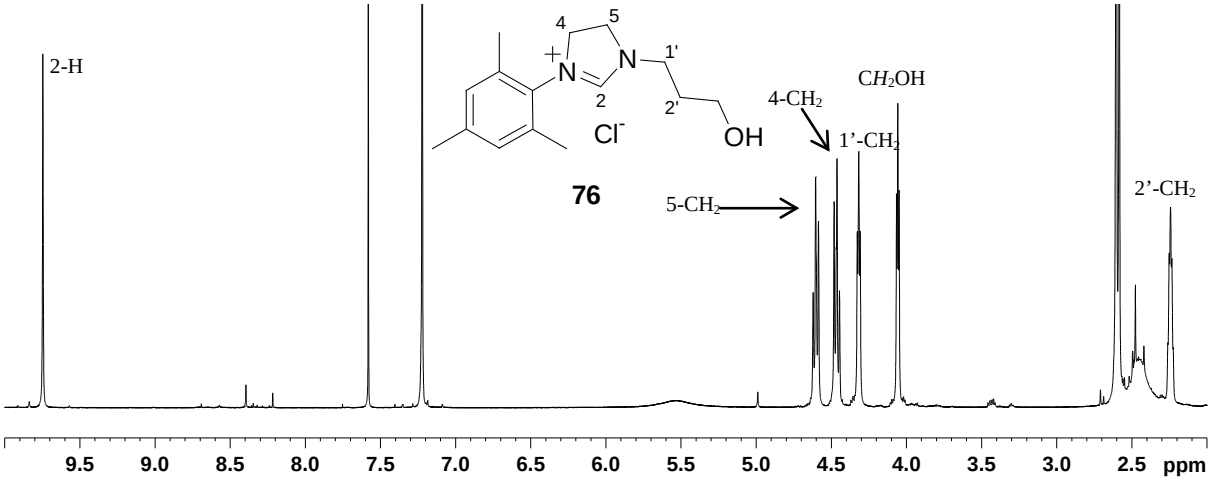

Figure 4.2 400 MHz ^{1}H NMR spectrum for the imidazolinium salt **76** in $CDCl_3$.

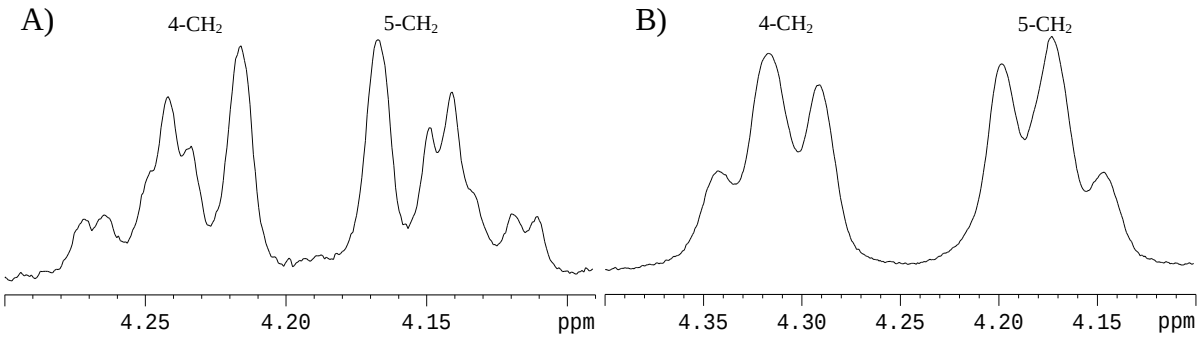

Figure 4.3 Partial ^{1}H NMR spectra of compound **76** in $CDCl_3$ at A) 400 MHz and B) 600 MHz.

These imidazolinium salts were readily characterised by mass spectrometry since the highest *m/z* peak (247.1808) corresponds to the parent cation, following loss of the chloride counterion.

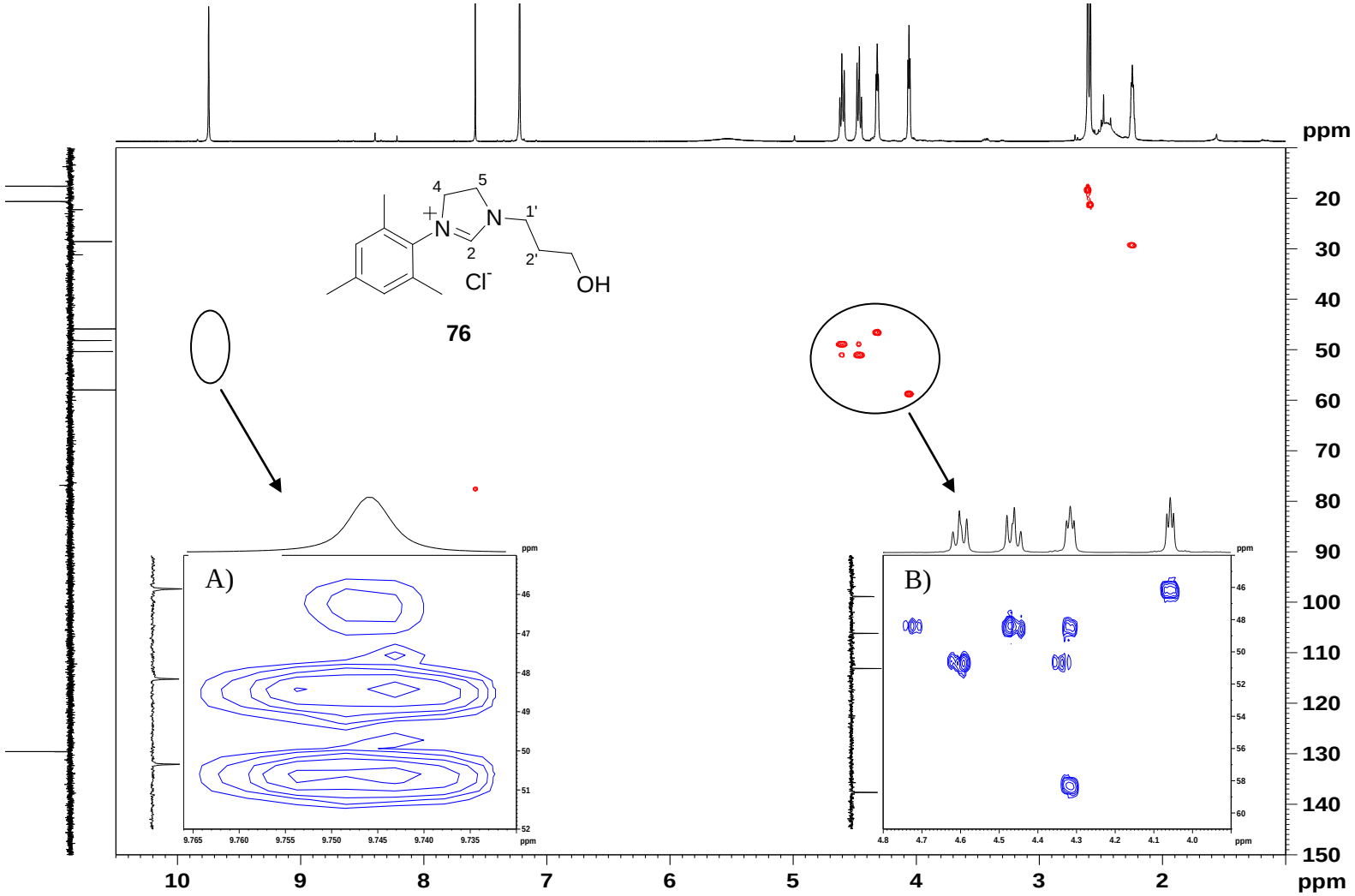

Figure 4.4 1– and 2–D NMR spectra for the imidazolinium salt **76** in $CDCl_3$ (400/100 MHz): ^1H NMR (top); DEPT 135 (left); HMBC (blue peaks) and HSQC (red peaks).

With the bidentate pro–ligand **76** in hand, the platform for the pursuit of a tridentate system was in place. Following the investigations by Sabbagh[100] and Millward,[102] we hoped to tether a malonate moiety in place of the hydroxyl group to provide the chelating 'pincer'. In order to facilitate linkage of the malonate, a suitable leaving group was required and compound **76** was reacted with thionyl chloride to form the chloro derivative **81**.[11, 105] This halide substitution proceeded readily, boasting 100 % yield with no further purification being necessary. Comparison of the ^{1}H NMR spectra for the substrate **76** and the product **81** (Figure 4.5) revealed a shift of the 1'– and 2'–methylene proton signals to higher field where they overlap with the other methylene and *o*–methyl proton signals, respectively.

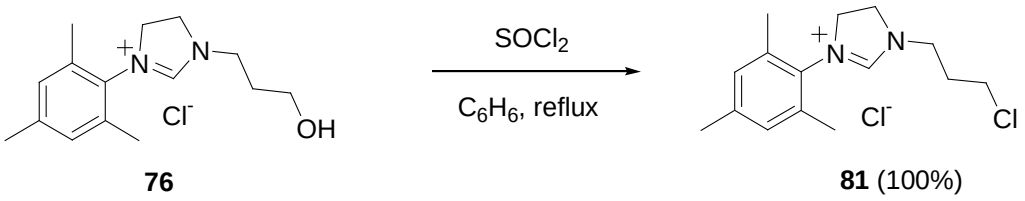

Scheme 4.5 Preparation of the chloropropyl imidazolinium salt **81**.

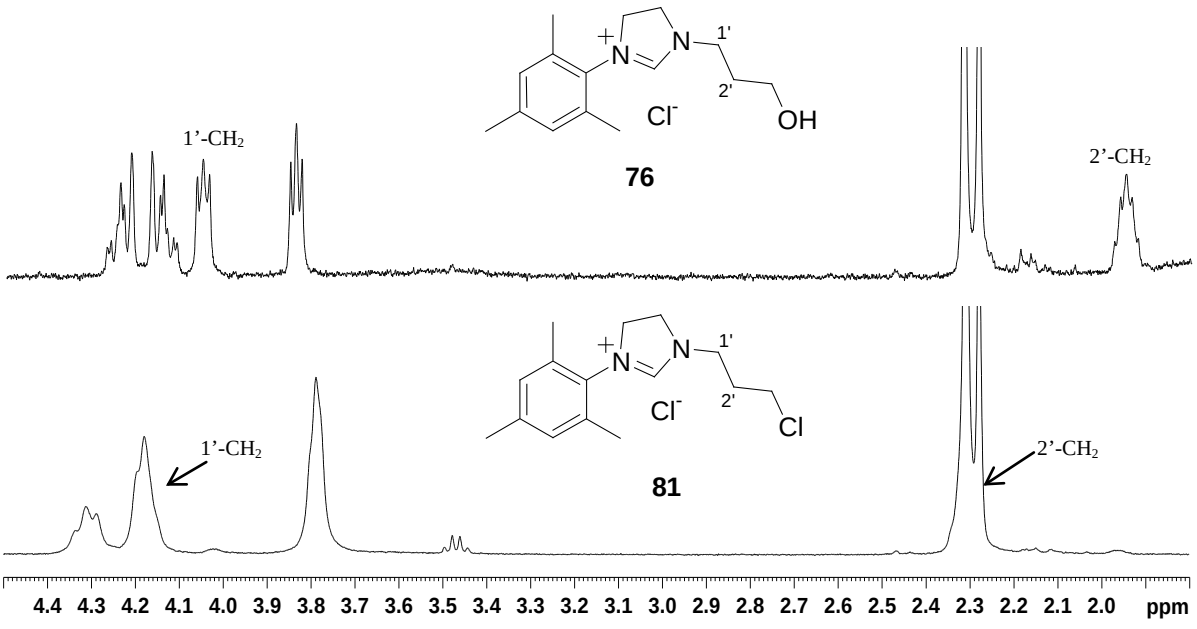

Figure 4.5 Partial 400 MHz ^{1}H NMR spectra for compounds **76** and **81** in $CDCl_3$.

We expected that the labile chloride could be displaced by the enolate anion **84**, generated by reaction of diethyl malonate **83** with NaH in THF[106] or with Na metal in EtOH[102] (Scheme 4.6). Both approaches to the enolate **84** were explored and various procedures were employed in the unsuccessful attempt to isolate the reaction product(s), including preparative layer chromatography, reverse phase chromatography and recrystallization. A more labile leaving group was considered and the bromo analogue **82** was prepared by treating the alcohol **76** with PBr_3.[107] Nucleophilic displacement of bromide by the enolate **84** was attempted but was also unsuccessful.

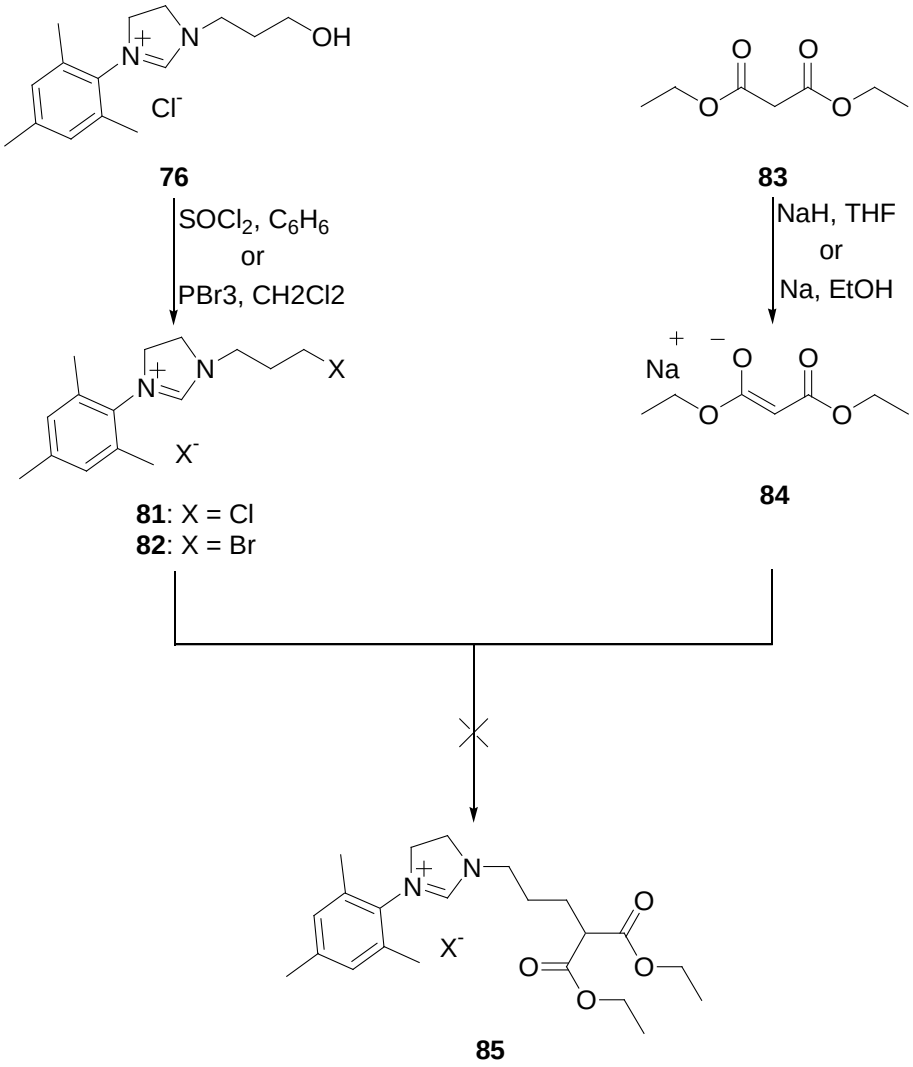

Scheme 4.6 Synthetic routes followed in the pursuit of malonyl derivative **85**.

^{1}H NMR analysis showed that the methine signal in the ^{1}H NMR spectrum of the precursor **82** (δ_H 9.43 ppm) had disappeared and it was possible that an unstable carbene was formed, which was capable of binding electron deficient species that may have been present in the reaction mixture.

Figure 4.6 shows IR data for compounds **76** and **82**, the former characterized by the OH (3189 cm^{-1}) and C=N (1644 cm^{-1}) absorption bands, the latter by the absence of the OH absorption band and the presence of a new C–Br band at 760 cm^{-1}.

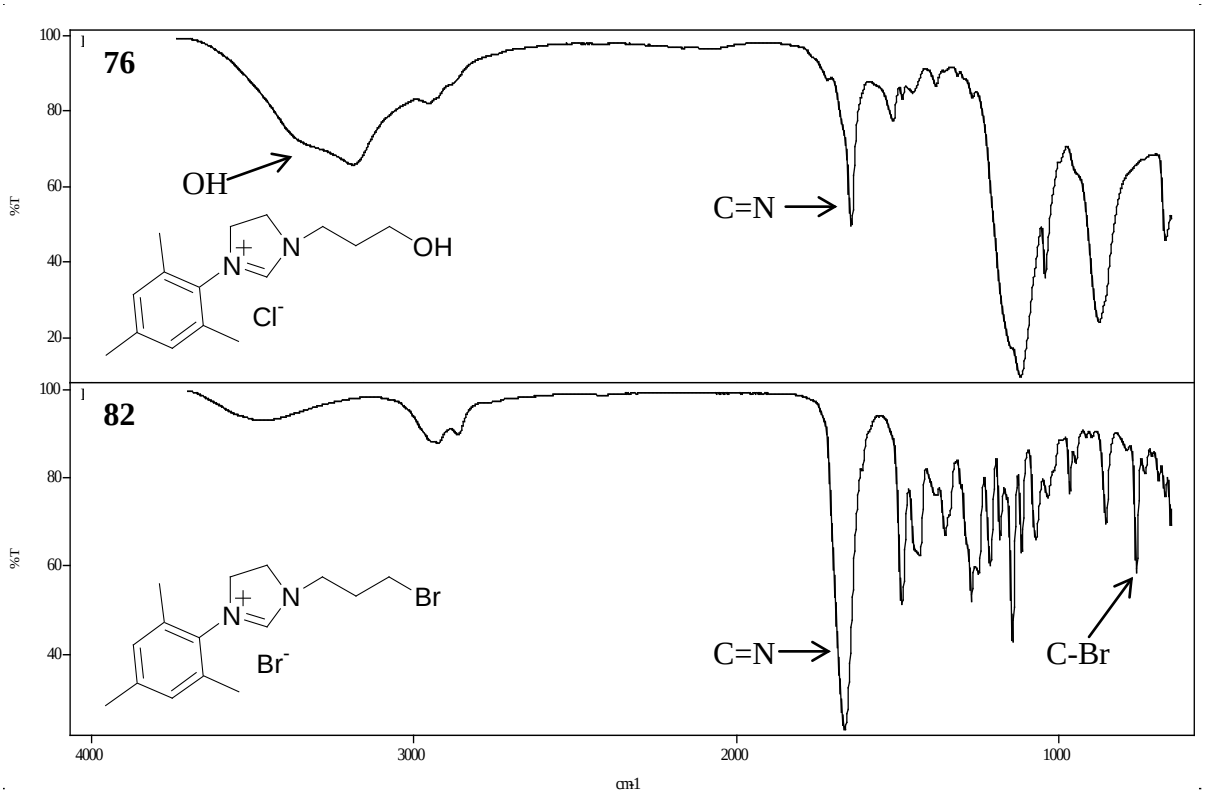

Figure 4.6 IR spectra for imidazolinium salts **76** and **82**.

At this point, an alternative approach became necessary since attempts to attach the malonyl moiety to the preformed imidazolinium salt had been unsuccessful. It was decided to explore the possibility of attaching the malonate moiety to the halogenated diamides **86** and **87** prior to cyclization, as indicated in the retrosynthetic analysis outlined in Scheme 4.7, whereby the halide derivatives of **75** might be more susceptible to nucleophilic displacement than the

imidazolinium salts **81** and **82** were, furnishing a diamido propylmalonate that could provide a vital precursor towards the imidazolinium salt **85**.

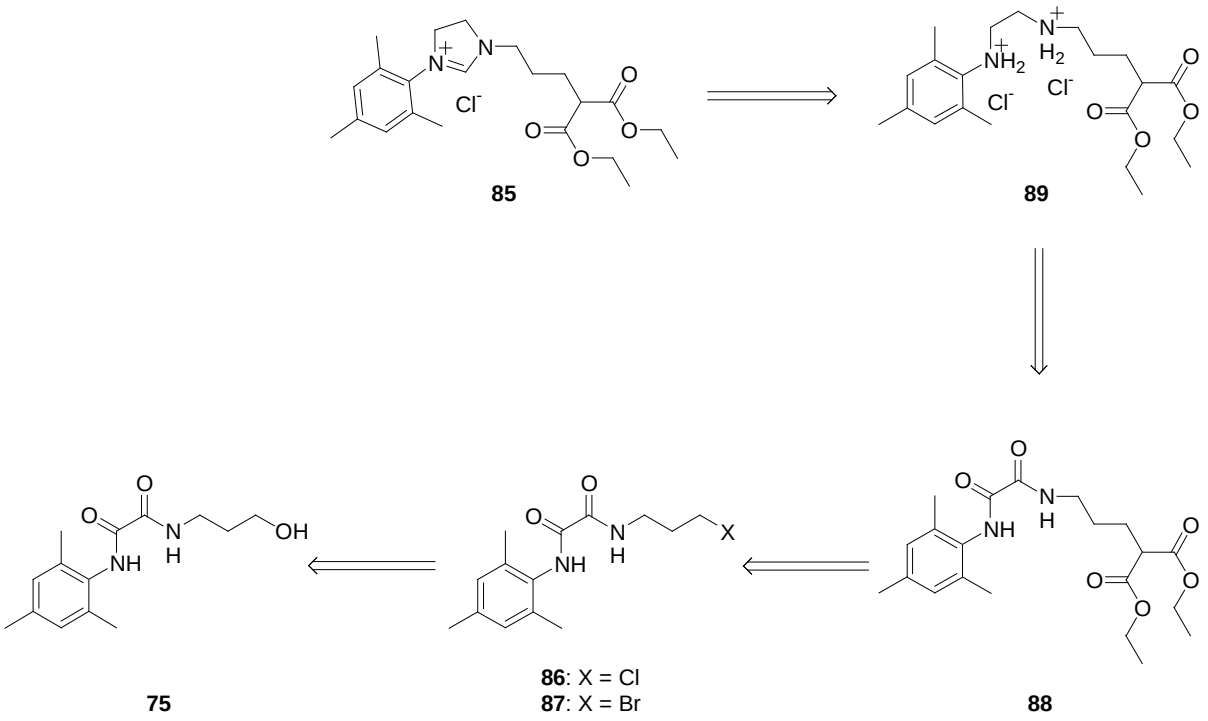

Scheme 4.7 Retro–synthetic analysis indicating an alternative route to compound **85**.

The halogenated analogues **86** and **87** were therefore prepared by treating the hydroxyalkyl oxamide **75** with $SOCl_2$ and PBr_3 respectively (Scheme 4.8). Nucleophilic displacement of the halide by diethyl malonate enolate **84** was attempted with both halogenated compounds **86** and **87**. The chloro derivative **86** proved to be unreactive but the more labile bromo analogue **87** reacted to afford the desired substituted malonate **88**, which was isolated as a solid by flash chromatography in 54% yield. The structure of compound **88** was confirmed by the 1– and 2–D NMR (Figure 4.7–4.9) and HRMS analysis. The ^{1}H NMR spectrum (Figure 4.7) reveals the presence of two equivalent methyl groups, resonating as a six proton triplet at 1.28 ppm. and two equivalent oxymethylene groups, resonating as a quartet at 4.20 ppm; signals for the trimethylene are shifted to higher field values.

The COSY spectrum (Figure 4.8) shows correlations between the protons on carbons 1–7, the most important of which is the interaction between the 4–methine and 5–methylene protons, confirming attachment of the malonyl moiety to the trimethylene side chain.

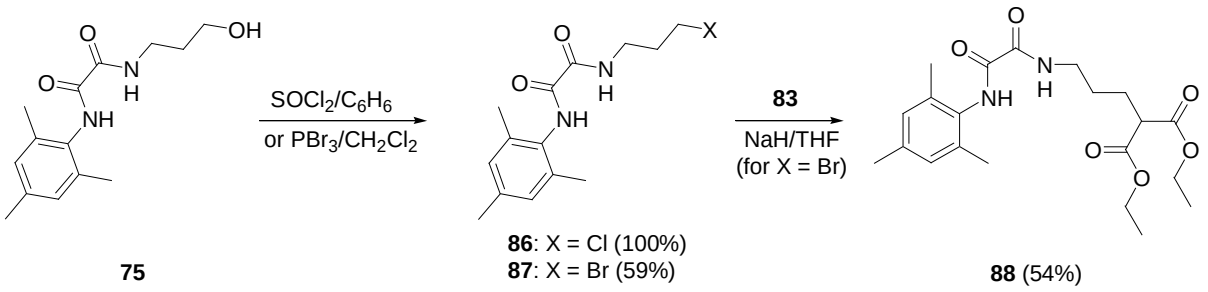

Scheme 4.8 Preparation of halo anologues of **75** followed by preparation of diamido propylmalonate **88**.

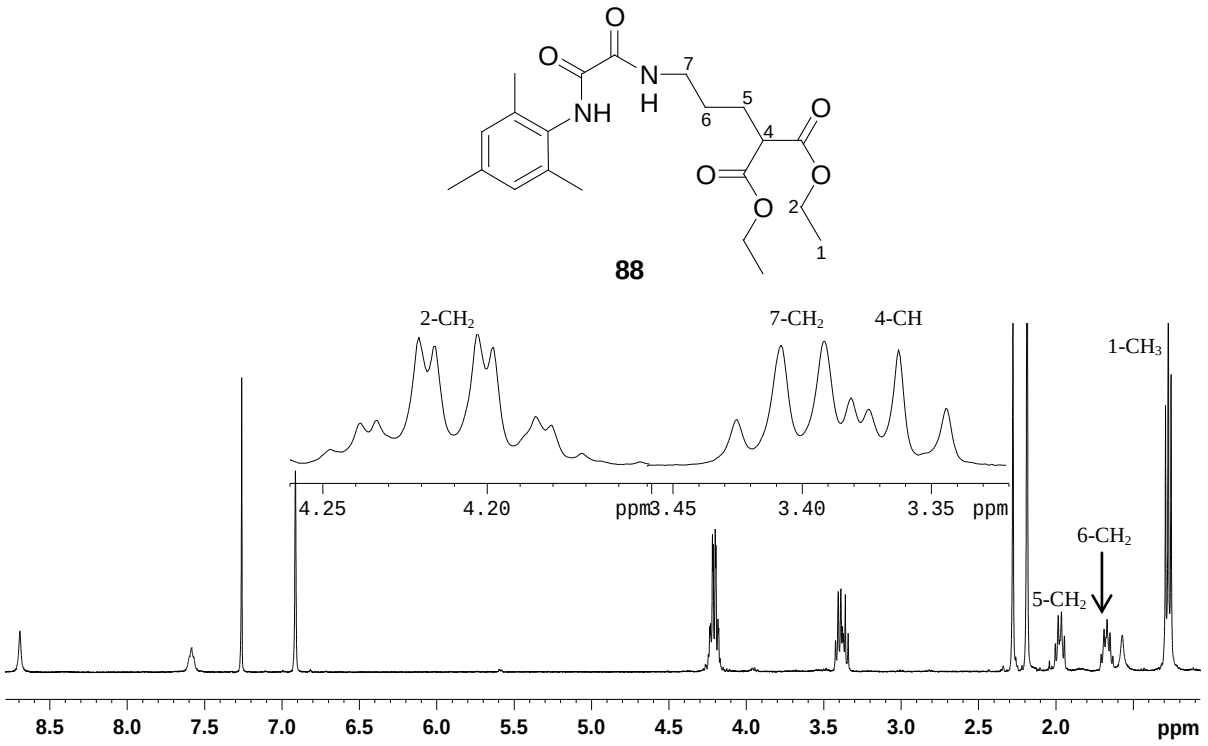

Figure 4.7 400 MHz ^{1}H NMR spectrum of compound **88** in $CDCl_3$ with expanded region (3.4 – 4.3 ppm) as insert.

The HMBC and HSQC data are shown in Figure 4.9, with attention being drawn to the ^{13}C signal at 169.1 ppm due to the equivalent ester carbonyl groups and the HMBC correlations (blue peaks I, II and III) between the ester carbonyl carbons and the 2– and 5–methylene and the 4–methine protons, respectively. The lower field amide carbonyl signal at 159.9 ppm exhibits an HMBC correlation with the 7–methylene protons. The HSQC data (red peaks) were used to correlate the ^{13}C and the ^{1}H NMR signals, permitting assignment of the individual ^{1}H NMR signals in Figure 4.7.

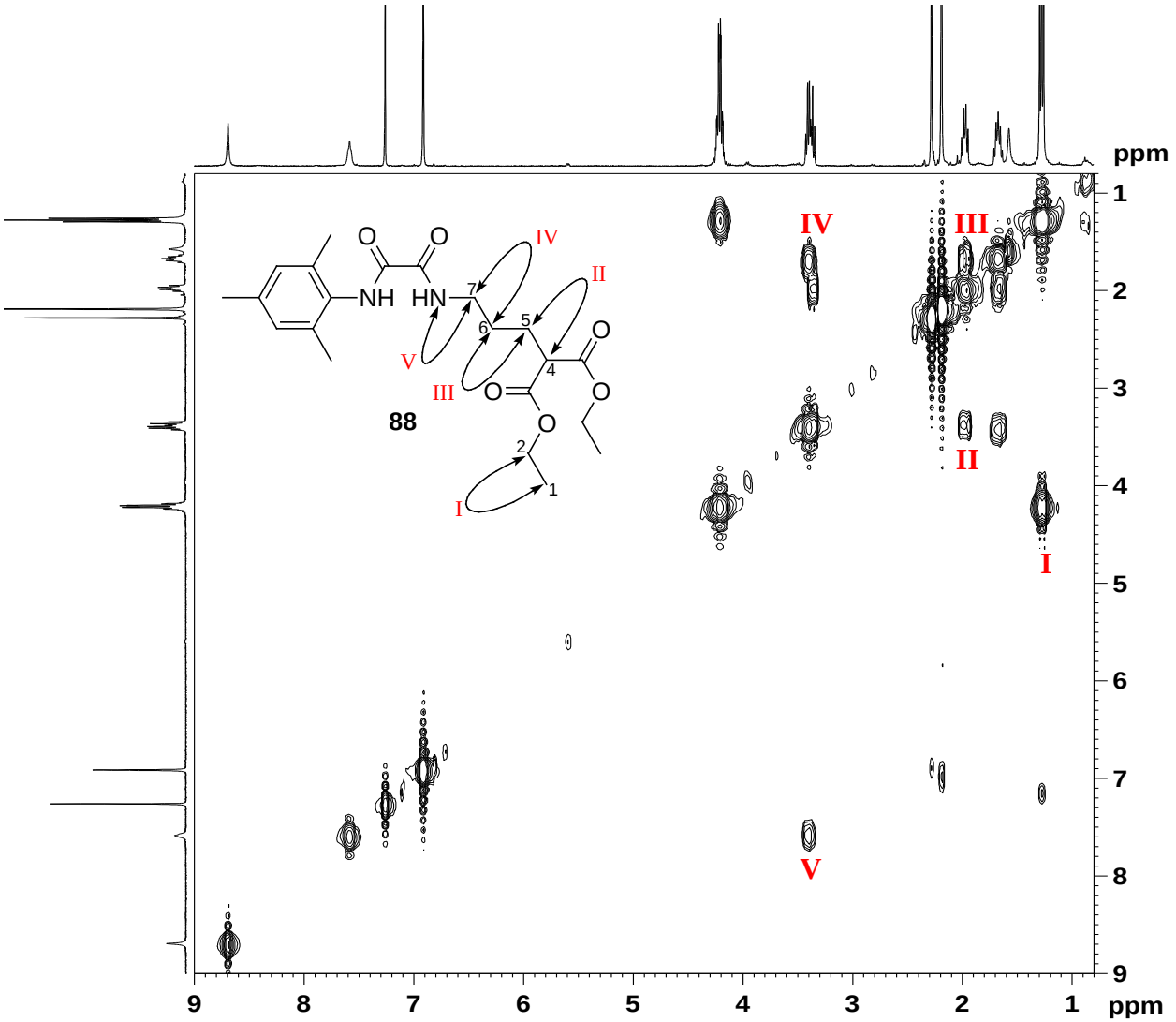

Figure 4.8 400 MHz COSY spectrum of compound **88** in $CDCl_3$.

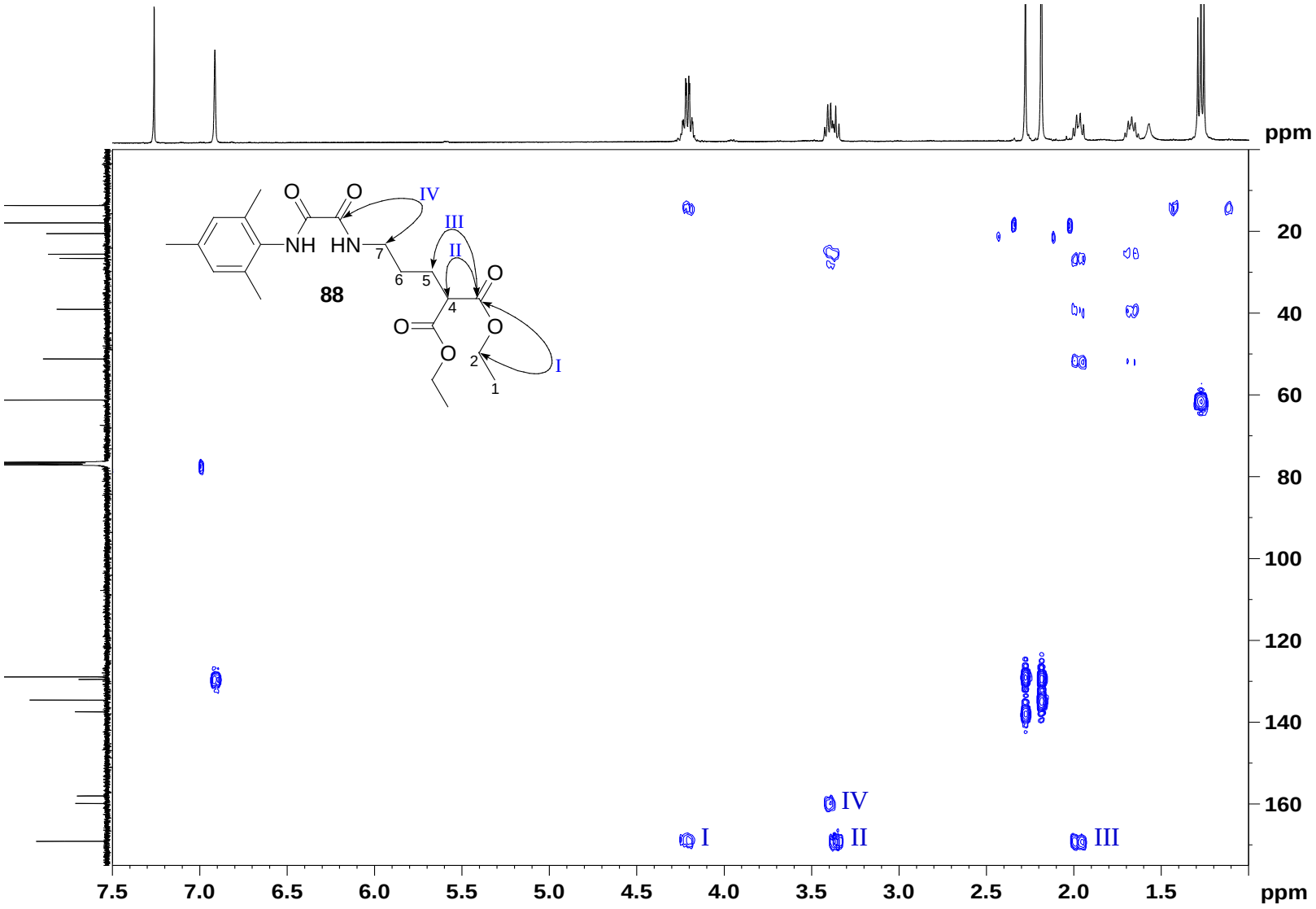

Figure 4.9 NMR spectra for compound **88**: HMBC (blue peaks) and HSQC (red peaks) in $CDCl_3$.

As before, a dihydrochloride salt was needed for cyclization, but it was suspected that reduction of the amide functionalities in compound **88** might be accompanied by concomitant reduction of the diester to a diol. Consequently, selective reduction was attempted several times with both $LiAlH_4$ and BH_3–THF, but was unsuccessful. Reaction times and purification procedures were varied, with reactions under reflux extending to as long as 26 hours. Compound **88** was treated with up to 16 equivalents of $LiAlH_4$ in the hope of reducing the diamide to a diamine and the diacid to a diol, thus forming 2–(hydroxymethyl)–5–[2–(mesitylamino)ethylamino]pentanol **90**. However, each reaction resulted in a cascade of products – intractable mixtures presumed to contain amides and amines, esters and alcohols.

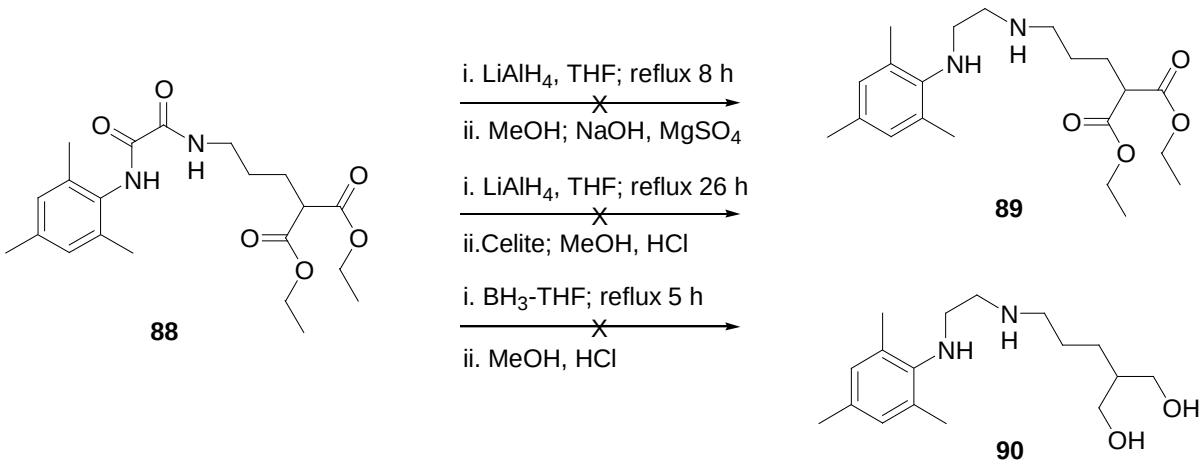

Scheme 4.9 Attempted reduction of the diamide **88**.

The idea of attaching the malonate moiety prior to cyclization still seemed the most feasible approach and in order to overcome the difficulties encountered in attempting to reduce the diamide functionality in compound **88**, the bromopropyl diamine **91** was targeted as a possible intermediate (Scheme 4.10). The successful preparation of compound **88** had proved the viability of the enolate substitution and compound **91** was expected to provide access to the cyclised product **85**.

The preparation of compound **91** was attempted using two different precursors. Treatment of the diamine **79** with PBr_3 resulted in an intractable mixture, purification of which was attempted by flash chromatography but no identifiable products were obtained. The reduction of the diamide **87,** on the other hand, resulted in reduction of the bromide. Chromatographic

separation of the crude mixture obtained from the latter reaction afforded two novel compounds, *N*–propyl–*N'*–mesityloxamide **92** and *N*–propyl–(2–mesityl)aminoacetamide **93.**

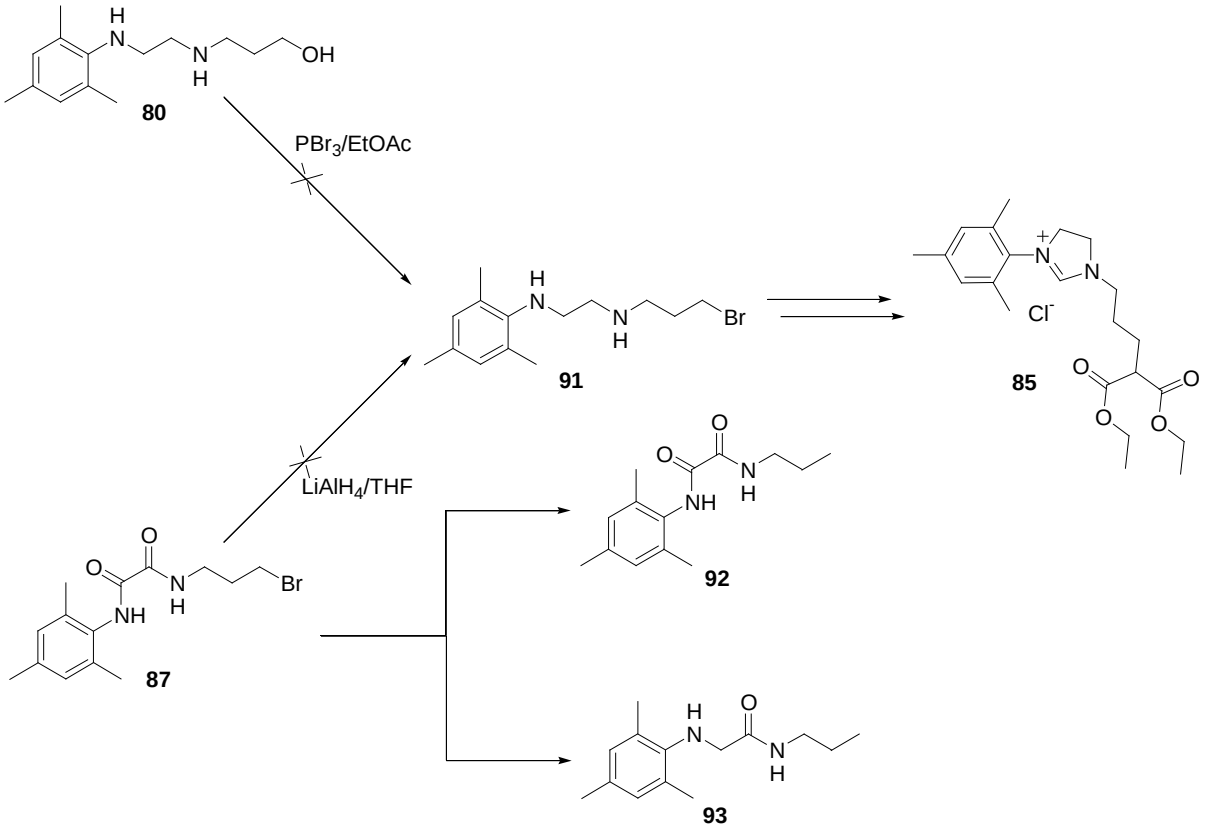

Scheme 4.10 Attempted synthetic routes towards compound **85**.

Figure 4.10 details the ^{1}H and ^{13}C NMR spectra for compounds **92** and **93**. Of particular significance in the ^{1}H NMR spectrum of the acetamide **93** is the singlet at 3.58 ppm, corresponding to the α–methylene protons and the single amide proton signal at 7.25 ppm, compared to the two amide proton signals at 7.52 and 8.51 ppm in the spectrum of the diamide **92**. Furthermore, two carbonyl signals at 158.3 and 159.8 ppm are observed in the ^{13}C NMR spectrum of compound **92** as opposed to a single carbonyl signal at 171.0 ppm for compound **93**. The structures were confirmed by HRMS analysis, giving *m/z* values of 249.1616 and 235.1804 respectively.

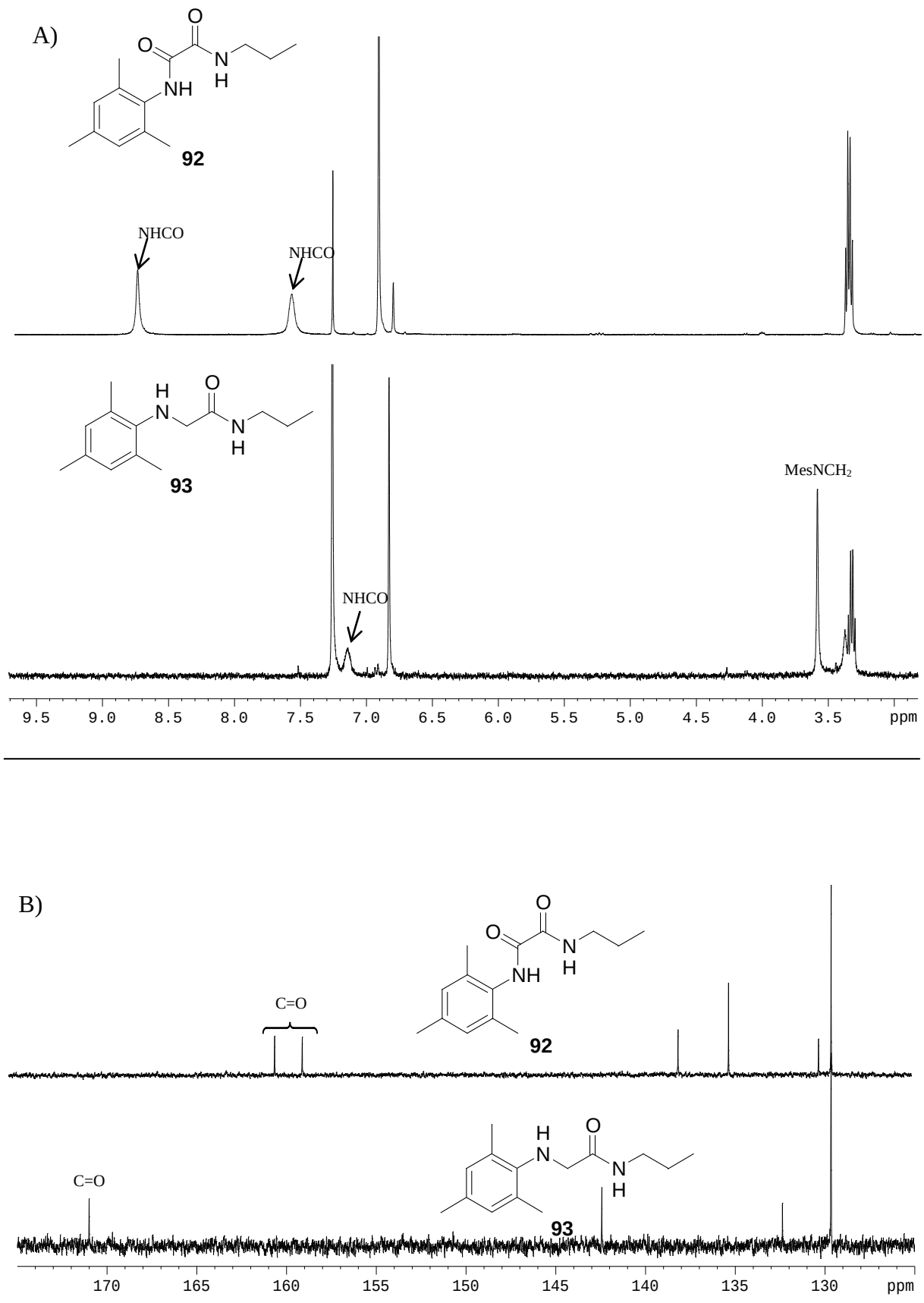

Figure 4.10 A) Partial 400 MHz ^{1}H NMR spectra for **92** and **93** and B) partial 100 MHz ^{13}C NMR spectra for **92** and **93** in $CDCl_3$.

As an alternative to the malonate functionality, malononitrile and malonaldehyde systems were investigated as potential chelating ligands since the nitrile or acid functionalities might react more favourably under reducing conditions than an ester. Following procedures similar to that used with diethyl malonate, the novel malononitrile derivative **94** was prepared from the bromo derivative **87** and malononitrile. Flash chromatography and further purification by HPLC afforded the dinitrile **94** as a pure compound, but in disappointing yield, raising concerns about the viability of this pathway. The structure was elucidated using 1– and 2–D NMR and HRMS data and by the precence of a C≡N IR absorption band at 2255 cm^{-1}.

The preparation of the malonaldehyde–based system **98** was attempted using the sodium enolate salt **97**, obtained *via* the acid hydrolysis of tetramethoxypropane **96** (Scheme 4.11).[109] Attempted coupling of the enolate **97** with the bromo derivative **87** unfortunately failed to afford the desired product **98.** Time constraints prevented further investigation of routes to tridentate ligands.

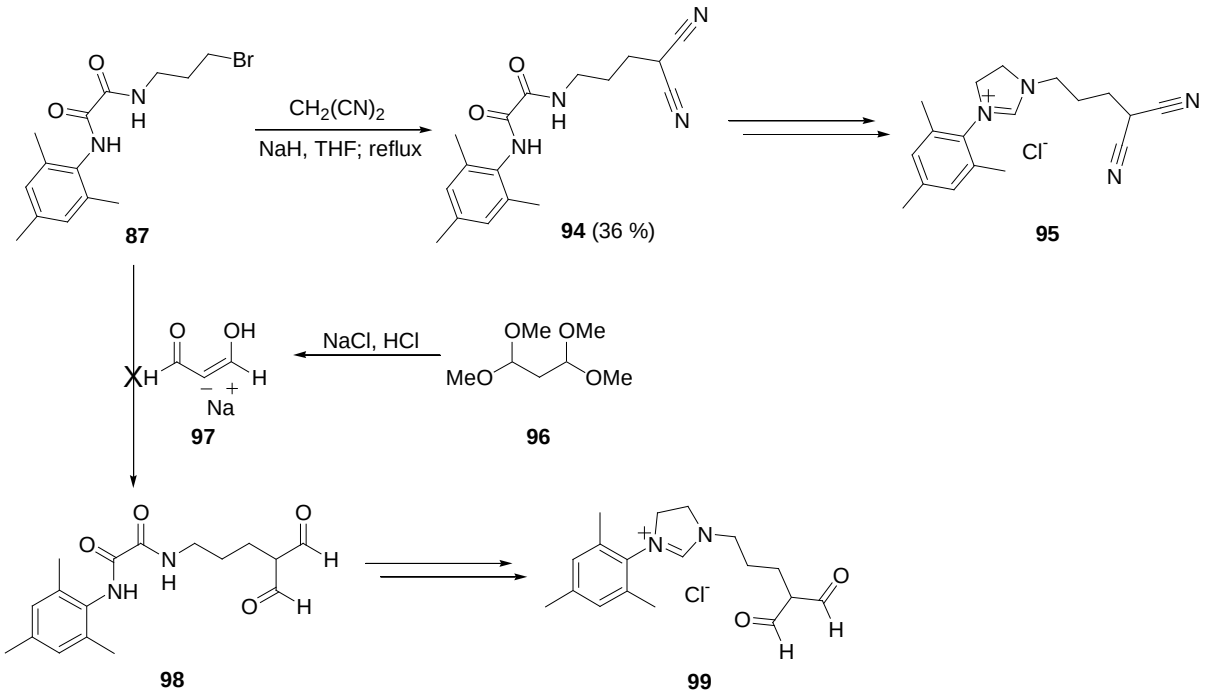

Scheme 4.11 Alternative pathways towards tridentate ligands using malononitrile and malonaldehyde.

4.2. Preparation of imidazolium pro–ligands

In addition to the highly reactive, saturated NHC pro–ligands (imidazoliniums), we investigated the related family of imidazoliums as precursors to carbenic imidazol–2–ylidenes. Imidazolium salts are attractive as stable NHC precursors due mainly to the simplicity and versatility of their preparation. Our interest in the unsaturated *N*–substituted mesitylimidazoliums was prompted by the practical difficulties encountered in the preparation and isolation of tridentate imidazolinium species as carbene precursors.

The retrosynthetic analysis in Scheme 4.12 shows how the bi– and tridentate pro–ligands **100** and **101**, respectively, might be prepared in as few as two steps, following an established methodology,[110] whereby *N*–mesitylimidazole **102**, first prepared by Arduengo,[111] provides access to a wide range of substituted mesitylimidazoliums.

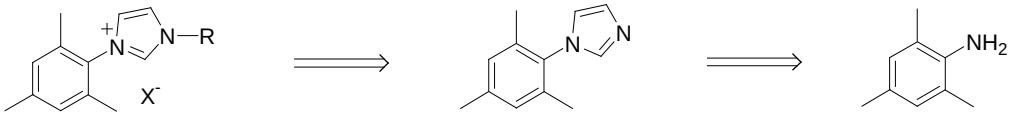

100: R = $(CH_2)_3OH$
101: R = $(CH_2)_3CH(CO_2Et)_2$

102 **73**

Scheme 4.12 Retro–synthetic strategy for the preparation of imidazolium salts.

2,4,6–Trimethylaniline **73** was treated with phosphoric acid to afford the anilinium salt **103** which was subsequently reacted with glyoxal **104**, paraformaldehyde **105** and ammonium chloride to give *N*–mesitylimidazole **102** (Scheme 4.13),[110] which was recrystallized several times from ethyl acetate and obtained in a yield of 98%.

With the precursor **102** in hand, alkylation with various halogenated systems was investigated. The alkylation of *N*–mesitylimidazole **102** has been described for many substrates, from simple alkyl halides to complex aromatic and even chiral substrates, as efficient yet very slow and time consuming – involving long periods under reflux, in some cases extending to several days.[95, 99, 107, 110, 112–121]

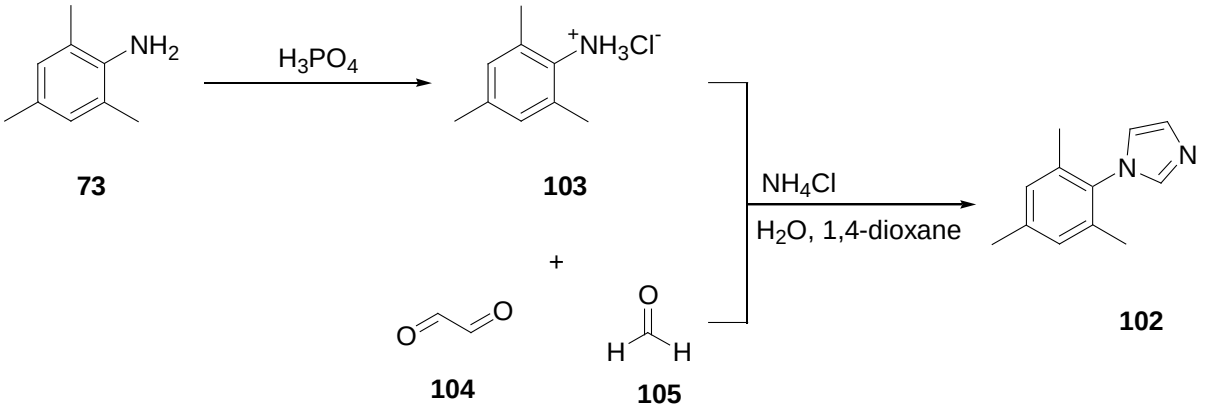

Scheme 4.13 Preparation of *N*–mesitylimidazole **102**.

Reaction of *N*–mesitylimidazole **102** with 3–chloropropanol **106** was attempted under reflux, initially in THF for a period of 16 h and then in toluene for a period of up to 5 days without any reaction having taken place. It became obvious that conventional heating methods would not suffice for the preparation of this system and we began to investigate the use of microwave irradiation as an alternate energy source.

Microwave assisted organic synthesis (MAOS) is a relatively young technique, although it has received considerable attention since the first independent reports by Giguere and Majetich[122] and by Gedye[123] in 1986. While Gedye *et al.*[123] reported "remarkable rate enhancement and dramatic savings in reaction times" in acid hydrolysis, oxidation, esterification and nucleophilic substitution of simple substrates, Giguere and Majetich[122] discussed improvements in the reaction times of Diels–Alder, Claisen and ene reactions using domestic microwave ovens.

Although it was apparent that microwave irradiation provided a very efficient energy source, the use of microwave irradiation in chemical synthesis was not widely accepted, mainly due to poor reproducibility of chemical transformations and lack of control in domestic microwave ovens. This was coupled with a lack of understanding of microwave heating and the inherent dangers associated with heating flammable organic solvents in a microwave field.[124] The first dedicated microwave reactors were made available in the 1990's and since then, the use of microwave irradiation in organic transformations has increased exponentially. These microwave reactors provide online temperature, power and pressure monitoring and the modern trend is to use only dedicated, controllable microwave equipment and to overlook scientific results produced using domestic microwaves.[125]

Microwave irradiation has had a profound impact on 'green' synthesis and sustainable chemistry,[126] with many reactions under microwave irradiation having shown considerable improvements in yield and selectivity compared to conventional heating methods.[126] Microwave heating has been proven to reduce reaction times from hours to minutes, reduce side reactions, increase yields and improve the reproducibility of transformations.[124]

Microwave irradiation lies in the frequency range 0.3 – 300 GHz and all microwave supply equipment, whether domestic or controlled, provide microwaves at a frequency of 2.45 GHz, thereby avoiding interference with telecommunication frequencies. The energy of a resultant microwave photon at 2.45 GHz is 0.0016 eV, *i.e.* lower than the energy of Brownian motion and unable to break chemical bonds. Such microwave energy is thus incapable of inducing chemical reactions and will have no effect on chemical structure[124, 127, 128] – the effect is purely kinetic.[127]

Microwave heating is based upon dielectric heating, which is dependent on the ability of a substance to absorb microwave energy and subsequently convert it into heat. Dipole rotation and ionic conduction are the mechanisms responsible for heating in a microwave field. Irradiation of a substance by microwaves results in dipolar or ionic alignment within the applied, oscillating electric field. Realignment of the dipole or ion field of the substances results in emission of heat *via* molecular friction and dielectric loss.[124, 127, 128]

Thus, the efficiency with which a particular substance may absorb microwave irradiation is dependent on the substance's dielectric properties and the ability to convert microwave irradiation into thermal energy depends on its loss factor (tan δ).[124] The mechanism of microwave heating involves heat transfer in the reaction medium and the problems associated with conventional heating methods (such as the existence of "hot spots" or "wall effects") are non–existent under microwave irradiation.[124] The thermal efficiency of microwaves means that solvents may be "super–heated" above their boiling point in a matter of seconds and cooled just as quickly, as the only residual heat once the electric field has been removed is latent heat.[127]

Microwave assisted organic synthesis (MAOS) is being utilized to make advances in many areas of synthesis and comprehensive reviews have been published illustrating its impact in modern chemistry.[124, 127, 129, 130]

In exploring the microwave–assisted reaction of *N*–mesitylimidazole **102** with 3–chloropropanol **106** (Scheme 4.14), consideration was given to the reaction time, thermal properties of the reactants and potential solvents. As a pilot reaction, the reactants were irradiated in a single mode, dedicated microwave reactor in the absence of solvent for a total of 60 minutes (150 W, 85–90^{o}C) with the progress of the reaction being monitored periodically by ^{1}H NMR spectroscopy.

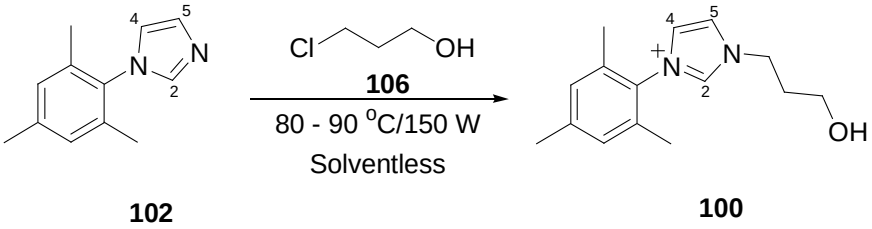

102 **100**

Scheme 4.14 Microwave–assisted preparation of the hydroxypropyl imidazolium salt **100**.

Changes in the aromatic region of the ^{1}H NMR spectrum (Figure 4.11) indicated that the reaction was in fact, proceeding. The observed changes were the progressive disappearance of the substrate *N*–methine proton signals at 6.88 and 7.23 ppm, to be replaced by emerging signals at 7.16 and 8.11 ppm, corresponding to the 4– and 5–methine protons, respectively in the product **100**. The imidazole 2–methine proton signal at 7.43 ppm was seen to disappear over time, which was coupled to the appearance of the characteristic low–field singlet at 10.10 ppm (Figure 4.12) due to the acidic 2–methine proton of the imidazolium salt **100**. After 60 minutes under microwave irradiation, the product was extracted into H_2O and isolated as a white solid in 58 % yield.

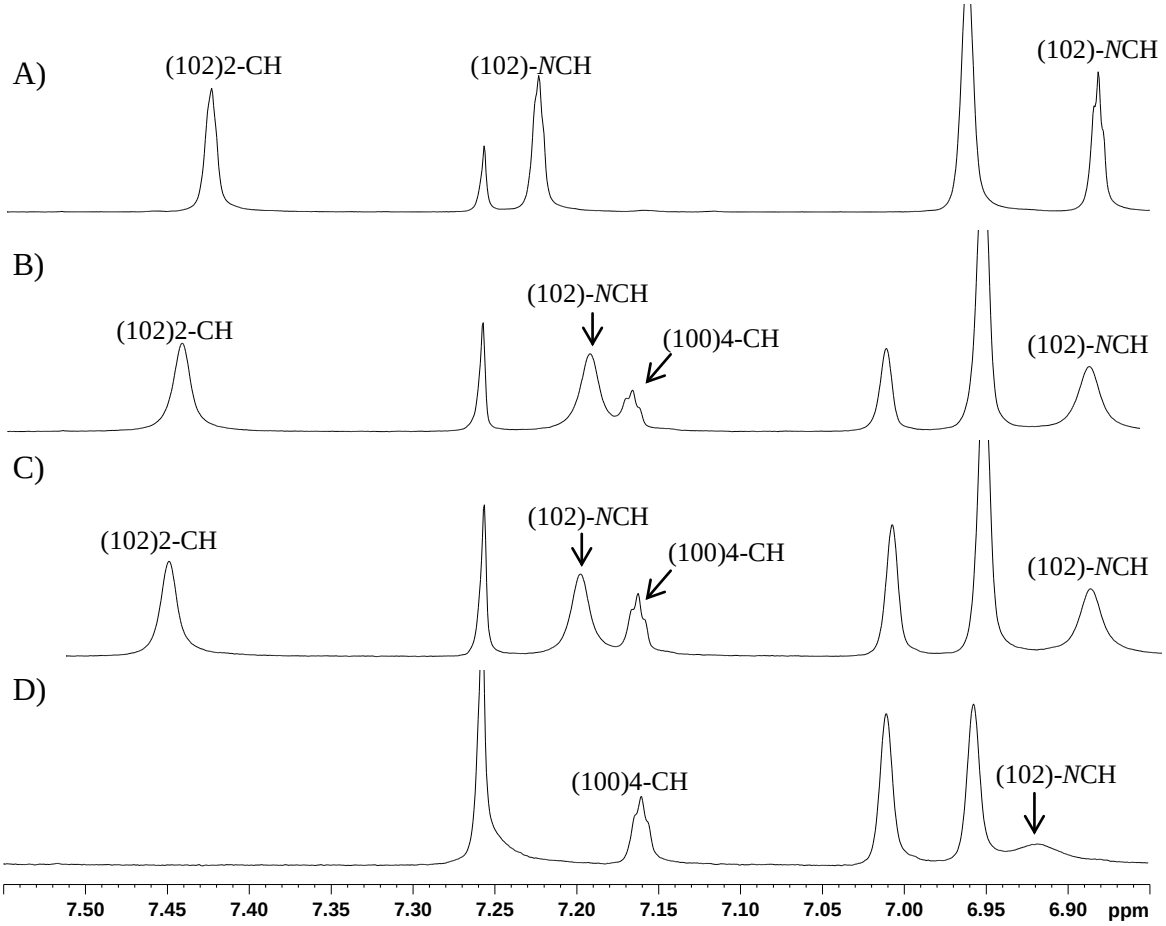

Figure 4.11 Partial 400 MHz ^{1}H NMR spectra in $CDCl_3$ of the microwave–assisted alkylation of compound **102** to give the imidazolium salt **100**: A) t = 0; B) t = 20 min; C) t = 40 min; and D) t = 60 min.

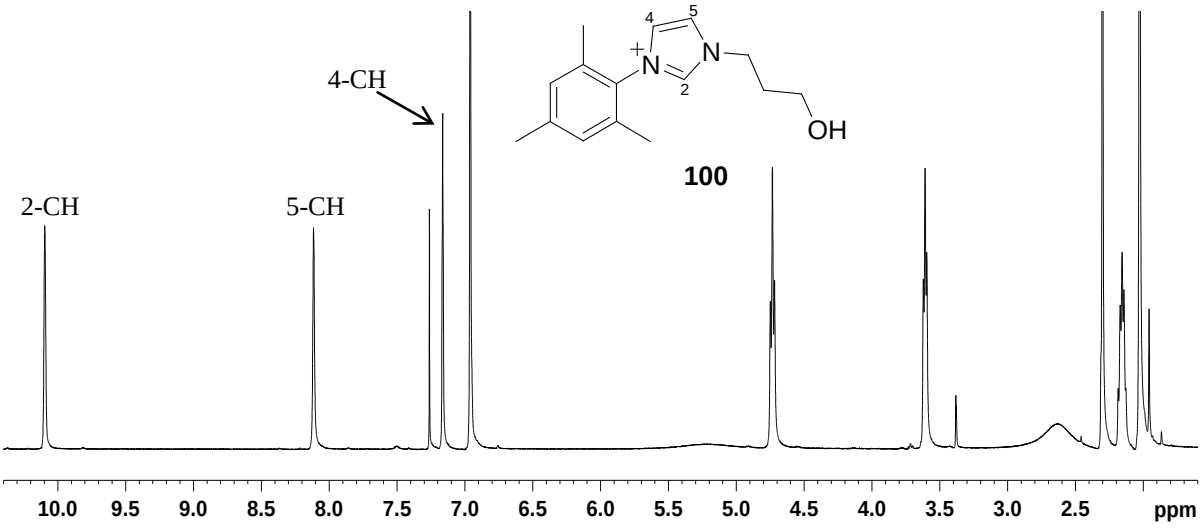

Figure 4.12 400 MHz ^{1}H NMR spectrum of the imidazolium salt **100** in $CDCl_3$.

1–D and 2–D NMR, HRMS and IR spectral data were used to confirm the structure of the imidazolinium salt **100.** In Figure 4.13, the DEPT 135 spectrum (left hand axis) shows the presence of three methylene groups, corresponding to the nuclei of the trimethylene side chain. The high field methyl signals correspond to the *o*– and *p*–methyl groups, and the signals in the aromatic region to the imidazolium and the equivalent aromatic methine protons. The ^{13}C NMR signals were assigned with the aid of the HSQC correlations (red peaks) and are consistent with the bonding relationships reflected by the HMBC (blue peaks) and COSY correlations (insert of Figure 4.13). For example, the HMBC correlations between the 2–methine carbon and the 4– and 5–methine protons (indicated as I and II) are confirmed by the COSY correlations (I and II); the HMBC and COSY correlations between the 4– and 5–methine groups are also evident (III).

Following the success of the reaction with neat reactants, consideration was given to the possible use of different solvents. Despite the obvious advantages of a solvent–free approach in terms of 'green chemistry', it was reasoned that, since the product is a salt, an organic solvent with low polarity might possibly dissolve the reagents but not the product, simplifying the purification procedure. Similar reported transformations under conventional heating[95, 99, 107, 110, 112–121] were considered and the two solvents that seemed most suitable were THF and toluene. The reaction was repeated in toluene under microwave irradiation and after 90 minutes a solid had, in fact, precipitated, and was rinsed with toluene and acetone to give the pure product.

Solvents for use in microwave–assisted reactions can be classified into three main groups in terms of their loss factor tan δ. Toluene (tan δ 0.04) is indicated to be a poor solvent for such reactions.[124] However, it is important to consider the entire reaction medium, taking into account the loss factors of the reagents (which are unknown) as well as the solvent. Hayes[127] describes poor microwave absorbers, such as toluene, as possible "heat sinks," drawing heat away from the reactants. Experiments were then performed with the same reagents, but using as solvents:– acetonitrile (tan δ 0.062),[124] described as a medium absorber;[127] and EtOH (tan δ 0.941),[124] described as a very good microwave absorber.[127] However, the reactions conducted in these solvents failed to run to completion in the same reaction time as those performed in toluene.

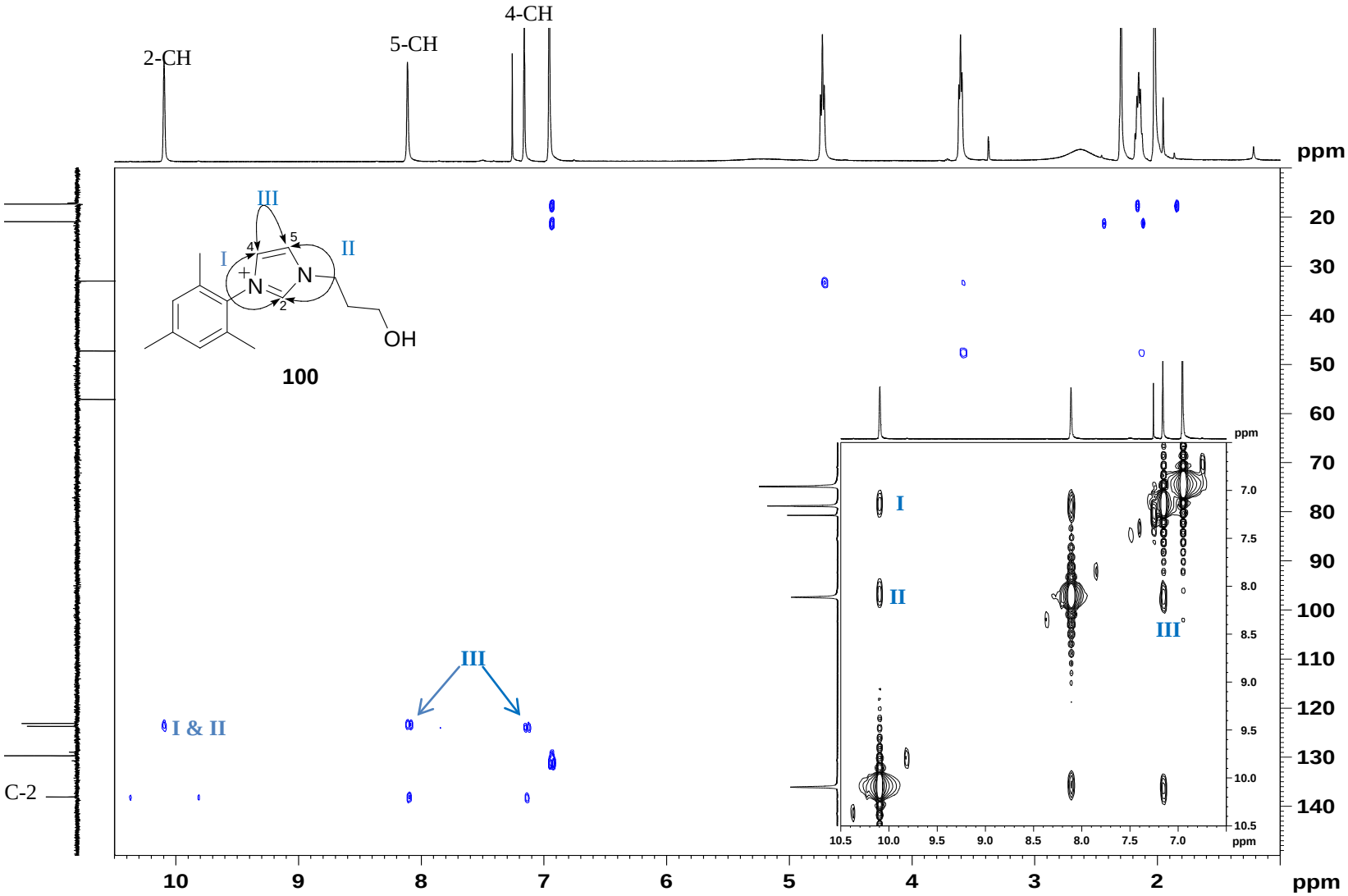

Figure 4.13 NMR Spectra for the imidazolium salt **100** in $CDCl_3$: ^1H NMR (top); DEPT 135 (left); HMBC (blue peaks); HSQC (red peaks) and partial COSY as insert (black peaks).

The dramatic improvement in the reaction rate for the transformation of this particular pair of substrates, compared to those in the literature[99, 107] constituted a novel and improved method for the preparation and isolation of strategically important mesitylimidazolium salts – critical precursors to imidazol–2–ylidene carbenes. Consequently, a small library of compounds was prepared, following the procedure for the preparation of imidazolium salt **100** in toluene. Scheme 4.15 summarises the successful synthesis of eight imidazolium salts and Table 4.1 details the reaction conditions and corresponding yields.

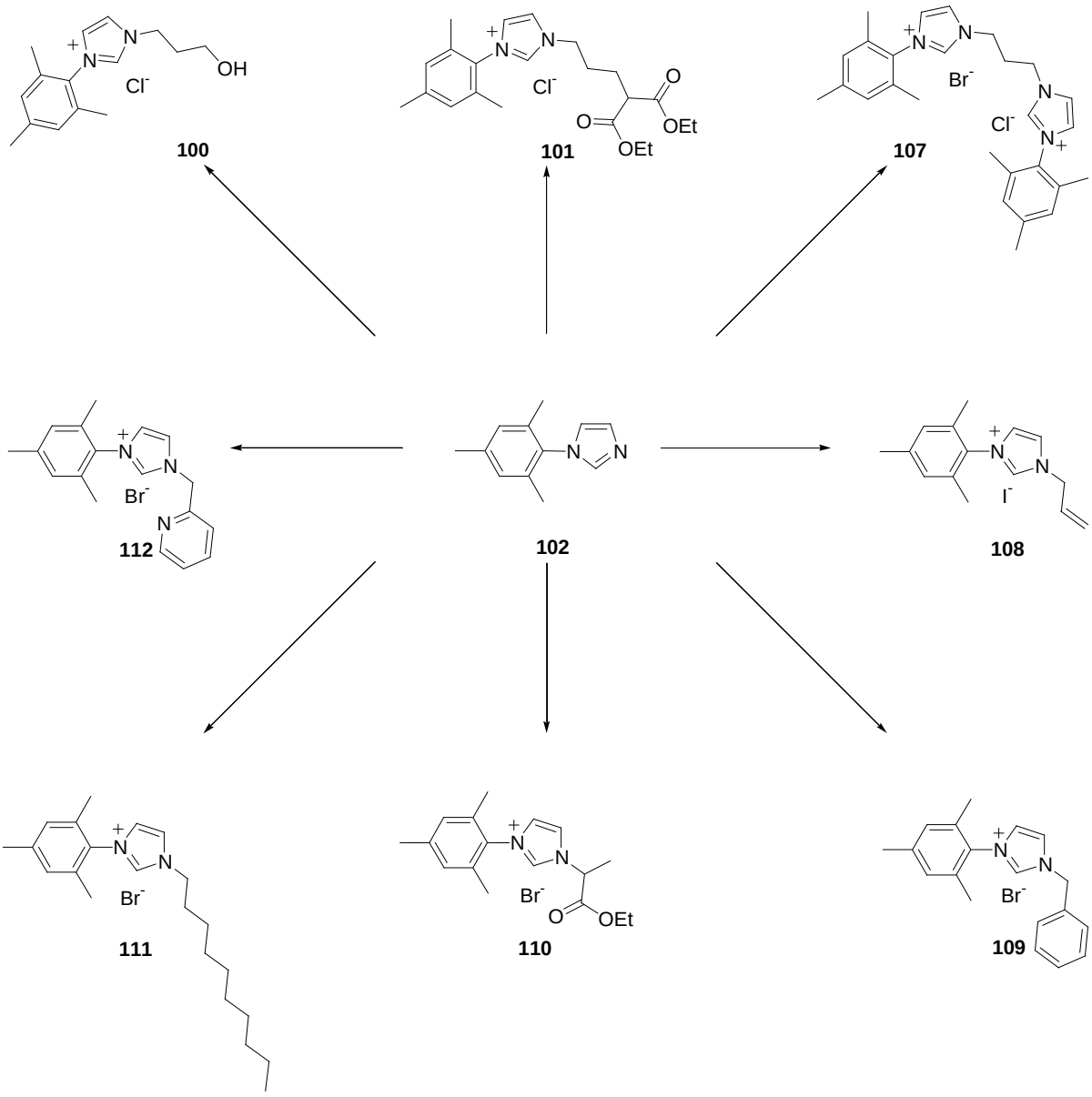

Scheme 4.15 Microwave–assisted preparation of substituted mesitylimidazolium salts from *N*–mesitylimidazole and various alkyl halides.

Table 4.1 Microwave–assisted preparation of substituted mesitylimidazolium salts[a].

Product	Reactant	Time (mins)	Isolated yield (%)
100	3–chloropropanol **106**	60	74
101	compound **113** (Scheme 4.16)	120	7
107	1–bromo–3–chloropropane **114**	30	70
108	allyl iodide	30	69
109	benzyl bromide	30	80
110	ethyl 2–bromopropionate	30	77
111	1–bromodecane	30	61
112[b]	2–bromomethyl pyridine. HBr	30	39

a) All reactions were performed at 85 °C and 150 W.

b) All reactions were performed in toluene except **112,** which was in ethanol.

Unfortunately, the critical tridentate pro–ligand **101** was obtained in the lowest yield (7 %) and efforts were focused on optimizing the reaction conditions in this particular case. *N*–mesitylimidazole **102** was alkylated with diethyl 2–(3–chloropropyl)malonate **113** (Scheme 4.16), prepared by the selective nucleophilic displacement of bromide from 1–bromo–3–chloropropane by the sodium enolate of diethyl malonate **84**; no further purification was necessary for the latter reaction, which was performed using equimolar quantities of both reactants and allowed to run to completion. Reaction conditions and purification procedures were varied in an attempt to optimize the microwave–assisted preparation of imidazolium **101** (Table 4.2).

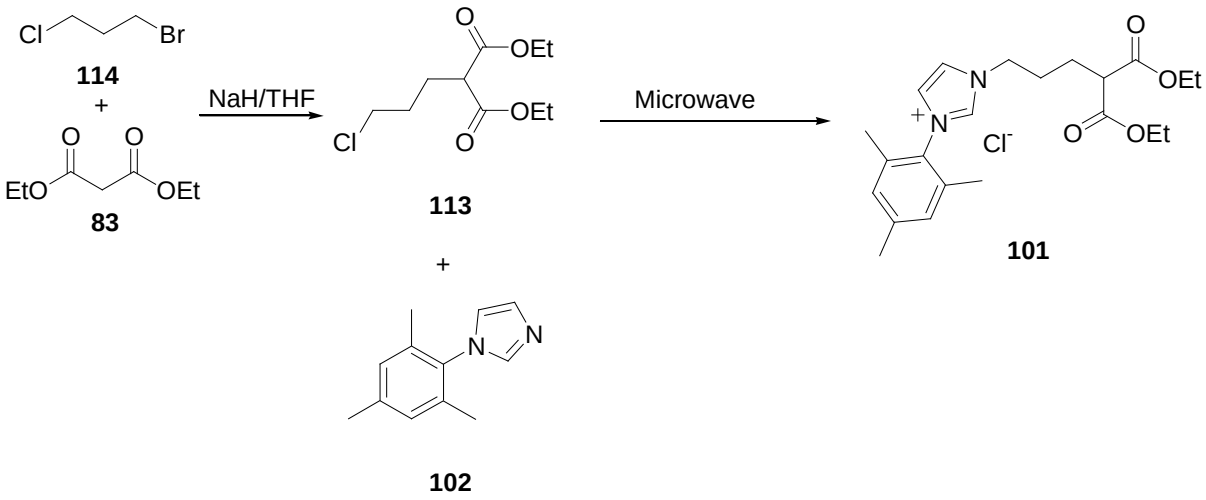

Scheme 4.16 Attempts to optimize the preparation of the malonate derivative **101**.

Table 4.2 Different reaction conditions used in the preparation of the malonate derivative **101**.

Method	Rxn time (h)	Temp (°C)	Power (W)	Solvent	Work–up
1	1–3	80–85	150–200	nil	phase seperation (acetone; tol.; EtOAc/H_2O)
2	1.0	80	150	EtOH	nil
3	3.0	92	150	MeCN	nil
4	2.0	95–100	180	DCM	nil
5	1–3.5	85–95	150	toluene	phase seperation (tol.; EtOAc/H_2O)
6	1.5	85	150	toluene	recryst. from MeOH, EtOAc and DCM
7	2.0	80	150	toluene	phase seperation (EtOAc/Aq. NaCl)
8	2.0	95	180	toluene	flash chromatography
9	2.0	90	150	toluene	HP20 chromatography

The reaction that provided the product **101** in high purity involved microwave irradiation in toluene at 85 ºC for 2 h, with two successful purification procedures:- a phase separation using aq. NaCl solution and ethyl acetate; and HP–20 chromatography with gradient elution of methanol–water. Although the yields were consistently low, the isolation of the imidazolium salt **101** represented a major step towards accessing the envisaged tridentate ligands and their use in the preparation of halide–free ruthenium catalysts. The structure of the malonyl derivative **101** was confirmed by HRMS and 1– and 2–D NMR analysis (Figure 4.14).

The low–field 2–methine signal (δ_H 10.64 ppm; δ_C 139.2 ppm) is, as indicated previously, characteristic of the imidazolium salt. The HMBC correlations (blue peaks) observed between the *N*–methylene at 4.80 ppm and the imidazolium methine carbon C–2 at 139.2 ppm; I and C–5 at 122.4 ppm; II indicate attachment of the side chain at N–3. COSY correlations (insert of Figure 4.14) between the 1'–methyl and 2'–methylene (III) and between the 4'– and 5'–methylene protons (IV) indicate adjacent pairs of nuclei and confirm the orientation and the linkage of the malonyl moiety *via* the trimethylene chain to the heterocyclic ring.

The structure of imidazolium salt **101** was further confirmed by comparing the IR spectra of the product with those of the two starting materials, compounds **102** and **113**, as shown in Figure 4.15. The C=N absorption band is evident in the spectra of *N*–mesitylimidazole **101** (1499 cm^{-1}) but not as easily identified in the *N*–substituted product **101**. The ester absorption band is observed in the spectrum of **113** (1728 cm^{-1}) and the product **101** (1722 cm^{-1}), indicating attachment of the alkyl malonate to form the product **101**.

The ester oxymethylene protons (H_a and H_b in Figure 4.16) of the malonate functionality in diethyl malonate resonate as expected – as a quartet (δ_H 4.00), since the protons couple to the terminal methyl groups. However, when diethyl malonate is attached to the chloropropyl chain to afford compound **113** these protons ($H_a$and H_b) in each ester moiety become diastereotopic and further splitting is evident due to their magnetic inequivalence. The effect is even more evident when the steric bulk is increased further, as in the spectrum of the imidazolium salt **101**, which shows a poorly resolved, overlapping pair of double quartets.

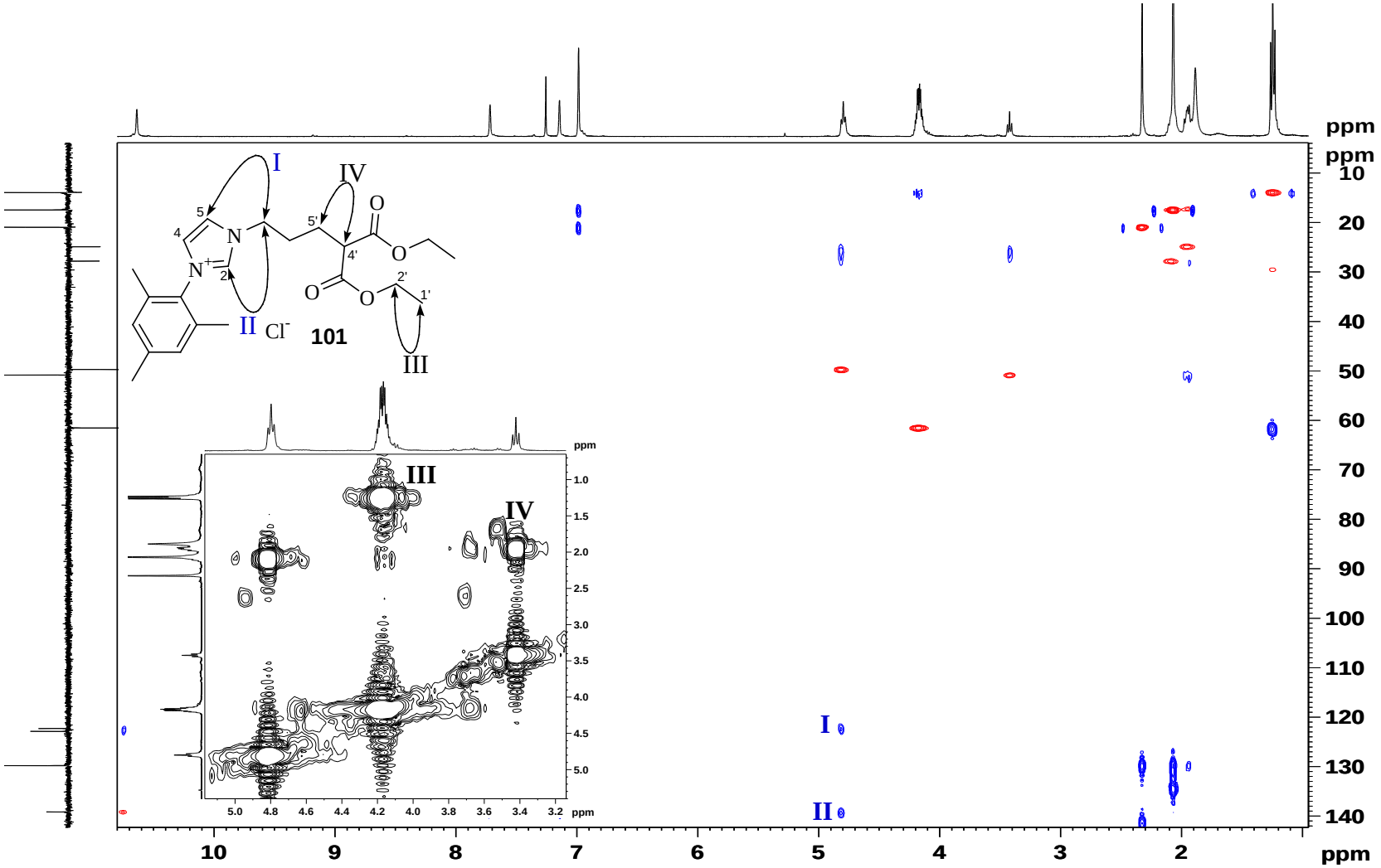

Figure 4.14 NMR spectra for the imidazolium salt **101**:[1]H NMR (top axis), DEPT 135 (left hand axis), HSQC (red peaks), HMBC (blue peaks) and partial COSY (black peaks) as insert.

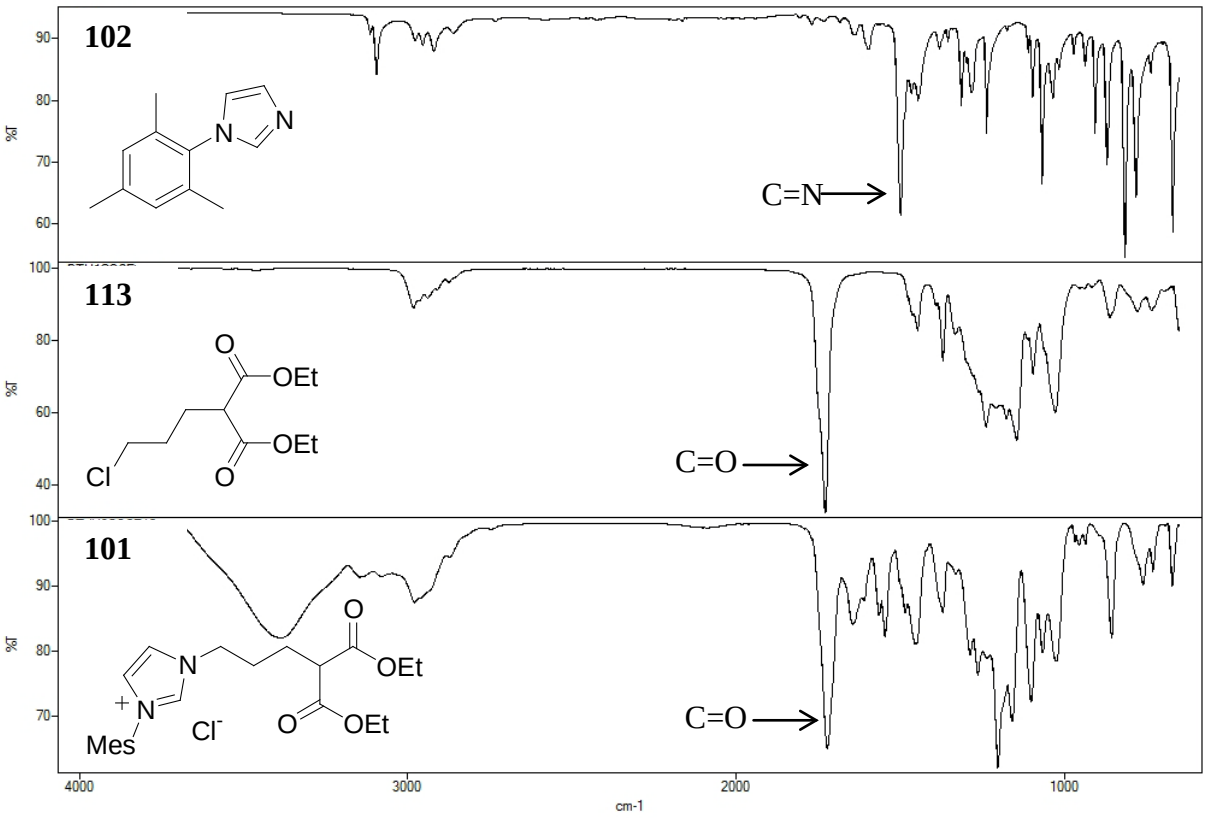

Figure 4.15 ATR IR spectra for compounds **102, 113** and **101**.

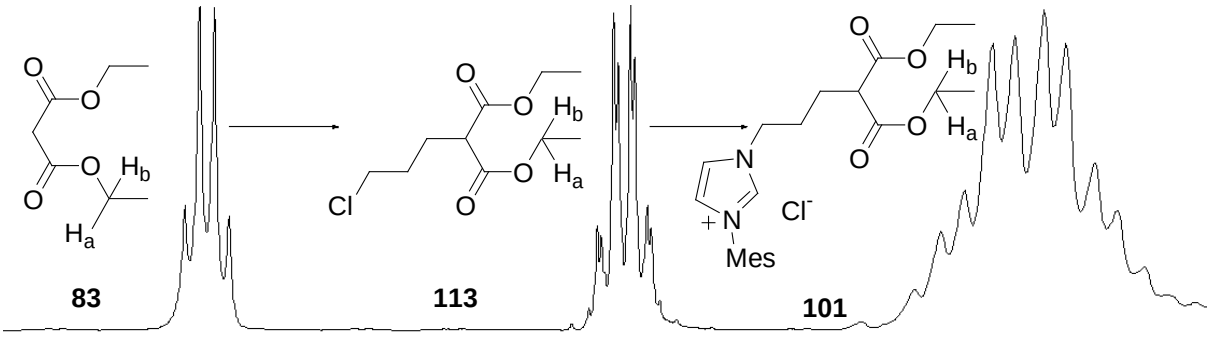

Figure 4.16 400 MHz ^{1}H NMR data showing the oxymethylene signals (H_a and H_b) for the malonate moiety in diethyl malonate **83**, chloroalkyl malonate **113** and imidazolium salt **101**.

Except for the malonyl derivative **101**, the imidazolium salts were generally obtained in average to good yield (up to 80%). The ^{1}H NMR spectroscopic analysis of compound **108** also presented interesting coupling effects. Figure 4.17 shows the region of the ^{1}H NMR

spectrum containing the allylic methylene and methine signals, resonating as three distinct multiplets. The terminal vinylic protons H_E and H_Z resonate as two distinct doublets of doublets (dd). This is as a result of the protons coupling with each other as well as with the vinylic methine proton H_A. The upfield signal at 5.50 ppm corresponds to H_Z and the lower–field signal at 5.56 ppm to H_E, which is *trans* to H_A and thus exhibits a larger vicinal coupling constant than the *cis*–proton H_Z. The methine proton signal H_A (δ_H 6.16 ppm) affords a more complicated splitting pattern, coupling to each of the vinylic protons H_E and H_Z and to the *N*–methylene protons to afford a doublet of double triplets (ddt).

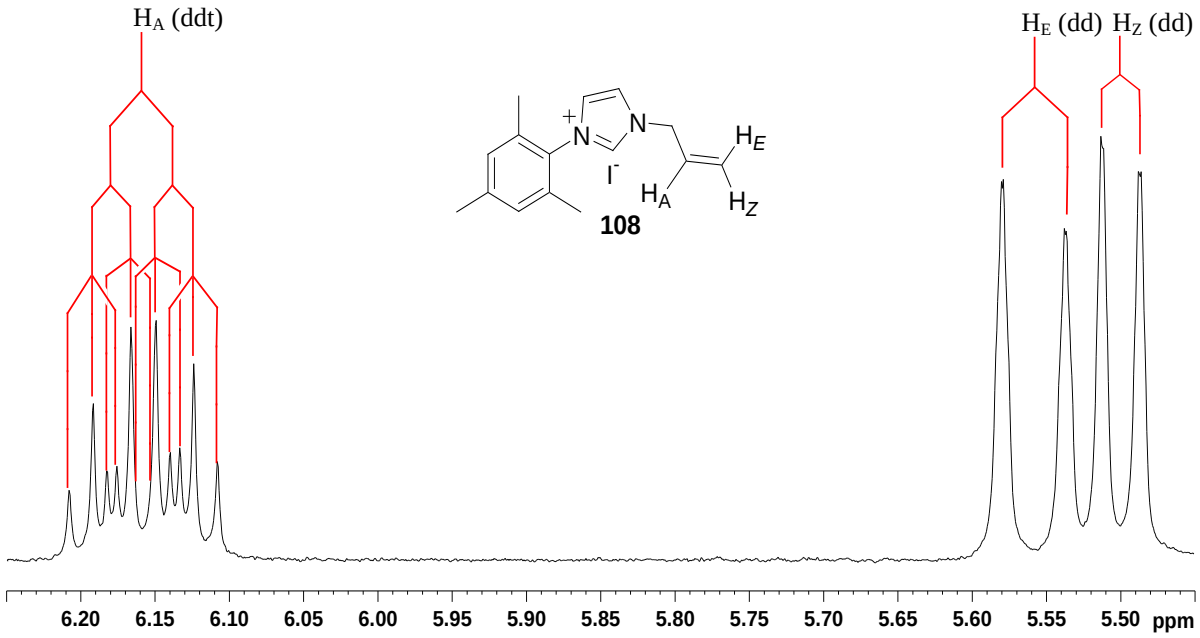

Figure 4.17 Partial 400 MHz ^{1}H NMR spectrum of compound **108** in $CDCl_3$.

The COSY relationships between the three nuclei are shown in Figure 4.17, with the methine proton H_A coupling with the vinylic protons H_Z and H_E as well as to the neighbouring methylene protons.

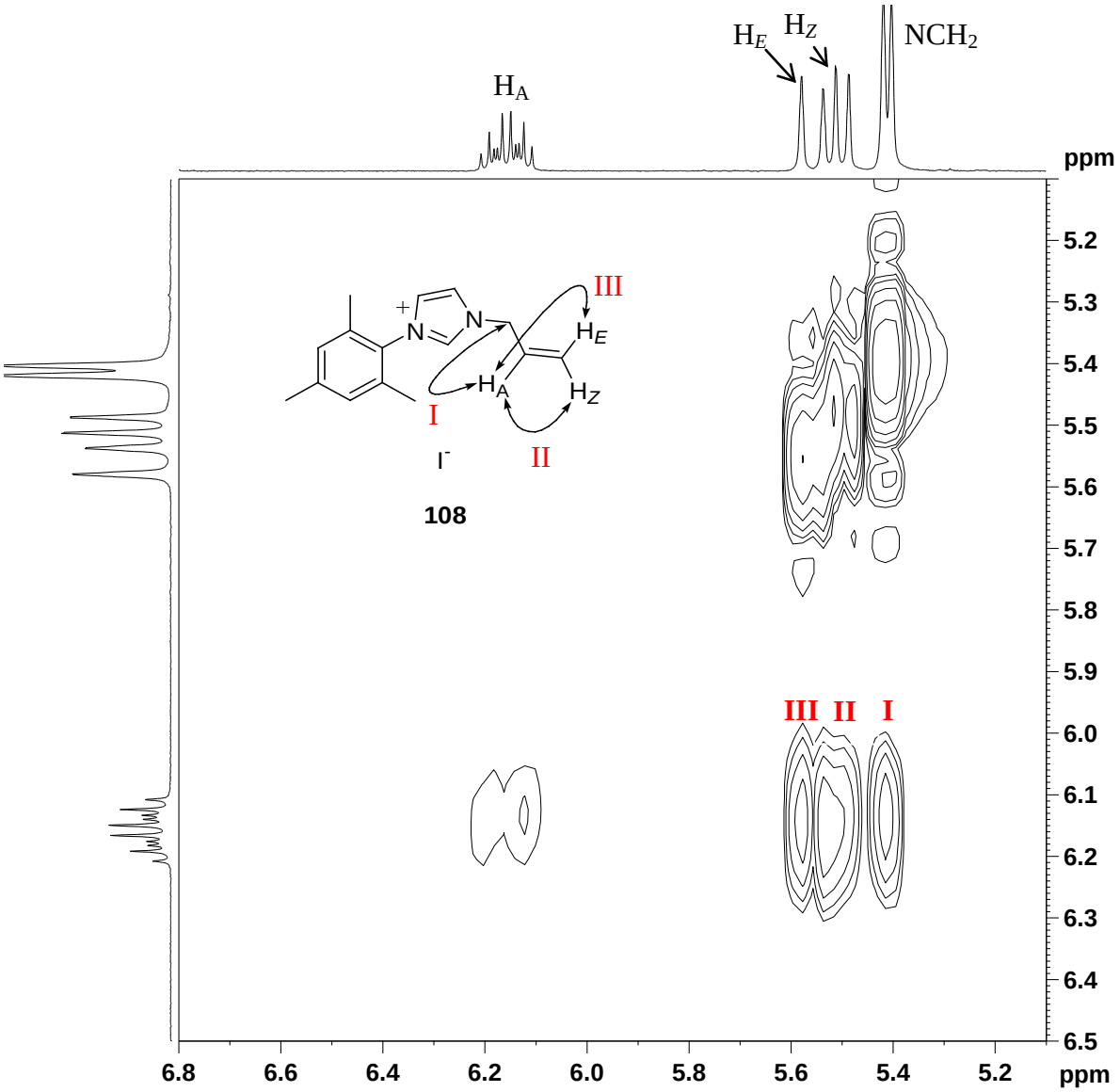

Figure 4.18 Partial 400 MHz COSY spectrum of imidazolium salt **108** in $CDCl_3$.

4.3. Coordination studies

In the course of this research, a number of well–defined pro–ligands were prepared, bearing both imidazolinium and imidazolium moieties, which could possibly coordinate to a metal centre such as ruthenium. In order to explore the coordination potential of selected ligands, two approaches to the formation of ruthenium complexes were explored, *viz*., the use of stable silver–carbene complexes as intermediates, which can undergo transmetallation upon reaction with the Hoveyda–Grubbs catalyst **35**, and reaction of an NHC carbene with the Grubbs I catalyst **25**.

The use of silver as a transmetallation agent in coordination reactions involving NHCs is becoming increasingly popular since the deprotonation of the imidazolium species by silver oxide is very selective and occurs under mild conditions, forming silver–carbenes that are stable to air and moisture. This technique eliminates unwanted deprotonation to N–functionalised NHCs and enables one to work with stable carbenes in subsequent coordination reactions.[131]

The relative σ– and π–bonding interactions of various NHC–metal complexes have been studied[72, 132–136] using charge decomposition analysis (CDA). The degree of NHC→metal σ–donation (*d*) and the NHC←metal π–back–donation (*b*) have been determined[67, 137, 138] and a high *d/b* ratio represents an effective σ–donor ligand, while a lower *d/b* ratio indicates a greater back–bonding relationship between the metal and the ligand. A high degree of π–back bonding was evident in Pd–NHC complexes, with *d/b* values between 2.59 and 3.99,[72, 134] while Au–NHC complexes exhibited values between 5.23 and 5.88.[132, 133] The powerful σ–bonds of Ag–NHCs exhibited *d/b* ratios between 7.80 and 12.68,[132, 135, 136] providing evidence as to why NHC–silver complexes exhibit such great stability.[67] Imidazolinium salt **76** was reacted with Ag_2O over 4 Å molecular sieves at room temperature[131] and excess silver was removed *via* filtration to afford the air–stable silver complex **115** (Scheme 4.17). The successful formation of complex **115** was established by the presence of a weak, low–field ^{13}C carbene signal at 164.0 ppm and by the absence of a corresponding low–field methine ^{1}H NMR signal (Figure 4.19). Without X–ray crystal analysis of the silver complex, we can only speculate as to the formal state of the metal since silver alkoxycarbenes have been known to form dimeric compounds and even cubane clusters in these reactions.[94, 139, 140] Under normal

circumstances, however, the alkoxide is expected to be bound to the metal, hence the silver will be in the silver (I) state as shown in Scheme 4.17.

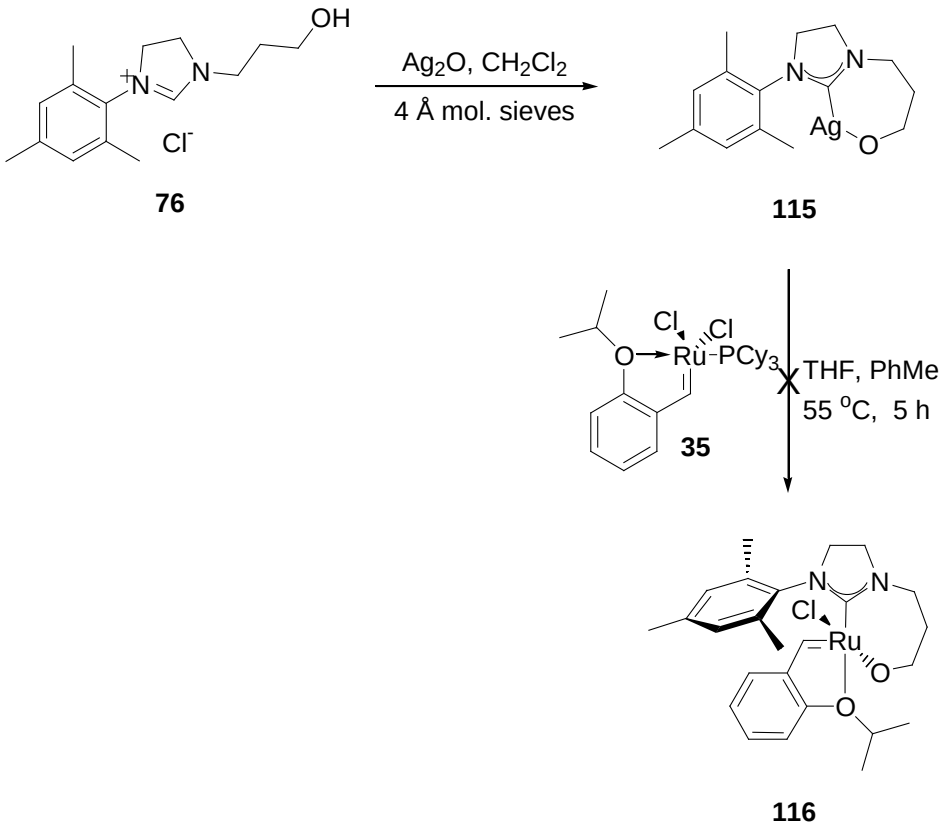

76 **115** **35** **116**

Scheme 4.17 Attachment of the bidentate NHC ligand **76** to the Hoveyda–Grubbs complex **35** *via* transmetallation with silver.

NHC–silver complex **115** and Hoveyda–Grubbs complex **35** were then reacted together at elevated temperature in THF–toluene,[94] and the suspension was filtered to remove AgCl. Chromatography on oven–dried silica gel under an atmosphere of Ar in dichloromethane unfortunately afforded only the Hoveyda–Grubbs starting material **35** almost quantitatively**.**

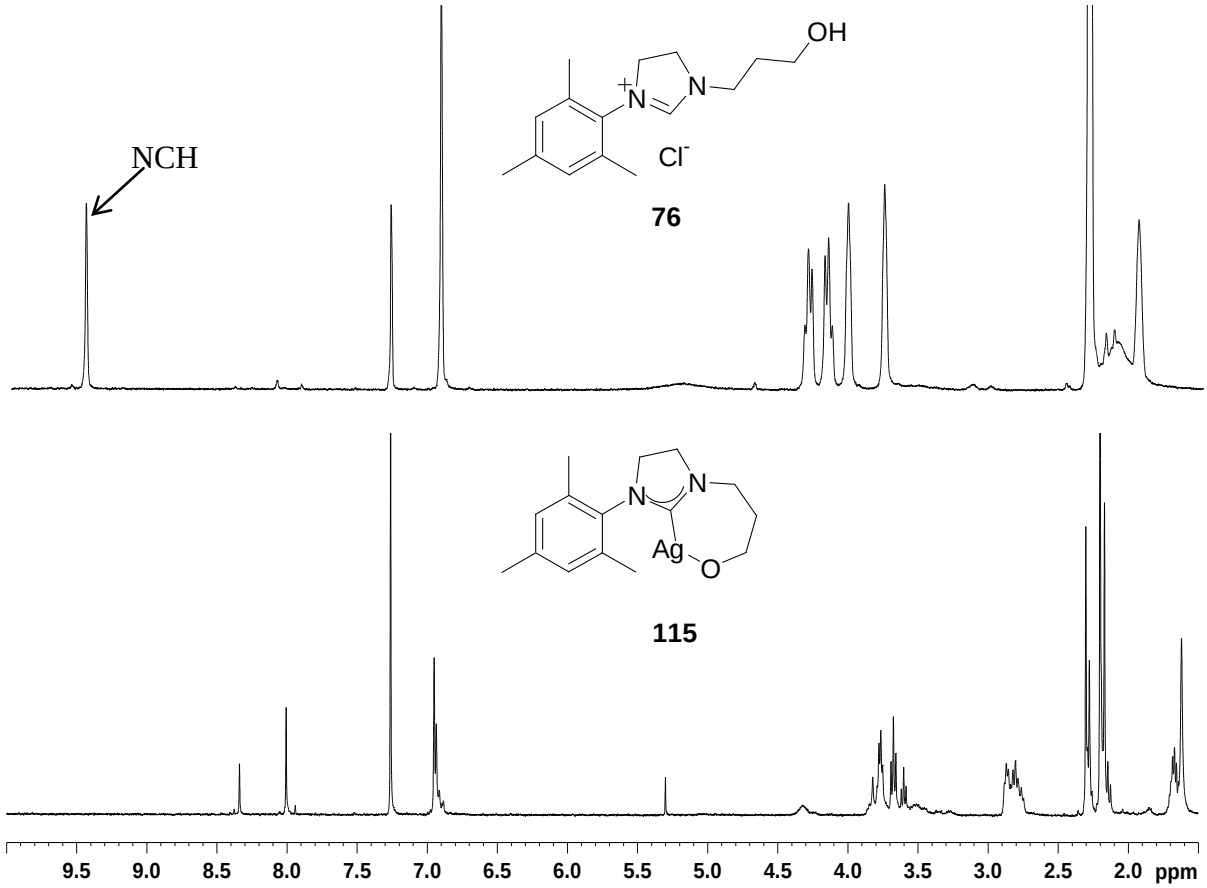

Figure 4.19 Partial 400 MHz ^{1}H NMR spectra of the pro–ligand **76** and the silver complex **115** in $CDCl_3$.

The structure of the putative complex **116** was geometry–optimized at the DFT level (Figure 4.20) since the simplest way to explore the steric and torsional effects in such a complex is to perform a geometry–optimization and analyse the bond–lengths and bond–angles (tabulated in Chapter 7). Of particular importance are the bond–lengths between the ruthenium atom and the NHC carbon, and between the ruthenium and the labile group (O*i*Pr). The NHC–Ru bond–length was found to be 2.02 Å, while that of Ru–O*i*Pr was 2.38 Å as opposed to 2.37 Å for the Ru–P bond of complex **35,** indicating a less labile leaving group than that of the commercial catalyst. The NHC–Ru–O^{i}Pr angle was 176.55º, consistent with the desired *trans* arrangement.

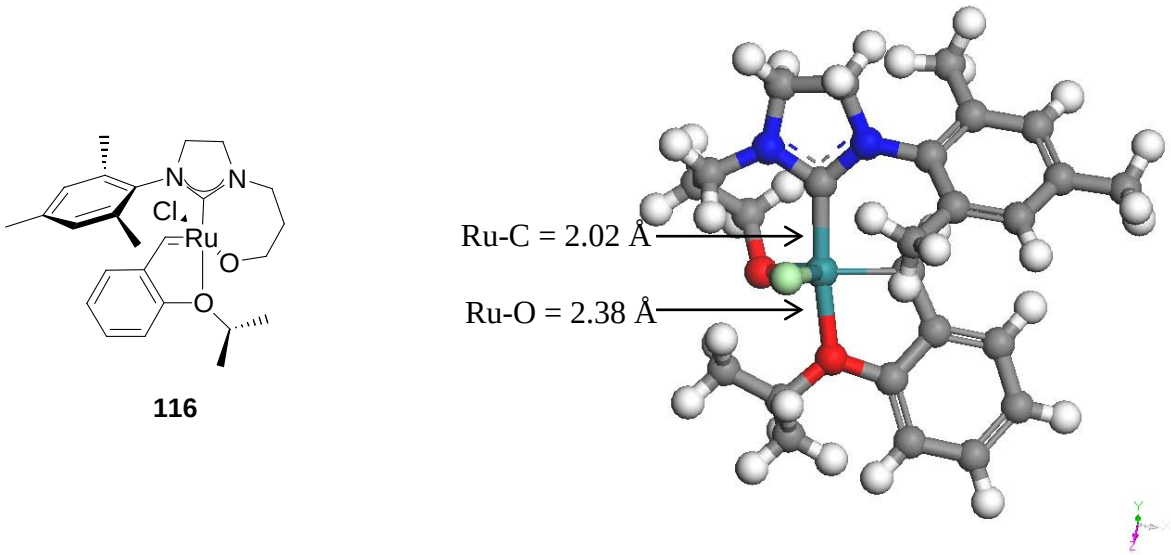

116

Figure 4.20 DFT Geometry–optimized model of the putative complex **116**.

In order to form Grubbs II–type complexes, NHC carbenes were obtained *in situ* by reacting the imidazolinium or imidazolium salt with a strong base, such as potassium hexamethyldisilazide (KHMDS) or butyllithium to remove the acidic proton and thus afford the imidazolin–2–ylidene or imidazol–2–ylidene respectively (Scheme 4.18).

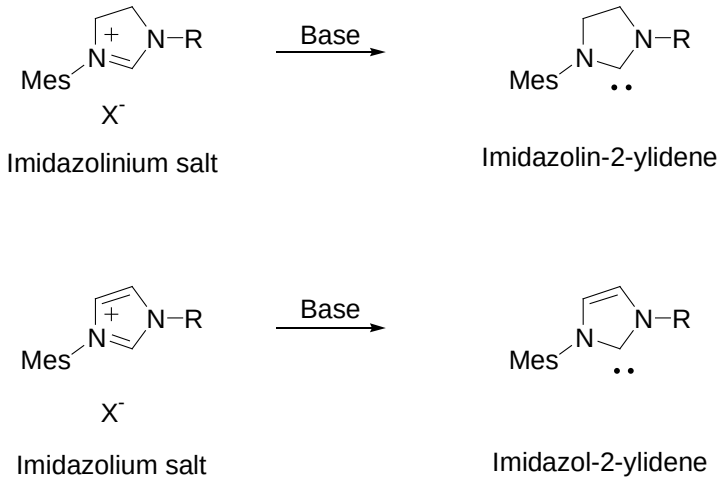

Scheme 4.18 Formation of imidazolin–2–ylidenes and imidazol–2–ylidenes.

The resulting nucleophilic carbenes were then reacted with the Grubbs I catalyst **25** to displace a phosphine moiety as illustrated for the imidazolium system **109** in Scheme 4.19.

KHMDS was used to generate the divalent carbene 1–benzyl–3–mesitylimidazol–2–ylidene **117**, which coordinated with complex **25** by displacing PCy_3. Upon completion, the residual catalyst **25** and free phosphine were removed by ultrasonic agitation in pentane,[141] causing the unwanted species to dissolve and the desired product to precipitate as a pink solid. The novel ruthenium complex **118** was sufficiently stable to permit full characterization by both 1–D and 2–D NMR, HRMS and IR analysis.

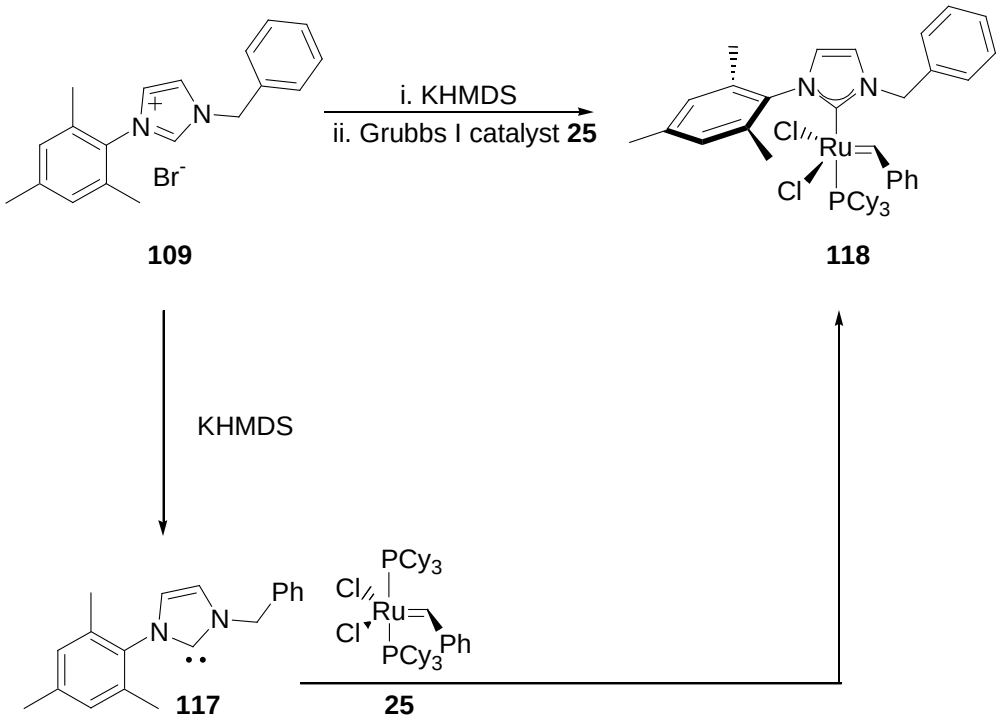

Scheme 4.19 Coordination of benzyl mesitylimidazolylidene **117** with the first–generation Grubbs catalyst **25**.

Figure 4.21 shows the ^1H NMR spectrum for complex **118.** The region between 1.0 and 3.0 ppm contains the cyclohexyl (PCy_3) and the *o*– and *p*–methyl signals, while the region between 6 and 8 ppm contains the benzylidene, benzyl and mesityl signals, with the imidazolylidene methines and the benzylic methylene protons resonating upfield of the aromatic protons. Of particular diagnostic importance is the carbene methine signal at very low–field (δ_H 19.44 ppm) resonating as a singlet, in contrast to the signal for the carbene proton of the Grubbs I catalyst **25**, which typically resonates as a doublet since it couples with the two phosphorus nuclei which are bound to the ruthenium. Owing to the strongly

electron–donating NHC, the electron density is increased at the metal centre and the carbene proton in complex **118** resonates at a slightly higher field (δ_H 19.44 ppm) than the corresponding methine in catalyst **25.** The carbon signals representing the two carbons bound to ruthenium are very weak and are not easily detected in the ^{13}C NMR spectrum, even at 600 MHz. Resonance data for the two nuclei were obtained by means of their 2–D interactions (Figure 4.22) with neighbouring nuclei. Hence, HSQC peaks (red) at 19.44 ppm and *ca.* 294 ppm reflect the C–H interaction of the Ru=CH moiety, while the two blue peaks at *ca.* 188 ppm, intersected by proton signals at 7.02 and 7.12 ppm represent HMBC correlations between the two imidazolylidene methine protons and the NHC carbon attached to the ruthenium, giving a good indication of the ^{13}C chemical shift for the NHC carbon nucleus.

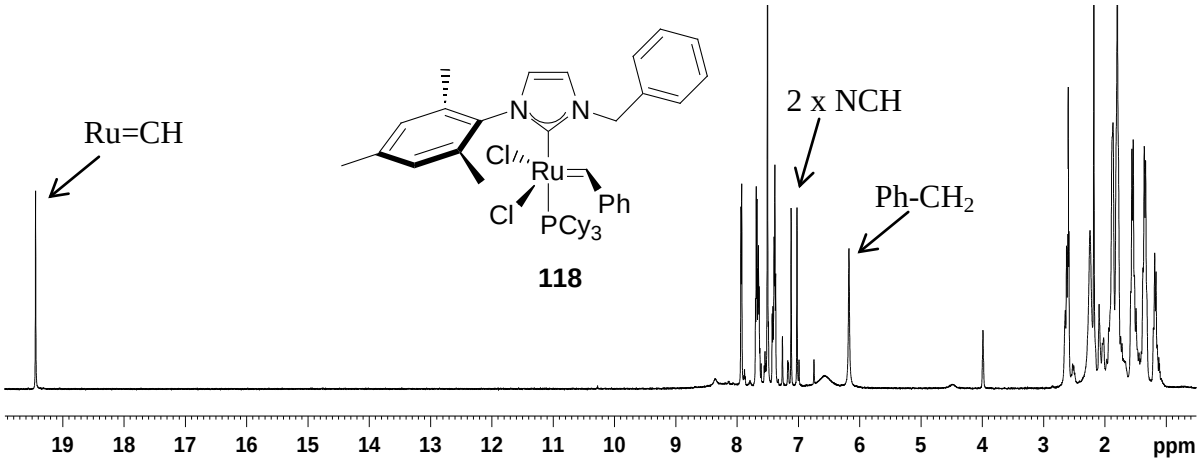

Figure 4.21 600 MHz ^1H NMR spectrum of the ruthenium complex **118** in $CDCl_3$.

The structure of complex **118** was geometry–optimized at the DFT level (Figure 4.23) and the bond–lengths and angles were compared to those of the commercial Grubbs catalysts, **25** and **29.** The NHC–Ru bond–length is longer in complex **118** than in the Grubbs II catalyst **29**, while the Ru–P bond in complex **118** was found to be shorter than the corresponding bond in either the Grubbs I or Grubbs II catalysts. The shorter bond to the leaving group could explain the stability that the novel complex **118** exhibits, since phosphine dissociation is implicated in the decomposition of these catalysts.[142]

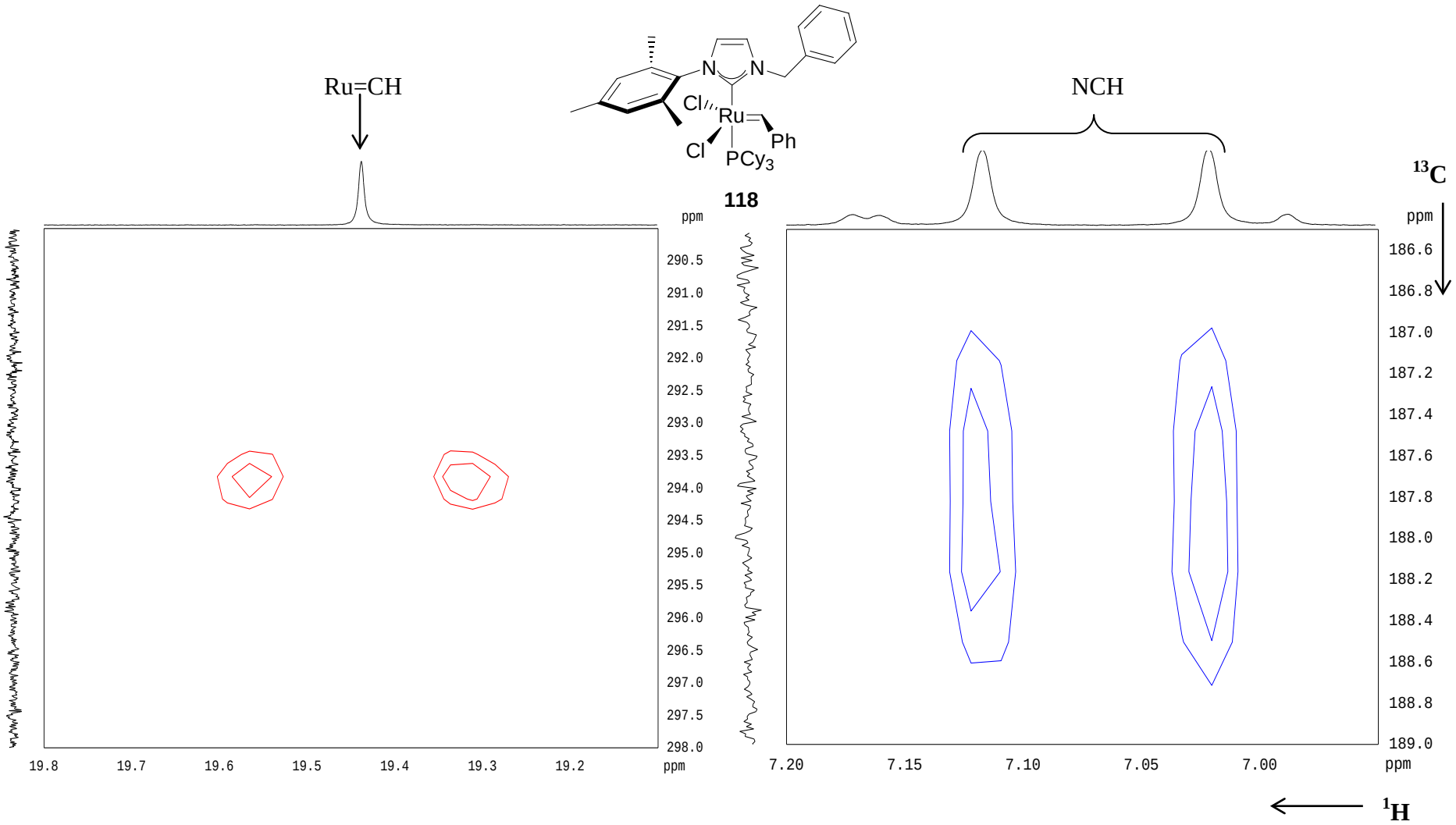

Figure 4.22 Partial HSQC (red peaks, left) and HMBC (blue peaks, right) spectra of the ruthenium complex **118** in $CDCl_3$.

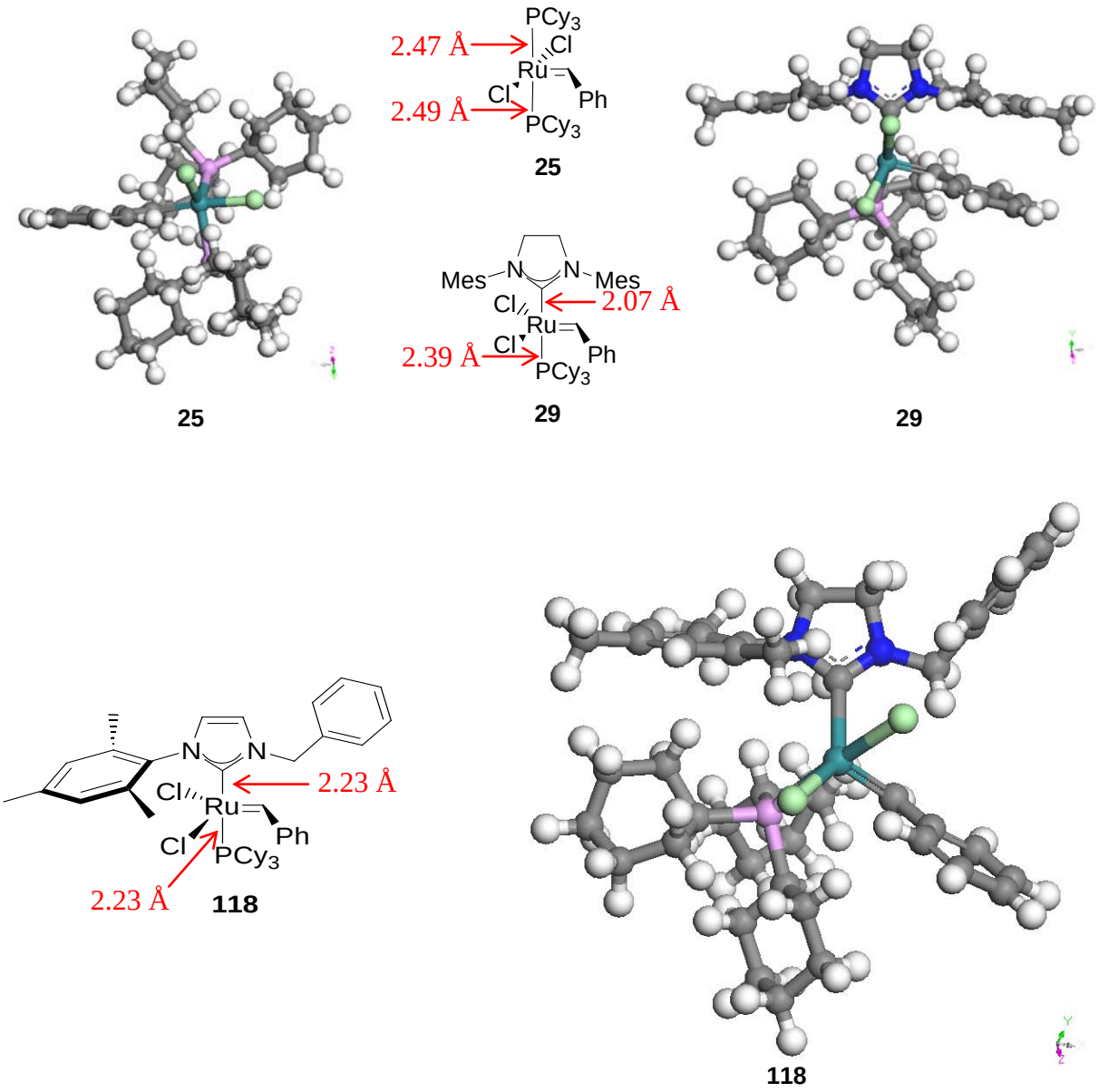

Figure 4.23 DFT geometry–optimized model of complex **118** compared to the Grubbs I and Grubbs II complexes **25** and **29** respectively.

One of the major problems associated with the preparation of metathesis catalysts is their tendency to decompose readily, and often, when a coordination reaction of this kind has not been successful it is because the catalyst has decomposed. Scheme 4.20 shows the general decomposition pathway for a simple metathesis catalyst, as proposed by Hong *et al.*[142] As is the case in the initiation of a metathesis reaction, the first step in decomposition involves the dissociation of a phosphine group. Under normal metathesis conditions, an olefinic substrate will coordinate the metal at the vacant site; however, in catalyst decomposition, the alkylidine

moiety undergoes nucleophilic attack by the free phosphine to afford an alkylphosphonium salt and an inactive catalyst.[142]

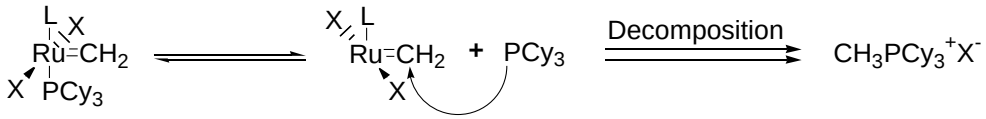

Scheme 4.20 Typical decomposition of Grubbs–type metathesis catalysts *via* phosphine activation.[142]

Following the successful formation of **118**, complexes **119**, **120** and **121** were prepared (Figure 4.24), using the same procedure. In each case, the pro–ligand was treated with a strong base (KHMDS or BuLi) and then reacted with the Grubbs I complex **25**. The reaction products emerged as dark solids and preliminary ^{1}H NMR analysis indicated the formation of Grubbs II–type complexes in each case, and although time did not permit the isolation and purification of analytical samples in each case, there are clear indications that complexes **119** – **121** were produced.

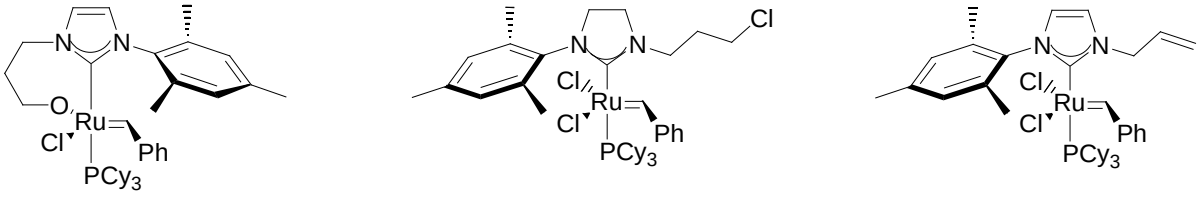

119 **120** **121**

Figure 4.24 Complexation products **119**, **120** and **121**.

Based on the proposal by Hong *et al.*,[142] a decomposed catalyst would have lost the alkylidene moiety due to phosphine activation and the high–field carbene signal would be absent from that compound's ^{1}H NMR spectrum. ^{1}H NMR data were acquired for the products obtained from the coordination reactions of complexes **119 – 121**. The ^{1}H NMR spectrum of **119** (Figure 4.25) clearly shows the presence of a singlet carbene signal slightly further downfield (δ_H 19.96 ppm) than would be expected for the starting material **25**,

indicating the presence of a 'Grubbs second–generation' type benzylidene. The spectra for complexes **120** and **121** contain a similar carbene signal in the same region. Thus, it seems that the catalysts did not decompose during coordination and that a phosphine group was lost in each case. Moreover, there is no indication of the low–field NHC methine signal characteristic of the imidazolium starting material. Therefore, it is not unreasonable to assume that the reactions of the carbenes derived from the pro–ligands **76, 81** and **108** with ruthenium (to form complexes **119**, **120** and **121**), respectively, were successful and that isolation of the well–defined coordination products simply requires further investigation.

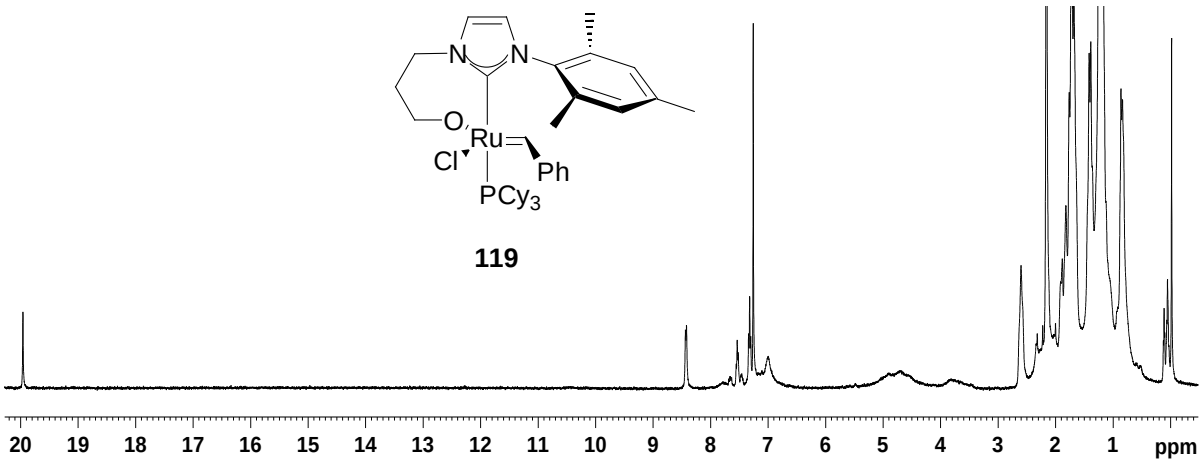

Figure 4.25 400 MHz ^{1}H NMR spectrum of the putative ruthenium complex **119** in $CDCl_3$.

The structures of complexes **119** and **120** were geometry–optimized at the DFT level and compared to the Grubbs I and Grubbs II complexes (Figure 4.26). The NHC–Ru bond for complex **119** was found to be 2.04 Å, *i.e.* shorter than the NHC–Ru bond of the commercial catalyst **29**. The Ru–P bond was 2.54 Å long, indicating a more labile leaving group than that on the Grubbs II catalyst **29**. This could indicate a stable complex with a more labile phosphine than the commercial catalysts **25** and **29**. However, the NHC–Ru–P bond was found to be 111°, deviating significantly from the desired *trans* arrangement of 180°.

Complex **120** was found to have a slightly longer NHC–Ru bond than the Grubbs II complex **29** as well as a longer Ru–P bond, indicating a more labile leaving group. The Ru–P bond was, however, shorter than the corresponding bonds in the Grubbs I analogue **25**. The NHC–Ru–P bond was 105.4°, again deviating from the preferred *trans* arrangement. The geometries described above appear to be somewhat anomalous and require further attention.

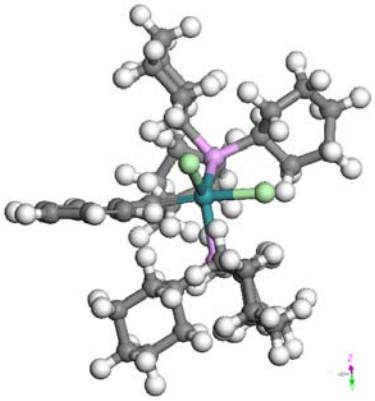

25

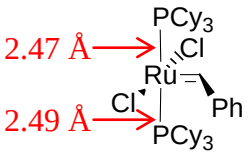

25

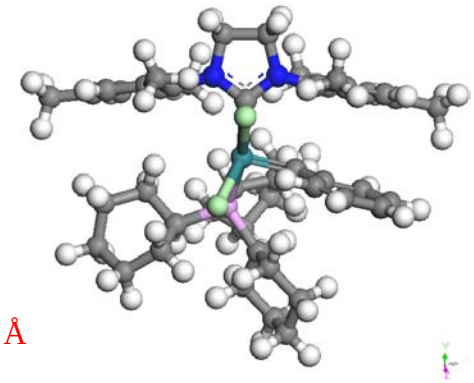

29

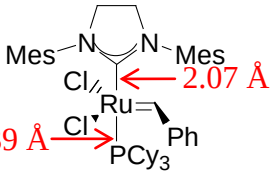

29

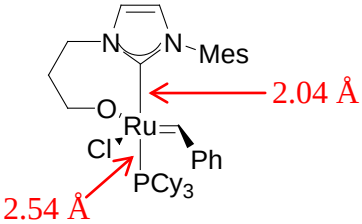

119

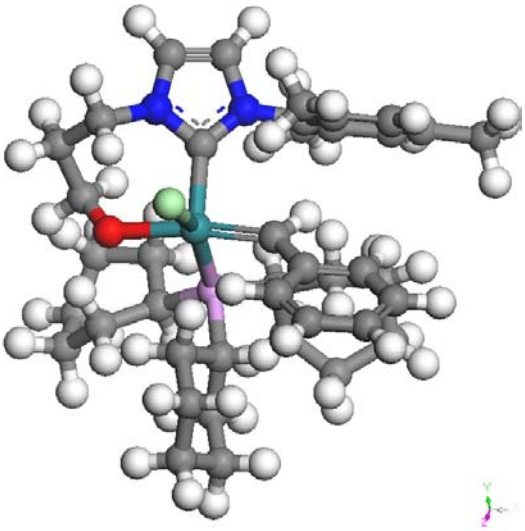

119

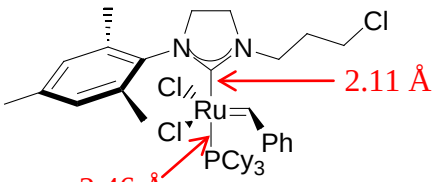

120

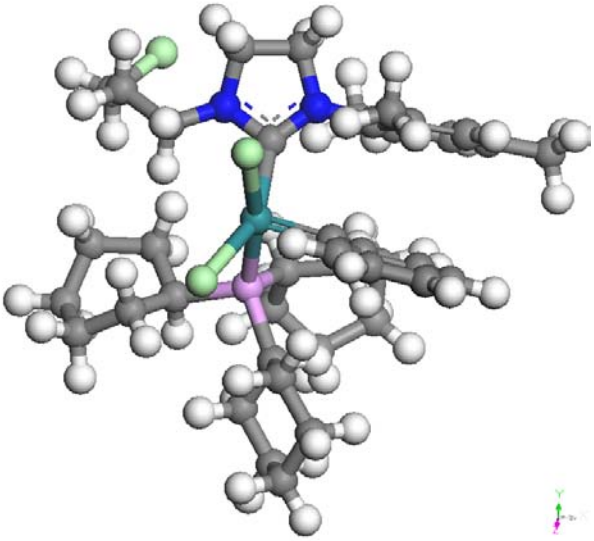

120

Figure 4.26 DFT geometry–optimized structures of complexes **119** and **120** compared with that of the Grubbs I and Grubbs II complexes, **25** and **29**.

5. Conclusions

Metathesis reactions are amongst the most important transformations in modern synthetic chemistry. Ruthenium–based metathesis catalysts can be tailored for specific reactions and, in the present study, we have explored various approaches to the preparation of novel, multidentate analogues of the established Grubbs and Hoveyda–Grubbs type catalysts.

Particular attention has been given to the development of imidazolinium and imidazolium salts as stable multidentate precursors to saturated and unsaturated NHC ligands, respectively, both of which are commonly used in the preparation of Ru–metathesis catalysts. The bidentate pro–ligand **76** was prepared by the cyclization of dihydrochloride salt **79**. Access to this precursor **79** was achieved *via* the sequential amidation of chlorooxoacetate **74** by the aryl amine **73** and aminopropanol **78**, followed by the reduction of the resulting oxamide **75**. The stable imidazolinium salt **76** provided a platform for further structural elaboration and, hence, subsequent halogenation using $SOCl_2$ and PBr_3 afforded the chloro and bromo derivatives **81** and **82** respectively. However, attempts to link the halogen derivatives **81** and **82** to a malonyl moiety to yield a tridentate ligand **85** proved unsuccessful. An alternative route towards the synthesis of imidazolinium **85** was therefore followed and this involved addition of diethyl malonate **83** to the bromide **87** *prior* to amide reduction of the resultant compound **88**. Unfortunately, due to complications in the reduction step, the desired diamine **89** could not be isolated. Further unsuccessful attempts to access compound **85** involved the preparation of the diamino alkylbromide **91** *via* two different strategies, *viz.*, bromination of the hydroxydiamine **80** and reduction of the bromoalkyl oxamide **87**.

Following the difficulties encountered in the preparation of the tridentate imidazolinium systems, the use of unsaturated imidazolium analogues was investigated. The bidentate hydroxyalkyl imidazolium **100** was successfully prepared by alkylating *N*–mesitylimidazole **102** with chloropropanol **106** using microwave irradiation. The use of this microwave–assisted approach for the alkylation of *N*–mesitylimidazole has greatly reduced reaction times (from 8 hours – 7 days to *ca.* 0.5 – 2 hours) for the series of eight imidazolium salts investigated. The novel, tridentate malonyl derivative **101** and the decylimidazolium salt **111** were both obtained using this improved methodology, the former, unfortunately in consistently low yields.

With a series of eleven pro–ligands in hand, coordination of the corresponding imidazolinylidene and imidazolylidene carbenes to ruthenium was explored in order to generate the desired second–generation Grubbs and Hoveyda–Grubbs type complexes. While coordination of the ligand **76** to silver afforded the novel alkoxy–NHC complex **115,** the intended transmetallation with ruthenium was unsuccessful. Three ruthenium complexes **119 – 121** were obtained (as indicated by ^{1}H NMR analysis) from the addition of the Grubbs I complex **25** to the respective carbenes. Finally, the benzyl mesitylimidazolium salt **109** has been used to prepare the well–defined Grubbs II–type novel complex **118**, which was fully characterized and showed very good stability in air.

DFT–level computational studies using the Accelrys DMol^{3} package of a selection of complexes (both proposed and isolated) has provided valuable insights into their likely geometries. The modelled structure of complex **118**, for example, indicated a slightly shorter Ru–P bond and an elongated NHC–Ru bond, as compared to those of the commercial catalysts **25** and **29** – factors which may affect catalytic activity.

Future avenues for this research could include:– i) structural elaboration of the imidazolium salts to develop multidentate ligands using our improved microwave–assisted technique; ii) optimization of the synthesis of malonyl derivative **101** to enable coordination studies; iii) further attempts to attach multidentate ligands to the Hoveyda–Grubbs complex **36** *via* transmetallation; and finally, iv) coordination of these ligands to the Grubbs I catalyst **25** using the *in situ* carbene generation approach.

EXPERIMENTAL

6. SYNTHESIS

6.1. General

All reagents were supplied by Aldrich and used without further purification unless stated otherwise. Dry solvents were prepared using methods described by Perrin and Armarego.[143] Thus, THF and toluene were distilled from Na/benzophenone ketyl and collected over molecular sieves (4 Å) N_2; CH_2Cl_2 and pentane were refluxed with CaH_2 and distilled over molecular sieves (4 Å) under N_2. All dry solvents were stored over molecular sieves under N_2 or Ar and handled under the same conditions; N_2 and Ar gas was supplied by Afrox and passed through Drierite® prior to use.

Normal phase thin layer chromatography (TLC) was performed on Merck silica gel 60 PF254 plates, while reverse phase TLC was performed on Fluka Analytical RP–18 silica gel glass plates. Normal phase flash chromatography was performed using Merck silica gel 60 (particle size 0.040 – 0.063 mm) and preparative TLC on glass plates, prepared with Merck silica gel PF254 containing $CaSO_4$. Reverse–phase flash chromatography was carried out using Waters C_{18} Sep–Pak cartridges [Vac 35cc (10g)]. Visualization on silica was achieved using either iodine vapor or UV light at 254 nm. Dianion® HP–20 (particle size 200–600 mm, Mitsubishi Chemical Co., Tokyo, Japan) supplied by Supelco, was used as adsorbent for HP–20 chromatography and was recycled by washing with acetone and MeOH. Normal phase HPLC was conducted on a Whatman Partisil 10 Magnum 6 column using a Spectra–Physics P100 isocratic pump and a Waters R1410 differential refractometer detector.

NMR data was obtained using Bruker 400 MHz Avance and 600 MHz Avance II spectrometers at 303 K in the specified deuterated solvent. NMR spectra were generated and optimized using XWIN–NMR v3.5 and Bruker Topspin v2.1. All chemical shifts are given in ppm and coupling constants in Hz and spectra were calibrated on residual protonated solvent signals ($CDCl_3$: ^1H – 7.26 ppm; ^{13}C – 77.00 ppm; DMSO–d_6: ^1H – 2.50 ppm; ^{13}C – 39.51 ppm; D_2O: ^1H – 4.80 ppm; MeOH–d_4: ^1H – 3.35 ppm; ^{13}C – 49.15 ppm). Low–resolution mass spectrometry was performed using a Finnigan MAT GCQ mass spectrometer in the electron ionization EI mode

at 70 eV. High–resolution mass spectrometry was performed on a Waters API Q–TOF Ultima instrument using electro–spray ionization in the positive ion mode (ESI+) by the University of Stellenbosch Central Analytical Facility. Melting points were determined using a hot–stage microscope and are uncorrected. Infrared spectral data was obtained on a Perkin–Elmer Spectrum 100 FT–IR and manipulated using Perkin–Elmer Spectrum v6.35 and Essential FTIR v1.50.252 software.

6.2. Preparation of imidazolinium pro–ligands

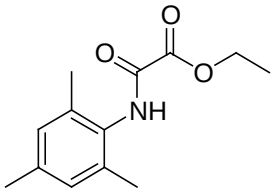

Ethyl 2–(mesitylamino)oxoacetate **77**[104]

A solution of 2,4,6–trimethylaniline **73** (1.0 mL, 7.0 mmol) and triethylamine (2.0 mL, 14 mmol) in dry THF under N_2 was cooled to 0 °C. Ethyl chlorooxoacetate **74** (0.8 mL, 7 mmol) was added and the mixture was stirred at room temperature for 3 h, then filtered and the solid washed with EtOAc. The filtrate and washings were combined and concentrated *in vacuo* to give a solid which was recrystallized from EtOAc–Hexane (1:5) to afford ethyl 2–(mesitylamino)oxoacetate **77** (3.28g, 50%) as a tan solid, mp 84–86 °C (from EtOAc–Hexane) (lit.,[144] 76–78 °C); ν_{max}/cm^{-1} 1724 and 1674 (C=O) ; δ_H (400 MHz; $CDCl_3$) 1.45 (3H, t, *J* 7.1, CH_2CH_3), 2.17 (6H, s, 2 x *o*–CH_3), 2.28 (3H, s, *p*–CH_3), 4.42 (2H, q, *J* 7.1, CH_2), 6.92 (2H, s, 2 x ArH) and 8.34 (1H, br s, NH); δ_C (100 MHz; $CDCl_3$) 14.0 (q, CH_2CH_3), 18.4 (q, *o*–CH_3), 20.9 (q, *p*–CH_3), 63.5 (t, CH_2), 129.0 (d, 2 x ArCH), 129.4, 134.7 and 137.7 (3 x s, 4 x ArC), 154.7 and 160.9 (2 x s, 2 x C=O); *m/z* 236 ([M+H], 43%) and 102 (100%).

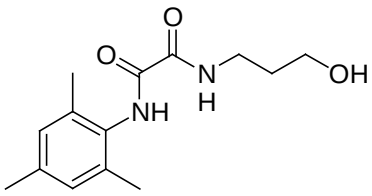

N–*(3–Hydroxypropyl)*–N'–*(mesityl)oxamide* **75**[102]

A solution of ethyl 2–(mesitylamino)oxoacetate **77** (7.60 g, 32.3 mmol) in 3–aminopropanol **78** (12.3 mL, 161 mmol) was stirred at 110 °C for 8 h under N_2 in a Schlenk flask. Upon cooling, a solid formed which was filtered off, dissolved in EtOAc and washed with brine (3x

20 mL) to remove excess 3–aminopropanol **78**, dried over anhydrous $MgSO_4$ and concentrated *in vacuo* to yield N–*(3–hydroxypropyl)*–N'*–mesityloxamide* **75** (7.25 g, 85%) as a white solid, mp 146–148 °C (from EtOAc); *m/z* 264.1486 (M^+. $C_{14}H_{20}N_2O_3$ requires 264.1474); ν_{max}/cm^{-1} 1659 (CONH) and 1502; δ_H (400 MHz; $CDCl_3$) 1.80 (2H, quintet, *J* 6.0, $CH_2CH_2CH_2$), 2.17 (6H, s, 2 x *o*–CH_3), 2.28 (3H, s, *p*–CH_3), 2.60 (1H, br s, OH), 3.52 (2H, q, *J* 6.6, NCH_2), 3.69 (2H, t, *J* 5.6, CH_2OH), 6.90 (2H, s, 2 x ArH), 7.93 (1H, br s, NH) and 8.75 (1H, br s, NH); δ_C (100 MHz; $CDCl_3$) 18.2 (q, 2 x *o*–CH_3) , 20.9 (q, *p*–CH_3) , 31.6 (t, $CH_2CH_2CH_2$), 36.7 (t, NCH_2), 59.5 (t, CH_2OH), 129.0 (d, 2 x ArCH), 129.6, 134.7 and 137.6 (3 x s, 4 x ArC), 158.0 and 160.5 (2 x s, 2 x C=O); *m/z* 265 (MH^+, 48%) and 161 (100%).

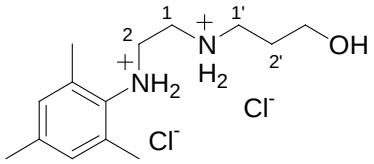

N–*(3–Hydroxypropyl)*–N'*–mesitylethylenediamine dihydrochloride* **79**

Method 1.

A solution of *N*–(3–hydroxypropyl)–*N*'–(mesityl)oxamide **75** (3.38 g, 12.8 mmol) in dry THF was added dropwise to a stirred suspension of $LiAlH_4$ (1.31 g, 34.5 mmol) in dry THF at 0 °C under N_2. The mixture was gently refluxed for 8 h, after which it was cooled to room temperature before the reaction was quenched *via* the dropwise addition of methanol (until all effervescence had ceased) followed by a solution of NaOH (1.0 g) and $MgSO_4$ (1.0 g) in H_2O (20 mL). The mixture was filtered and the residual solid was washed with THF. The filtrate and washings were combined and concentrated *in vacuo* to give a yellow oil, NMR analysis of which confirmed formation of the desired product as the free amine. The oil was dissolved in MeOH (5 mL) and conc. HCl was added (2 eq). The solution was agitated and then concentrated *in vacuo* by azeotropic distillation with MeOH to give N–*(3–hydroxypropyl)*–N'*–mesitylethylenediamine dihydrochloride* **79** (2.38 g, 61%) as a hygroscopic yellow solid, *m/z* 236.1890 (M^+ – 2 HCl. $C_{14}H_{24}N_2O$ requires 236.1900); ν_{max}/cm^{-1} 1659 and 1502; δ_H (400 MHz; $CDCl_3$) 1.74 (2H, quintet, *J* 5.5, 2'–H_2), 2.22 (3H,

s, *p*–CH_3), 2.26 (6H, s, 2 x *o*–CH_3), 2.65 (1H, br s, OH), 2.82 (2H, t, *J* 5.7, 1–H_2), 2.90 (2H, t, *J* 5.8, 1'–H_2), 3.03 (2H, t, *J* 5.7, 2–H_2), 3.81 (2H, t, *J* 5.8, CH_2OH) and 6.82 (2H, s, 2 x ArH); δ_C (100 MHz; $CDCl_3$) 18.2 (q, *o*–CH_3), 20.5 (q, *p*–CH_3), 31.0 (t, C–2'), 48.1 (t, C–2), 49.6 (t, C–1'), 50.3 (t, C–1), 64.0 (t, *C*H_2OH), 129.4 (d, 2 x ArCH), 129.9, 131.6 and 143.2 (3 x s, 4 x ArC); *m/z* 236 (M^+ – 2 HCl, 18%) and 148 (100 %).

Method 2.[104]

N–(3–Hydroxypropyl)–*N*'–(mesityl)oxamide **75** (100 mg, 0.38 mmol) was placed in a dry flask under N_2. BH_3–THF (1M; 3 mL, 3 mmol) was added to the flask and the mixture was refluxed for 16 h under N_2. The reaction was cooled to room temperature before being quenched *via* the dropwise addition of MeOH, followed by conc. HCl (0.75 mL, 32%). The solvent was removed *in vacuo* by azeotropic distillation with MeOH to give a white solid. Chromatography [reverse–phase flash on C_{18} silica gel; elution with brine–MeOH (3:1)] proved unsuccessful and no pure organic products were isolated.

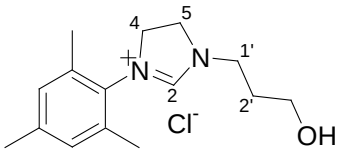

1–(3–Hydroxypropyl)–3–mesitylimidazolin–2–ium chloride **76**

A stirred solution of *N*–(3–hydroxypropyl)–*N'*–mesitylethylenediamine dihydrochloride **79** (5.82 g, 18.8 mmol) in $HC(OEt)_3$ **80** (31.30 mL, 188.9 mmol) was heated at 135 ºC for 1 h. The solution was cooled to room temperature and concentrated *in vacuo* to remove the EtOH formed during the reaction before the residue was chromatographed [HP20 polystyrene beads; gradient elution with MeOH–H_2O in 4 elutions (100:0, 50:50, 75:25, 10:90)]. The 10% MeOH eluent was concentrated *in vacuo* by azeotropic distillation with MeOH to give *1–(3–hydroxypropyl)–3–mesitylimidazolin–2–ium chloride* **76** (1.6 g, 30%) as a white–yellow solid, mp 167–169 ºC; ν_{max}/cm^{-1} 3189 (OH), 1644 (C=N), 1124 and 876; *m/z* 247.1808 (M^+. $C_{15}H_{23}N_2O$ requires 247.1810); δ_H (600 MHz; $CDCl_3$) 1.91 (2H, quintet, *J* 5.4, 2'–H_2), 2.26 (6H, s, 2 x *o*–CH_3), 2.29 (3H, s, *p*–CH_3), 3.73 (2H, t, *J* 5.2, CH_2OH), 4.05 (2H, t, *J* 5.5, 1'–

H_2), 4.15 (2H, t, *J* 10.7, 4–H_2), 4.24 (2H, t, 10.7, 5–H_2), 6.90 (2H, s, 2 x ArH) and 9.56 (1H, s, 2–H); δ_C (150 MHz; $CDCl_3$) 19.0 (q, 2 x *o*–CH_3), 21.0 (q, *p*–CH_3), 28.9 (t, C–2'), 46.2 (t, C–1'), 48.5 (t, C–5'), 50.7 (t, C–4'), 58.3 (t, *C*–OH), 129.9 (d, 2 x ArCH), 130.5, 135.3 and 140.2 (3 x s, 4 x ArC) and 159.8 (d, C–2); *m/z* 247 (M^+, 18.5%) and 245(100 %).

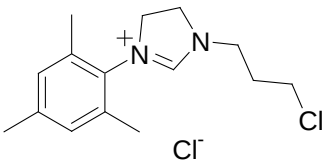

1–(3–Chloropropyl)–3–mesitylimidazolin–2–ium chloride **81**

A solution of 1–(3–hydroxypropyl)–3–mesitylimidazolin–2–ium chloride **76** (360 mg, 1.27 mmol) and $SOCl_2$ (0.19 mL, 2.6 mmol) in benzene was refluxed under a $CaCl_2$ guard–tube for 30 min. The solvent and excess $SOCl_2$ were removed *in vacuo* to yield *1–(3–chloropropyl)–3–mesitylimidazolin–2–ium chloride* **81** (445 mg, 100%) as a dark oil; ν_{max}/cm^{-1} 3370, 1643 (C=N), 1263, 1120 and 731 (C–Cl); *m/z* 265.1483 (M^+. $C_{15}H_{22}N_2Cl$ requires M^+: 265.1472); δ_H (400 MHz; $CDCl_3$) 2.29 (3H, s, *p*–CH_3), 2.31 (6H, s, 2 x *o*–CH_3), 2.30 – 2.34 (2H, m, overlapping, $CH_2CH_2CH_2$), 3.79 (2H, t, *J* 5.2 Hz, NCH_2), 4.13 – 4.24 (4H, m, overlapping NCH_2 and CH_2Cl), 4.28 – 4.38 (2H, m, NCH_2), 6.93 (2H, s, 2 x ArH) and 9.47 (1H, s, NCHN); δ_C (100 MHz; $CDCl_3$) 18.0 (q, 2 x *o*–CH_3), 21.0 (q, *p*–CH_3), 29.3 (t, $CH_2CH_2CH_2$), 42.3 (t, NCH_2), 46.6 (t, CH_2Cl), 49.1 (t, NCH_2), 51.1 (t, NCH_2), 129.9 (d, 2 x ArCH), 130.5, 135.4 and 140.1 (3 x s, 4 x ArC) and 159.2 (d, NCHN); *m/z* 265 (M^+, 4.86%) and 227 (100 %).

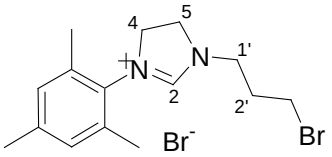

1–*(3–Bromopropyl)–3–mesitylimidazolin–2–ium bromide* **82**

PBr_3 (760 mg, 2.8 mmol) was slowly added to a solution of 1–(3–hydroxypropyl)–3–mesitylimidazolin–2–ium chloride **76** (318 mg, 1.12 mmol) in CH_2Cl_2 (5 mL) at 0 °C. The mixture was stirred at room temperature for 20 h, diluted with CH_2Cl_2 (20 mL) and then added to a satd. aq. solution of $NaHCO_3$ at 0 ºC. The organic phase was separated and washed with cold aq. $NaHCO_3$, dried over anhydrous $MgSO_4$, filtered and concentrated *in vacuo* to give *1–(3–bromopropyl)–3–mesitylimidazolin–2–ium bromide* **82** (275 mg, 63%) as a yellow oil; ν_{max}/cm^{-1} 1644 (C=N), 1488, 1271, 1144 and 760 (C–Br); δ_H (400 MHz; $CDCl_3$) 2.41 (2H, quintet, *J* 6.2, 2'–H_2), 2.28 (3H, s, *p*–CH_3), 2.33 (6H, s, *o*–CH_3), 3.62 (2H, t, *J* 6.0, 1'–H_2), 4.13 (2H, t, *J* 6.5, CH_2Br), 4.26 (2H, t, *J* 10.4, 4–H_2), 4.41 (2H, t, *J* 10.4, 5–H_2), 6.93 (2H, s, 2 x ArH) and 9.43 (1H, s, 2–CH); δ_C (100 MHz; $CDCl_3$) 18.2 (q, 2 x *o*–CH_3), 20.8 (q, *p*–CH_3), 43.5 (t, CH_2), 45.7 (t, CH_2), 46.9 (t, CH_2) 66.6 (t, 2 x CH_2), 129.6 (d, 2 x ArCH), 136.0, 138.4 and 153.4 (3 x s, 4 x ArC) and 164.0 (d, C–2); *m/z* 310.1 ($[M+H]^{2+}$, 30 %) and 291.2 (100 %).

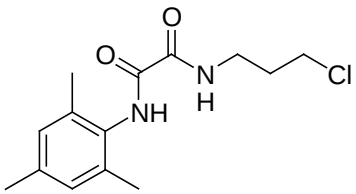

N–*(3–Chloropropyl)*–N'–*mesityloxamide* **86**

A solution of *N*–(3–hydroxypropyl)–*N*'–mesityloxamide **75** (120 mg, 0.45 mmol) and $SOCl_2$ (0.070 mL, 0.91 mmol) in benzene was refluxed for 30 min. under a $CaCl_2$ guard–tube. The solvent and excess $SOCl_2$ were removed *in vacuo* to yield N–*(3–chloropropyl)*–N'–*mesityloxamide* **86** (125 mg, 100%) as a yellow solid, mp 130 – 132 ºC (from C_6H_6); ν_{max}/cm^{-1} 3310, 3246, 2919, 1655, 1508, 1235 and 745 (C–Cl); *m/z* 283.1236 (MH^+. $C_{14}H_{20}N_2O_2Cl$ requires 283.1213); δ_H (400 MHz; $CDCl_3$) 2.10 (2H, quintet, *J* 6.5,

$CH_2CH_2CH_2$), 2.19 (6H, s, 2 x *o*–CH_3), 2.28 (3H, s, *p*–CH_3), 3.56 (2H, q, *J* 6.5, NCH_2), 3.63 (2H, t, *J* 6.5, CH_2Cl), 6.92 (2H, s, 2 x ArH), 7.80 and 8.80 (2H, 2 x br s, 2 x NH); δ_C (100 MHz; $CDCl_3$) 18.4 (q, 2 x *o*–CH_3), 20.9 (q, *p*–CH_3), 31.7 (t, $CH_2CH_2CH_2$), 37.2 (t, NCH_2), 42.0 (t, CH_2Cl), 129.0 (d, 2 x ArCH), 129.5, 134.7 and 137.6 (3 x s, 4 x ArC), 158.0 and 160.1 (2 x s, 2 x C=O).

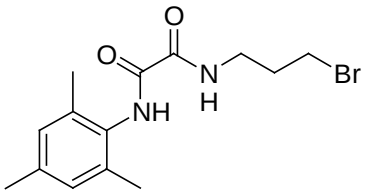

N–*(3–bromopropyl)*–N'–*mesityloxamide* **87**

To a stirred suspension of *N*–(3–hydroxypropyl)–*N*'–mesityloxamide **75** (500 mg, 1.89 mmol) in EtOAc was added PBr_3 (0.40 mL, 3.7 mmol) dropwise over 20 min. The reaction mixture was heated at 75 ºC for 90 min., cooled to room temperature, poured into ice water and then extracted into $CHCl_3$. The extract was washed with aq. $NaHCO_3$ (3 x 10 mL) then H_2O (10 mL) and dried over anhydrous $MgSO_4$ before being concentrated *in vacuo* to afford N–*(3–bromopropyl)*–N'–*mesityloxamide* **87** (362 mg, 59%) as a yellow solid, mp 159 – 160 ºC (from EtOAc);ν_{max}/cm^{-1} 3300, 1661, 1493, 1439, 1221 and 708; *m/z* 327.0701 (MH^+. $C_{14}H_{20}N_2O_2Br$ requires 327.0708); δ_H (400 MHz; $CDCl_3$) 2.14 – 2.17 (2H, m, $CH_2CH_2CH_2$), 2.19 (6H, s, 2 x *o*–CH_3), 2.30 (3H, s, *p*–CH_3), 3.47 (2H, t, *J* 6.5, CH_2Br), 3.55 (2H, q, *J* 6.5, NCH_2) and 6.92 (2H, s, 2 x ArH); δ_C (100 MHz; $CDCl_3$) 18.3 (q, 2 x *o*–CH_3), 20.9 (q, *p*–CH_3), 30.2 (t, CH_2Br), 31.8 (t, $CH_2CH_2CH_2$), 38.3 (t, NCH_2), 129.0 (d, 2 x ArCH), 129.6, 134.6 and 137.5 (3 x s, 4 x ArC), 158.0 and 160.1 (2 x s, 2 x C=O).

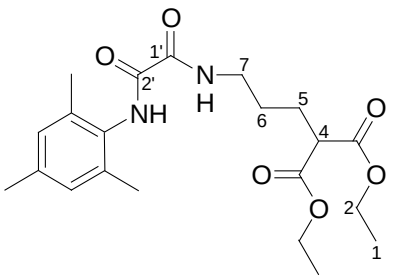

Diethyl 2{3–[(2–mesitylaminooxalyl)amino]propyl}malonate **88**

Method 1.

A solution of NaH (60% dispersion in oil; 75 mg, 1.8 mmol) in dry THF (5 mL) was added to diethyl malonate **83** (0.3 mL, 1.8 mmol) under Ar and the resultant solution stirred until clear before being transferred dropwise under Ar to a solution of *N*–(3–bromopropyl)–*N'*–mesityloxamide **87** (200 mg, 0.610 mmol) in dry THF (5 mL). The reaction mixture was refluxed for 16 h under N_2, cooled to room temperature and neutralized with aq. NH_4Cl. The organic layer was extracted with EtOAc (3 x 10 mL) and concentrated *in vacuo* to give an oil, which was purified by chromatography [flash on silica gel; elution with EtOAc–Hexane (1:3)] to afford *diethyl 2{3–[(2–mesitylaminooxalyl)amino]propyl} malonate* **88** (107 mg, 53.5%) as a silver–white crystalline solid, mp 90.5 – 91.5 ºC (from EtOAc); ν_{max}/cm^{-1} 3389, 3249, 1749 and 1722 (CO_2Et), 1652 (CONH) and 1510 (CONH); *m/z* 407.2200 (MH^+. $C_{21}H_{31}N_2O_6$ requires 407.2182); δ_H (400 MHz; $CDCl_3$) 1.28 (6H, t, *J* 7.1, 2 x 1–H_3), 1.67 (2H, quintet, *J* 7.5, 6–H_2), 1.98 (2H, q, *J* 7.8, 5–H), 2.19 (6H, s, 2 x *o*–CH_3), 2.29 (3H, s, *p*–CH_3), 3.36 (H, t, *J* 7.4, 4–H), 3.39 (2H, q, *J* 6.8, 7–H_2), 4.20 (4H, qd, *J* = 7.1, 1.9, 2 x 2–H_2), 6.91 (2H, s, 2 x ArH), 7.26 and 8.69 (2H, 2 x br s, 2 x NH); δ_C (100 MHz; $CDCl_3$) 14.2 (q, 2 x C–1) , 18.3 (q, 2 x *o*–CH_3), 20.9 (q, *p*–CH_3), 25.9 (t, C–5), 27.0 (t, C–6), 39.4 (q, C–7), 51.5 (d, C–4), 61.5 (t, 2 x C–2), 129.0 (d, 2 x ArCH), 129.6, 134.7 and 137.6 (3 x s, 4 x ArC), 158.1 and 159.9 (2 x s, 2 x C=O) and 169.1 (2 x OC=O).

Method 2.

A solution of NaH (60% dispersion in oil; 8.5 mg, 0.35 mmol) in dry THF (5 mL) was added to diethyl malonate **83** (0.054 mL, 0.35 mmol) under Ar and stirred until clear before being transferred to a solution of *N*–(3–chloropropyl)–*N'*–mesityloxamide **86** (80 mg, 0.30 mmol) in dry THF (5 mL). The mixture was refluxed for 8 h under N_2, cooled to room temperature

and neutralized with aq. NH_4Cl. The organic layer was extracted into EtOAc (20 mL) and concentrated *in vacuo* to give the crude material. Upon recrystallization from MeOH the starting material **86** was recovered.

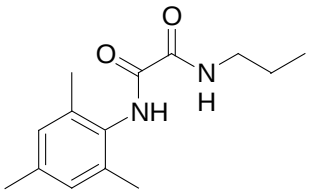

N–*Propyl*–N'–*mesitylethanediamide* **92**

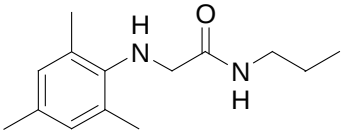

N–*Propyl–2–(mesitylamino)acetamide* **93**

A solution of *N*–(3–bromopropyl)–*N'*–mesityloxamide **87** (500 mg, 1.53 mmol) in dry THF (5 mL) was added dropwise to a suspension of $LiAlH_4$ (157 mg, 4.13 mmol) in dry THF (10 mL) at 0 ºC under N_2. The reaction was gently refluxed for 8 h, cooled to room temperature and the excess $LiAlH_4$ was quenched *via* the dropwise addition of H_2O (until bubbling ceased). A white precipitate formed, which was filtered and washed with THF (20 mL). The filtrate and washings were concentrated *in vacuo* and purified by chromatography [flash on silica gel; elution with EtOAc–Hexane (1:1)] to give two fractions.

i) N–*Propyl*–N'–*mesitylethanediamide* **92** (35 mg, 9.0%) as a white solid, mp 233–234 ºC (from EtOAc); ν_{max}/cm^{-1} 3308, 3265, 2963, 1656, 1508 and 758; *m/z* 249.1616 (MH^+. $C_{14}H_{23}N_2O_2$ requires 249.1603); δ_H (400 MHz; $CDCl_3$) 0.99 (3H, t, *J* 7.4, CH_2CH_3), 1.65 (2H, sextet, *J* 7.2, $CH_2CH_2CH_2$), 2.19 (6H, s, 2 x *o*–CH_3), 2.28 (3H, s, *p*–CH_3), 3.47 (2H, q, *J* 6.9, NCH_2), 6.92 (2H, s, 2 x ArH), 7.52 (1H, br s, NH) and 8.71 (1H, br s, NH); δ_C (100 MHz; $CDCl_3$) 11.3 (q, CH_2CH_3), 18.3 (q, 2 x *o*–CH_3), 20.9 (q, *p*–CH_3), 22.5 (t, $CH_2CH_2CH_2$), 41.5 (t, NCH_2), 129.0 (d, 2 x ArCH), 129.7, 134.7 and 137.5 (3 x s, 4 x ArC), 158.3 and 159.8 (2 x s, 2 x C=O).

ii) N–*Propyl–2–(mesitylamino)acetamide* **93** (25 mg, 7.0%) as a brown solid, mp 65–67.5 ºC (from EtOAc); ν_{max}/cm^{-1} 3300, 2965, 1646 (CONH), 1562 (NH bending), 1483 and 1440; *m/z* 235.1804 (MH^+. $C_{14}H_{21}N_2O_2$ requires 235.1810); δ_H (400 MHz; $CDCl_3$) 0.97 (3H, t, *J* 7.4, CH_2CH_3), 1.59 (2H, sextet, *J* 7.2, $CH_2CH_2CH_2$), 2.23 (3H, s, *p*–CH_3), 2.25 (6H, s, 2 x *o*–CH_3), 3.32 (2H, q, *J* 6.9, NCH_2CH_2), 3.58 (2H, s, $MesNCH_2$) 6.83 (2H, s, 2 x ArH) and 7.15 (1H, br s, NHCO); δ_C (100 MHz; $CDCl_3$) 11.4 (q, CH_2CH_3), 18.1 (q, 2 x *o*–CH_3), 20.5 (q, *p*–CH_3), 22.9 (t, $CH_2CH_2CH_2$), 40.9 (t, NCH_2CH_2), 52.2 (t, $MesNCH_2$) 129.7 (d, 2 x ArCH), 129.7, 132.4 and 142.4 (3 x s, 4 x ArC) and 171.0 (s, C=O).

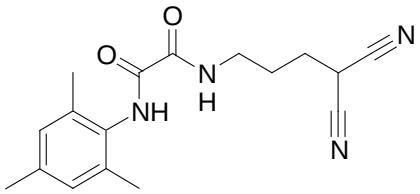

N–*(4,4–Dicyanobutyl)*–N'–*mesityloxamide* **94**

Propanedinitrile (250 mg, 0.760 mmol) was added dropwise to a suspension of NaH (60% dispersion in oil; 230 mg, 5.73 mmol) in dry THF (10 mL) and the resultant solution stirred for 20 min. before being transferred to a solution of *N*–(3–bromopropyl)–*N'*–mesityloxamide **87** (250 mg, 0.764 mmol) in dry THF (10 mL), and the reaction mixture was refluxed for 8 h. After 1 h under reflux the solution had turned from white to yellow and after 8 h the solution was a dark orange. The reaction mixture was neutralized *via* the dropwise addition of aq. NH_4Cl, transferred to a separating funnel and extracted with EtOAc. The organic layer was dried over anhydrous $MgSO_4$ and concentrated *in vacuo.* The crude product was purified by chromatography [flash on silica gel; elution with EtOAc–Hexane (1:1) and then HPLC; elution with EtOAc–Hexane (1:1)] to give N–*(4,4–dicyanobutyl)*–N'–*mesityloxamide* **94** (78 mg, 36%) as a brown solid, mp 164.5 – 165.5 ºC (from EtOAc); ν_{max}/cm^{-1} 3321, 3247, 3219, 2255 (C≡N), 1654 and 1513; *m/z* 313.1667 (MH^+. $C_{17}H_{21}N_4O_2$ requires 313.1665); δ_H (400 MHz; $CDCl_3$) 1.83 (2H, quintet, *J* 7.1, $CH_2CH_2CH_2$), 1.99 (2H, q, *J* 7.5, CH_2CH), 2.19 (6H, s, 2 x *o*–CH_3), 2.31 (3H, s, *p*–CH_3), 3.39 (2H, q, *J* 6.4, NCH_2), 3.60 (1H, t, *J* 7.2 Hz, CH), 6.95 (2H, s, 2 x ArH), 8.13 (1H, br s, NH) and 8.78 (1H, br s, NH); δ_C (100 MHz; $CDCl_3$) 18.3 (q, 2 x *o*–CH_3), 20.9 (q, *p*–CH_3), 21.6 (d, CH), 26.1 (t, $CH_2CH_2CH_2$), 27.9 (t, CH_2CH),

37.8 (t, NCH_2), 112.4 (s, C≡N), 129.2 (d, 2 x ArCH), 129.5, 134.8 and 138.1 (3 x s, 4 x ArC), 158.2 and 160.3 (2 x s, 2 x C=O).

6.2.1. Attempted Syntheses

1–*[4,4–Bis(ethoxycarbonyl)butyl]–3–mesitylimidazolin–2–ium chloride* **85**

Method 1.

Diethyl malonate **83** (0.30 mL, 2.0 mmol) was added dropwise to a suspension of NaH (60% dispersion in oil; 40 mg, 0.80 mmol) in dry THF (5 mL) and the resulting suspension was stirred until a clear solution was obtained, which was transferred *via* syringe under Ar to a solution of 1–(3–chloropropyl)–3–mesitylimidazolin–2–ium chloride **81** (100 mg, 0.33 mmol) in dry THF (5 mL). The reaction was refluxed for 5 h under N_2, cooled to room temperature and then poured into ice cold HCl (0.04M, 15 mL). The solution was washed with EtOAc (3 x 15 mL) to separate the organic fraction as an oil. The oil was washed with Et_2O (10 mL). The oil was chromatographed [preparative layer chromatography on silica gel; elution with EtOAc–Hexane (1:1)] but no identifiable products were isolated.

Method 2.

The enolate of diethyl malonate **84** was prepared as before and added to a solution of 1–(3–chloropropyl)–3–mesitylimidazolin–2–ium chloride **81** in dry THF. The mixture was refluxed for 5 h under N_2 then cooled to room temperature. Upon addition of conc. HCl (2–3 drops, until neutral) the mixture solidified and upon addition to $CHCl_3$, a precipitate formed. The precipitate and supernatant were collected separately and the supernatant was concentrated *in vacuo* to give an oil, which was recrystallized from MeOH to afford the starting material **81**.

Method 3.

Na metal (30.8 mg, 1.40 mmol) was added to dry EtOH (20 mL), and once gas evolution had ceased, diethyl malonate **83** (0.18 mL, 1.1 mmol) was added and the resulting solution heated at 50 $^{\circ}$C for 30 min. 1–(3–chloropropyl)–3–mesitylimidazolin–2–ium chloride **81** (350 mg, 1.12 mmol) was added to the solution, which was then refluxed for 8 h and stirred at room temperature overnight. The solvent was removed *in vacuo* and the remaining slurry was taken

up in EtOAc (20 mL) and H_2O (20 mL). The aqueous fraction was washed with EtOAc (5 x 10 mL) and the organic layer and washings were combined and dried over anhydrous $MgSO_4$ before being concentrated *in vacuo* and chromatographed [reverse–phase flash on C_{18} silica; elution with methanol–brine (2.5:1)]. No identifiable products were isolated.

Method 4.

The enolate of diethyl malonate **84** was prepared as before and added to a solution of 1–(3–bromopropyl)–3–mesitylimidazolin–2–ium bromide **82** (92 mg, 0.24 mmol) in dry THF. The mixture was refluxed for 8 h under N_2, then cooled to room temperature and neutralised *via* the dropwise addition of super–saturated aq. NH_4Cl. The product was extracted with CH_2Cl_2, dried over anhydrous $MgSO_4$ and concentrated *in vacuo* to give a light oil, NMR analysis of which indicated no identifiable products.

Method 5.

Crude product material from 2–(hydroxymethyl)–5–[2–(mesitylamino)ethylamino]pentanol dihydrochloride **89** (100 mg) was heated to 135 ºC over 1 h with $HC(OEt)_3$ (1.0 mL, 8.2 mmol). The reaction mixture was cooled to room temperature and the organic and aqueous fractions were separated into EtOAc (10 mL) and H_2O (10 mL). Preliminary NMR analysis on both fractions showed no identifiable products.

2–(Hydroxymethyl)–5–[2–(mesitylamino)ethylamino]pentanol dihydrochloride **89**

Method 1.

A solution of diethyl 2{3–[(2–mesitylaminooxalyl)amino]propyl}malonate **88** (966 mg, 2.38 mmol) in dry THF (10 mL) was added dropwise to a suspension of $LiAlH_4$ (48.0 mg, 12.8 mmol) in dry THF (10 mL) at 0 ºC under N_2. The reaction was gently refluxed for 8 h, cooled to room temperature and then quenched *via* the dropwise addition of MeOH (until no further effervescence was observed). The solution was hydrolyzed with a solution of NaOH (1 g) and $MgSO_4$ (1 g) in H_2O (10 mL), filtered and the solid washed with THF (3 x 10 mL). The filtrate and washings were combined and concentrated *in vacuo* to give a yellow oil. The crude product was chromatographed [preparative; elution with EtOAc–Hexane–MeOH (1:1:2%)]. The desired product was not isolated and no pure organic compounds were identified.

Method 2.

The reaction was performed as before, with 2{3–[(2–mesitylaminooxalyl)amino]propyl} malonate **88** (200 mg, 0.49 mmol) and $LiAlH_4$ (298 mg, 7.85 mmol) under reflux for 16 h. The reaction was quenched *via* the dropwise addition of H_2O, until a granular precipitate formed. The suspension was filtered through a Celite column (5 mL) and the column washed with THF (20 mL). The eluent and washings were combined and concentrated *in vacuo* to give an oil, which was dissolved in MeOH and conc. HCL was added dropwise until a pH of 4 was reached. The mixture was transferred to a separating funnel and the organic and aqueous layers were separated and concentrated *in vacuo*. The aqueous fraction was neutralised *via* the addition of $NaHCO_3$ followed by extraction into EtOAc and drying over anhydrous $MgSO_4$. The residue was chromatographed [flash on silica gel; elution with EtOAc, acetone, MeOH (2 column lengths each)]. The desired product was not identified.

The reaction was repeated in the same manner, monitoring the progress *via* TLC to determine if the reaction would run to completion. The reaction was placed under reflux for a total of 26 h without running to completion with no less than 6 spots appearing on the TLC plate.

Method 3.

2{3–[(2–mesitylaminooxalyl)amino]propyl}malonate **88** (200 mg, 0.49 mmol) was placed in a flask under N_2 purge. BH_3–THF (68mg, 4.9 mL, 4.9 mmol) was added and the resultant solution was refluxed for 5 h, after which time a white precipitate had formed. The reaction was cooled to room temperature and quenched *via* the dropwise addition of MeOH followed by conc. HCl until a pH of 4 was attained. The solution was transferred to a separating funnel and the organic phase was extracted into EtOAc. Both fractions were concentrated *in vacuo* and NMR analysis indicated that the desired product was not present in either fraction.

N–*(3–bromopropyl)*–N'–*mesitylethylenediamine* **91**

Method 1.

To a stirred suspension of *N*–(3–hydroxypropyl)–*N'*–mesitylethylenediamine dihydrochloride **79** (600 mg, 2.54 mmol) in EtOAc (5 mL) was added PBr_3 (0.48 mL, 5.1 mmol) dropwise

over 20 min. The resultant solution was heated at 75 ºC for 90 min. After cooling to room temperature the reaction was poured into ice water (20 mL) and the product extracted with $CHCl_3$ (25 mL) in a separating funnel. The extract was washed with $NaHCO_3$ (3 x 10 mL), then H_2O (3 x 10 mL) and dried over anhydrous $MgSO_4$ before being concentrated *in vacuo* and chromatographed [flash on silica gel; elution with EtOAc–Hexane (1:1)]. The desired product was not isolated and no significant organic compounds were identified.

Method 2.

A solution of *N*–(3–bromopropyl)–*N'*–mesityloxamide **87** (500 mg, 1.53 mmol) in dry THF (5 mL) was added dropwise to a suspension of $LiAlH_4$ (157 mg, 4.13 mmol) in dry THF (10 mL) at 0 ºC under N_2. The reaction was gently refluxed for 8 h, cooled to room temperature and then quenched *via* the dropwise addition of H_2O (until bubbling ceased). A white precipitate had formed, which was filtered and washed with THF (20 mL). The filtrate and washings were concentrated *in vacuo*. Flash chromatography on silica gel (elution with EtOAc–Hexane) did not yield the desired product.

N–*[4,4–Bis(formyl)butyl]–N'–mesityloxamide* **98**

Solutions of 0.15M aq. NaCl (0.8 mL) and 6M HCl (0.03 mL) were added to 1,1,3,3–tetramethoxypropane **96** (251 mg, 0.25 mL, 1.53 mmol) and the solution was agitated using a vortex mixer, then washed with cold 0.15M aq. NaCl (3 x 5 mL) and dried over anhydrous $MgSO_4$. The product was concentrated *in vacuo* at room temperature then dissolved in dry THF (10 mL) and added to a solution of *N*–(3–bromopropyl)–N'–mesityloxamide **87** (250 mg, 0.76 mmol) in dry THF (10 mL). The reaction mixture was refluxed for 8 h under Ar, but the desired product was not generated.

2–{3–[2–(Mesitylamino]ethylamino]propyl}propanedinitrile **122**

A solution of crude product material of *N*–(4,4–dicyano–butyl)–*N'*–mesityloxamide **94** (0.5 mL) in dry THF (5 mL) was added to a suspension of $LiAlH_4$ (243 mg, 6.40 mmol) in dry THF (5 mL). The reaction was refluxed for 5 h and then stirred at room temperature for a further 36 h. The reaction was quenched *via* the dropwise addition of H_2O, dissolved in MeOH and the solid filtered off before conc. HCl was added dropwise until a pH of 4 was

reached. The solution was transferred to a separating funnel and the organic and aqueous fractions were seperated. Preliminary NMR analysis on the two fractions did not reveal signs of the desired product.

6.3. Preparation of imidazolium pro–ligands

Microwave assisted reactions were performed in a CEM Discover single–mode microwave apparatus, producing controlled irradiation at 2450 MHz, using standard 10 mL silicon–septum sealed glass pressure vials. Reactions were optimized using the temperature–time mode of operation and temperature was monitored by means of an IR sensor directed at the outside wall of the reaction vial. All reaction times described refer to hold times at the indicated temperature and not total irradiation times. Upon completion, reaction mixtures were cooled to below 50 ºC *via* propelled air flow.

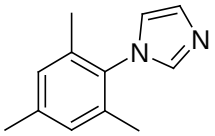

N–*mesitylimidazole* **102**[110]

An aqueous solution of NH_4Cl (5.35 g, 0.10 mol) in H_2O (20 mL) was added to a rapidly stirred solution of paraformaldehyde **105** (3.0 g, 19 mmol), 2,4,6–trimethylanilinium salt **103** [prepared by adding phosphoric acid to 2,4,6–trimethylaniline **73** (3.0 g, 19 mmol) in H_2O (10 mL) until a pH of 2 was reached] and glyoxal **104** (11.5 mL of a 40% aqueous solution) in H_2O (50 mL) and 1,4–dioxane (50 mL) at 100 ºC. After stirring for 2 h, the solution was cooled to 0 ºC and solid NaOH was added until the pH rose above 12 and a dark layer separated out. H_2O (50 mL) was added and the product was extracted with hexane (3 x 50 mL). The organic extracts were combined, dried over $MgSO_4$ and reduced *in vacuo* to give a dark brown solid which was recrystallized four times from EtOAc to give *N*–mesitylimidazole **102** (3.48 g, 98%) as a tan solid, mp 114 – 116^{o}C (from EtOAc) (*lit.*,[121] 107 – 109^{o}C *)*; ν_{max}/cm^{-1} 3096, 1499 (C=N), 816 and 672; δ_H (400 MHz; $CDCl_3$) 1.98 (6H, s, 2 x *o*–CH_3), 2.33 (3H, s, *p*–CH_3), 6.88 (1H, s, NCH), 6.96 (2H, s, 2 x ArH), 7.23 (1H, s, NCH) and 7.43 (1H, s, NCHN); δ_C (100 MHz; $CDCl_3$) 17.3 (q, 2 x *o*–CH_3), 21.0 (q, *p*–CH_3), 120.0 (d, NCH), 129.0 (d, 2 x ArCH), 129.6 (NCH), 133.4 and 135.4 (2 x s, 2 x ArC), 137.5 (d, NCHN) and 138.8 (s, ArC); *m/z* 188.10 ([M+2H], 100 %).

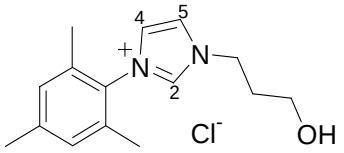

1–(3–hydroxypropyl)–3–mesitylimidazol–2–ium chloride **100**

Method 1.

A solution of *N*–mesitylimidazole **102** (500 mg, 2.69 mmol) and 3–chloropropanol **106** (254 mg, 2.69 mmol) in toluene (1 mL) was heated in the microwave apparatus for 60 min. (85 ºC,150 W). The precipitate was washed with toluene (3 x 5 mL) and acetone (3 x 5 mL) to give 1–(3–hydroxypropyl)–3–mesitylimidazol–2–ium chloride **100** (560 mg, 74%) as a white solid, mp 180 – 182 ºC (from MeOH) (lit.,[99, 107] no mp reported); ν_{max}/cm^{-1} 3248 (OH), 3050, 1541 (C=N), 1081, 1064 and 763; *m/z* 245.1643 (M^+. $C_{15}H_{21}N_2O$ requires 245.1654); δ_H (400 MHz; $CDCl_3$) 2.03 (6H, s, 2 x *o*–CH_3), 2.16 (2H, quintet, *J* 5.6, $CH_2CH_2CH_2$), 2.30 (3H, s, *p*–CH_3), 2.64 (1H, br s, OH), 3.61 (2H, t, *J* 5.0, CH_2OH), 4.73 (2H, t, *J* 6.2, NCH_2), 6.96 (2H, s, 2 x ArH), 7.16, (1H, s, 4–H), 8.11 (1H, s, 5–H) and 10.10 (1H, s, 2–H); δ_C (100 MHz; $CDCl_3$) 17.4 (q, 2 x *o*–CH_3), 21.0 (q, *p*–CH_3), 33.1 (t, $CH_2CH_2CH_2$), 47.4 (t, NCH_2), 57.2 (t, CH_2OH), 123.1 (d, C–4), 123.7 (d, C–5), 129.7 (d, 2 x ArCH), 130.7 and 134.2 (2 x s, 2 x ArC), 138.0 (d, C–2) and 141.1 (s, ArC).

Method 2.

A solution of 1–mesitylimidazole **102** (200 mg, 1.07 mmol) and 3–chloropropanol **106** (112 mg, 1.18 mmol) in THF (10 mL) was refluxed for 16 h before being cooled to room temperature and concentrated *in vacuo.* Preliminary NMR analysis of the crude product showed the presence of the starting materials but none of the desired product.

Method 3.

A solution of 1–mesitylimidazole **102** (200 mg, 1.07 mmol) and chloropropanol **106** (112 mg, 1.18 mmol) in toluene (10 mL) was refluxed for 5 days and the reaction was monitored periodically by ^1H NMR spectroscopy. After 5 days under reflux no reaction had taken place and only the starting materials remained.

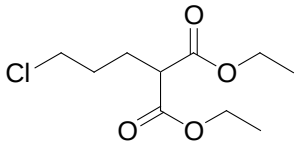

Diethyl 2–(3–chloropropyl)malonate **113**[147, 148]

Diethyl malonate **83** (1.54 mL, 10.16 mmol) was added to a suspension of NaH (60% dispersion in oil; 915 mg, 22.9 mmol) in dry THF (10 mL) under Ar and the mixture was stirred until a clear solution was observed before being transferred *via* cannula to a solution of 1–bromochloropropane **114** (3.00 g, 19.1 mmol) in dry THF (10 mL). The reaction mixture was refluxed for 8 h under Ar, cooled to room temperature and neutralized with a satd. NH_4Cl solution. The solution was transferred to a separating funnel and the organic layer was extracted with EtOAc, dried over anhydrous $MgSO_4$ and concentrated *in vacu*o to give diethyl 2–(3–chloropropyl)malonate **113** (2.28 g, 95%) as a clear liquid; ν_{max}/cm^{-1} 2983, 1728 (C=O), 1239, 1145 and 1028; *m/z* 237.0919 (MH^+. $C_{10}H_{18}Cl_2O_4$ requires 237.0894); δ_H (400 MHz; $CDCl_3$) 1.23 (6H, t, *J* 7.1, 2 x CH_2CH_3), 1.79 (2H, quintet, *J* 7.1, $CH_2CH_2CH_2$), 2.00 (2H, p, *J* 7.1, CH_2CH), 3.31 (1H, t, *J* 7.3, CH), 3.51 (2H, t, *J* 6.5, CH_2Cl) and 4.18 (4H, qd, *J* 7.1, 1.6, 2 x OCH_2); δ_C (100 MHz; $CDCl_3$) 14.0 (q, 2 x CH_2CH_3) , 26.1 (t, $CHCH_2$), 30.2 (t, $CH_2CH_2CH_2$), 44.1 (t, CH_2Cl), 51.2 (d, CH), 61.4 (t, 2 x OCH_2) and 169.0 (s, 2 x C=O).

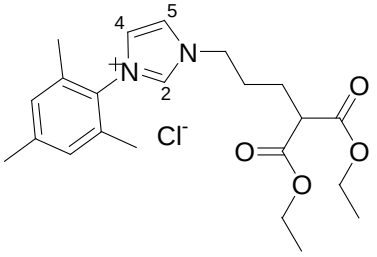

1–[4,4–Bis(ethoxycarbonyl)butyl]–3–mesitylimidazol–2–ium chloride **101**

A solution of *N*–mesitylimidazole **102** (100 mg, 0.54 mmol) and diethyl 2–(3–chloropropyl)malonate **113** (127 mg, 0.54 mmol) in toluene (1 mL) was heated in the microwave apparatus for 2 h (85 ºC, 150 W). The resulting precipitate was washed with toluene (3 x 5mL) then dissolved in water–EtOAc (1:1) and NaCl (spatula tip) was added.

The organic fraction was separated and concentrated *in vacuo* to give *1–[4,4–bis(ethoxycarbonyl)butyl]–3–mesitylimidazol–2–ium chloride* **101** (15 mg, 7%) as a brown oil; ν_{max}/cm^{-1} 3388, 1722 (C=O), 1546 (C=N), 1203, 1159 and 1102; *m/z* 387.2273 (M^+. $C_{22}H_{31}N_2O_4$ requires M^+: 387.2284); δ_H (400 MHz; $CDCl_3$) 1.25 (6H, t, *J* 7.1, 2 x CH_2CH_3), 1.91 – 1.99 (2H, m, CH_2CH), 2.07 (6H, s, 2 x *o*–CH_3), 2.04 – 2.11 (2H, m, $CH_2CH_2CH_2$), 2.33 (3H, s, *p*–CH_3), 3.42 (1H, t, *J* 7.0, CH), 4.17 (4H, qd, *J* 7.0, 3.1, 2 x OCH_2), 4.80 (2H, t, *J* 6.9, NCH_2), 6.98 (2H, s, 2 x ArH), 7.14 (1H, s, 4–H), 7.71 (1H, s, 5–H) and 10.64 (1H, s, 2–H); δ_C (100 MHz; $CDCl_3$) 14.0 (q, 2 x CH_2CH_3), 17.5 (q, 2 x *o*–CH_3), 21.0 (q, *p*–CH_3), 25.0 (t, CH_2CH), 27.9 (t, $CH_2CH_2CH_2$), 49.8 (t, NCH_2), 50.9 (d, CH), 61.6 (t, 2 x OCH_2), 122.4 (d, C–5), 123.0 (d, C–4), 129.8 (d, 2 x ArCH), 130.8 (s, ArC), 134.2 (s, 2 x ArC), 139.2 (d, C–2), 141.3 (s, ArC) and 168.9 (s, 2 x C=O).

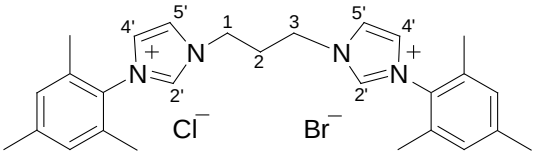

1,3–Bis–(3–mesitylimidazolium–2–yl)propane dihydrogen halide salt **107**[149]

A solution of *N*–mesitylimidazole **102** (52 mg, 0.28 mmol) and 1–bromochloropropane **114** (22 mg, 0.14 mmol) in toluene (1 mL) was heated in the microwave apparatus for 30 min. (85 ºC, 150 W). The precipitate was washed with toluene (2 x 10 mL) and recrystallized from acetone to give 1,3–bis–(3–mesitylimidazolium–2–yl)propane dihdrogen halide salt **107** (52 mg, 70%) as a white solid, mp 148–149 ºC; ν_{max}/cm^{-1} 3355, 3067, 1549 (C=N), 1204, 1160 and 831; *m/z* 413.2706 ([M–H]. $C_{27}H_{33}N_4$ requires 413.2705); δ_H (400 MHz; $CDCl_3$) 2.07 (12H, s, 4 x *o*–CH_3), 2.35 (6H, s, 2 x *p*–CH_3), 3.17 – 3.27 (2H, m, 2–H_2), 4.99 (4H, t, *J* 7.7, 2 x NCH_2), 7.01 (4H, s, 4 x ArH), 7.09 (2H, s, 2 x 4'–H), 8.51 (2H, s, 2 x 5'–H) and 9.98 (2H, s, 2 x 2'–H); δ_C (100 MHz; $CDCl_3$) 17.5 (q, 4 x *o*–CH_3), 20.9 (q, 2 x *p*–CH_3), 32.0 (t, C–2), 47.0 (t, 2 x NCH_2), 122.9 (d, 2 x C–4'), 124.8 (d, 2 x C–5'), 129.7 (d, 4 x ArCH), 130.6 (s, 2 x ArC), 134.1 (s, 4 x ArC), 137.1 (d, 2 x CH–2') and 141.2 (s, 2 x ArC).

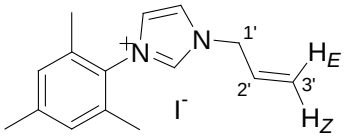

1–(Prop–2–enyl)–3–mesitylimidazol–2–ium iodide **108**[113]

A solution of *N*–mesitylimidazole **102** (52 mg, 0.28 mmol) and allyl iodide (47 mg, 0.28 mmol) in toluene (1 mL) was heated in the microwave apparatus for 30 min. (85 ºC, 150 W). The resultant precipitate was washed with toluene (3 x 5 mL) and recrystallized from CH_2Cl_2–Et_2O to give 1–(prop–2–enyl)–3–mesitylimidazol–2–ium iodide **108** (68.4 mg, 69%) as a brown solid, mp 166 – 167 ºC (from CH_2Cl_2–Et_2O); ν_{max}/cm^{-1} 3011, 1544 (C=N), 1199, 864 and 760; δ_H (400 MHz; $CDCl_3$) 2.11 (6H, s, 2 x *o*–CH_3), 2.34 (3H, s, *p*–CH_3), 5.41 (2H, d, *J* 6.4, 1'–H_2), 5.50 (1H, dd, *J* 10.1, 0.5, 3'–H_Z), 5.56 (1H, dd, *J* 16.9, 0.5, 3'–H_E) 6.16 (1H, ddt, *J* 16.9, 10.2, 6.4, 2'–H), 7.01 (2H, s, 2 x ArH), 7.20 (1H, t, *J* 1.7, NCH), 7.69 (1H, t, *J* 1.6, NCH) and 10.08 (1H, s, NCHN); δ_C (100 MHz; $CDCl_3$) 17.9 (q, 2 x *o*–CH_3), 21.1 (q, *p*–CH_3), 52.7 (t, C–1'), 122.7 (t, C–3'), 122.8 (d, NCH), 123.1 (d, NCH), 130.0 (d, 2 x ArCH), 130.1 (d, C–2'), 130.5 (s, ArC), 134.3 (s, 2 x ArC), 137.6 (d, NCHN) and 141.5 (s, ArC); *m/z* 227.84 ([M–H], 100 %).

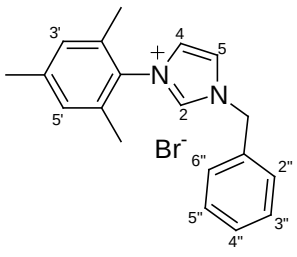

1–Benzyl–3–mesitylimidazol–2–ium bromide **109**

A solution of *N*–mesitylimidazole **102** (50 mg, 0.27 mmol) and benzyl bromide (47 mg, 0.27 mmol) in toluene (1 mL) was heated in the microwave apparatus for 30 min. (85 ºC, 150 W). The resultant precipitate was washed with toluene (3 x 5 mL) and recrystallized from CH_2Cl_2–Et_2O to give 1–benzyl–3–mesitylimidazol–2–ium bromide **109** (78 mg, 80%) as a white solid, mp 249 – 251 ºC (from CH_2Cl_2–Et_2O) (*lit.*,[112] 237 – 238 ºC); ν_{max}/cm^{-1} 2990, 1543 (C=N), 1196, 877, 755 and 715; δ_H (400 MHz; $CDCl_3$) 2.05 (6H, s, 2 x *o*–CH_3), 2.32

(3H, s, *p*–CH_3), 5.98 (2H, s, $PhCH_2$), 6.97 (2H, s, 3' and 5'–H), 7.11 (1H, t, *J* 1.7, 5–H), 7.38 (3H, m, 3 x ArH), 7.60 (2H, m, 2 x ArH), 7.66 (1H, t, *J* 1.5, 4–H) and 10.62 (1H, s, 2–H); δ_C (100 MHz; $CDCl_3$) 17.6 (q, 2 x *o*–CH_3), 21.0 (q, *p*–CH_3), 53.5 (t, $PhCH_2$), 122.6 (d, C–5), 123.0 (d, C–4), 129.1 (d, C–2'', 6''), 129.4 (d, C–3'', –4'' and –5''), 129.9 (d, C–3'and –5'), 130.6, 133.5 and 134.2 (3 x s, 4 x ArC), 138.1 (d, C–2) and 141.3 (s, ArC); *m/z* 278 ([M+H], 100 %).

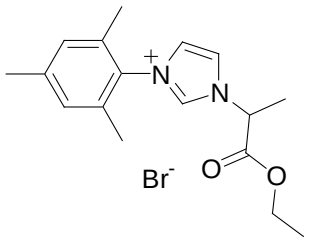

1–[(1–Ethoxycarbonyl)ethyl]–3–mesitylimidazol–2–ium bromide **110**[116]

A solution of *N*–mesitylimidazole **102** (46 mg, 0.25 mmol) and ethyl 2–bromopropionate (44 mg, 0.25 mmol) in toluene (1 mL) was heated in the microwave apparatus for 30 min. (85 ºC, 150 W). The resultant precipitate was washed with toluene (3 x 5 mL) and Et_2O (3 x 5 mL) to give 1–[(1–Ethoxycarbonyl)ethyl]–3–mesitylimidazol–2–ium bromide **110** (69 mg, 77%) as a yellow oil; δ_H (400 MHz; $CDCl_3$) 1.31 (3H, t, *J* 7.2, CH_2CH_3), 1.95 (3H, d, *J* 7.4, $CHCH_3$), 2.06 (3H, s, *o*–CH_3), 2.13 (3H, s, *o*–CH_3), 2.34 (3H, s, *p*–CH_3), 4.27 (2H, qd, *J* 7.2, 1.6, CH_2), 6.73 (1H, q, *J* 7.3, $CHCH_3$), 7.01 (2H, s, 2 x ArH), 7.18 (1H, t, *J* 1.7, NCH), 7.79 (1H, t, *J* 1.7, NCH) and 10.50 (1H, s, NCHN); δ_C (100 MHz; $CDCl_3$) 13.9 (q, CH_2CH_3), 17.3 (q, *o*–CH_3), 17.7 (q, *o*–CH_3), 18.1 (q, $CHCH_3$), 21.0 (q, *p*–CH_3), 57.7 (d, $CHCH_3$), 63.0 (t, CH_2), 121.4 (d, NCH), 122.7 (d, NCH), 129.8 (d, ArCH), 129.9 (d, ArCH), 130.5, 134.1 and 134.4 (3 x s, 3 x ArC), 139.9 (d, NCHN), 141.4 (s, ArC) and 169.0 (s, C=O); *m/z* 287.87 (M^+, 100 %).

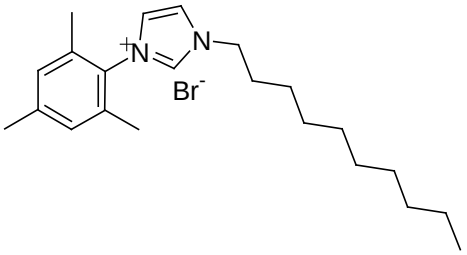

1–Decyl–3–mesitylimidazol–2–ium bromide **111**

A solution of *N*–mesitylimidazole **102** (50 mg, 0.27 mmol) and 1–bromodecane (52 mg, 0.27 mmol) in toluene (1 mL) was heated in the microwave apparatus for 30 min. (85 ºC, 150 W). The resultant precipitate was washed with toluene (3 x 5 mL) and Et_2O (3 x 5 mL) to give *1–decyl–3–mesitylimidazol–2–ium bromide* **111** (67 mg, 61%) as a grey solid, mp 105 – 106 ºC; ν_{max}/cm^{-1} 2919, 2849, 1541, 1456, 1199 and 859; *m/z* 327.2788 (M^+. $C_{22}H_{35}N_2$ requires 327.2800); δ_H (400 MHz; $CDCl_3$) 0.87 (3H, t, *J* 6.8, CH_2CH_3), 1.24 (10H, br s, 5 x CH_2), 1.31 – 1.43 (4H, m, 2 x CH_2), 1.98 (2H, t, *J* 7.2, CH_2), 2.08 (6H, s, 2 x *o*–CH_3), 2.33 (3H, s, *p*–CH_3), 4.74 (2H, t, *J* 7.2, NCH_2), 6.99 (2H, s, 2 x ArH), 7.15 (1H, s, NCH), 7.63 (1H, s, NCH) and 10.50 (1H, s, NCHN); δ_C (100 MHz; $CDCl_3$) 14.0 (q, CH_2CH_3), 17.7 (q, 2 x *o*–CH_3), 21.1 (q, *p*–CH_3), 22.6, 26.1, 29.0, 29.2, 29.3, 29.4, 30.6 and 31.8 (8 x t, 8 x CH_2), 50.6 (t, NCH_2), 122.4 (d, NCH), 123.0 (d, NCH), 129.9 (d, 2 x ArCH), 130.7 and 134.2 (2 x s, 2 x ArC), 138.6 (d, NCHN) and 141.4 (s, ArC).

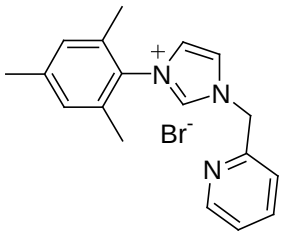

1–[(Pyridin–2–yl)methyl]–3–mesitylimidazol–2–ium bromide **112**

A solution of *N*–mesitylimidazole, **102** (204 mg, 1.09 mmol) and 2–chloromethylpyridine hydrobromide (221 mg, 0.870 mmol) in EtOH (1 mL) was heated in the microwave apparatus for 30 min. (85 ºC, 150 W). The resultant precipitate was purified by chromatography [HP20 polystyrene beads; gradient elution with MeOH–H_2O (10:1→1:10)]. The eluent was

discarded, while the column was stripped with acetone and the resultant eluent was concentrated *in vacuo* and recrystallized from CH_2Cl_2 to give 1–[(pyridin–2–yl)methyl]–3–mesitylimidazol–2–ium bromide **112** (120 mg, 39%) as a light brown solid, mp 131 – 132 ºC (from MeOH) (*lit.*,[139] 210 ºC [decomp.]); ν_{max}/cm^{-1} 3411, 2991, 1545 (C=N), 1438, 1202 and 783; *m/z* 278.1650 (M^+. $C_{18}H_{20}N_3$ requires 278.1657); δ_H (400 MHz; $CDCl_3$) 2.06 (6H, s, 2 x *o*–CH_3), 2.35 (3H, s, *p*–CH_3), 6.12 (2H, s, $PyCH_2$), 6.98 (2H, s, 2 x ArH), 7.08 (1H, t, *J* 1.6, NCH), 7.47 (1H, td, *J* 6.3, 0.8, PyH), 7.95 (1H, d, *J* 7.7, PyH), 7.97 (1H, td, *J* 7.6, 1.7, PyH), 8.29 (1H, t, *J* 1.5, NCH), 8.50 (1H, d, *J* 4.0, PyH) and 10.22 (1H, s, NCHN); δ_C (100 MHz; $CDCl_3$) 17.5 (q, 2 x *o*–CH_3), 21.0 (q, *p*–CH_3), 53.9 (t, $PyCH_2$), 122.5 (d, NCH), 123.8 (d, NCH), 123.9 (d, PyCH), 124.3 (d, PyCH), 129.8 (d, 2 x ArH), 130.6 (s, ArCH), 134.2 (s, 2 x ArC), 137.7 (d, PyCH), 138.1 (d, NCHN), 141.3 (s, ArC), 149.6 (d, PyH) and 152.6 (s, PyC).

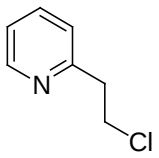

2–(2–Chloroethyl)pyridine **123**[150]

A solution of 2–(2–hydroxyethyl)pyridine (2g, 16mmol) and $SOCl_2$ (2.7mL, 32.5mmol) in C_6H_6 was refluxed for 30 min. under a $CaCl_2$ guard tube. Excess solvent and $SOCl_2$ were removed *in vacuo* and the residue was dissolved in $CHCl_3$–benzene (1:1) and washed with aq. $NaHCO_3$ until neutral, dried over anhydrous $MgSO_4$ and concentrated *in vacuo* to yield 2–(2–chloroethyl)pyridine **123** (2.28g, 60%) as a brown liquid; δ_H (400MHz; $CDCl_3$) 3.22 (2H, t, *J* 6.9, CH_2), 3.92 (2H, t, *J* 6.9, CH_2), 7.16 (1H, dd, *J* 7.2, 5.5, PyH), 7.19 (1H, d, *J* 7.7, PyH), 7.62 (1H, td, *J* 7.7, 1.8, PyH) and 8.55 (1H, d, *J* 4.7, PyH).

6.3.1. Attempted Syntheses

1–[2–(Pyridin–2–yl)ethyl]–3–mesitylimidazol–2–ium bromide **124**

A solution of *N*–mesityl imidazole **102** (1.0 g, 0.54 mmol) and 2–(2–chloroethyl)pyridine **123** (75 mg, 0.54 mmol) in toluene (1 mL) was heated in the microwave apparatus for 30 min. (85 ºC, 150 W). The resultant precipitate was washed with toluene (3 x 5mL) and Et_2O (3 x 5 mL) to give light brown solid. NMR analysis of the crude product indicated that the desired product was present but isolation of the pure product was not achieved.

2–(3–Chloropropyl)malondialdehyde **125**

6M HCl (0.15 mL) was added to 1,1,3,3–tetramethoxypropane **96** (3.34 g, 3.35 mL, 20.33 mmol) and stirred for 2 h. NaOH was added until the pH rose to 8 before 1–bromochloropropane **114** (1.60 g, 1.00 mL, 10.2 mmol) in THF (10 mL) was added and the reaction was stirred overnight. The yellow mixture with a pH of 10 was transferred to a separating funnel. A layer of $CHCl_3$ was added before HCl was added dropwise until the yellow colour had dissipated into the organic layer. The two layers were separated and the organic layer was chromatographed [flash on silica gel; elution with EtOAc] to afford the starting materials 1,1,3,3–tetramethoxypropane **96** and 1–bromochloropropane **114**.

5–Chloro–2–cyanobutanedinitrile **126**

Propanedinitrile (1.34 g, 1.28 mL, 20.3 mmol) was added to a suspension of NaH (60% dispersion in oil; 1.22 g, 30.5 mmol) in dry THF (10 mL) and stirred for 20 min. before the solution was added *via* syringe to a solution of 1–bromochloropropane **114** (3.20 g, 2.00 mL, 20.33 mmol) in dry THF (10 mL) and refluxed for 8 h. The reaction was neutralized *via* the dropwise addition of aq. NH_4Cl, extracted with EtOAc and concentrated *in vacuo* to give a red oil and a colorless oil, which were immiscible. The colorless oil was found to contain no relevant organic material and was discarded. The red oil was chromatographed [flash; elution with EtOAc–Hexane (1:3)] but no identifiable organic materials were found.

1–(4,4–Dicyanobutyl)–3–mesitylimidazol–2–ium chloride **127**

A solution of *N*–mesitylimidazole **102** (100 mg, 0.54 mmol) and a portion of crude material from (3–chloropropyl)propanedinitrile **126** (0.5 mL) in THF (10 mL) was refluxed for 16 h. Preliminary NMR analysis showed no evidence of any reaction taking place.

1–(Pyridin–2–yl)–3–mesitylimidazol–2–ium bromide **128**

A solution of *N*–mesitylimidazole **102** (50 mg, 0.27 mmol) and 1–bromopyridine (42 mg, 0.27 mmol) in toluene (1 mL) was heated in the microwave apparatus for 90 min. (95 ºC, 200W). No precipitate was observed and preliminary NMR analysis indicated only the presence of the starting materials and the reaction was not pursued.

1–(2–Methylpropyl)–mesitylimidazol–2–ium bromide **129**

A solution of *N*–mesitylimidazole **102** (50 mg, 0.27 mmol) and 1–bromo–2–methyl propane (37 mg, 0.27 mmol) in toluene (1 mL) was heated in the microwave apparatus for 45 min. (90 ºC, 200W). The resultant precipitate was washed with Et_2O and recrystallized from CH_2Cl_2–Et_2O to give a purple solid. Preliminary NMR analysis of the residue showed that the desired product was present, however purification proved to be difficult and the pure product was not isolated.

1–(3–Methylbut–2–enyl)–3–mesitylimidazol–2–ium chloride **130**

A solution of *N*–mesitylimidazole **102** (105 mg, 0.56 mmol) and dimethylallyl bromide (84 mg, 0.56 mmol) in toluene (1 mL) was heated in the microwave apparatus for 15 min. (70 ºC, 150 W). The resultant precipitate was washed with Et_2O (3 x 5 mL) and precipitated from CH_2Cl_2–Et_2O. Preliminary NMR analysis indicated the presence of the desired product, but purification was not achieved and the pure product was not isolated.

6.4. Complexation Studies

6.4.1. 'Air–Free' Preparation and Handling Techniques

All organometallic reactions and handling of products was conducted in oven–dried glassware under an atmosphere of Ar using standard Schlenk and vacuum techniques on a double manifold connected directly to the Ar source and a vacuum pump. The double manifold allows for the evacuation and subsequent flushing with Ar of Schlenk glassware, as well as the evaporation of solvents by condensation into the cooling traps. The Argon line consisted of an Argon bottle, connected to the manifold *via* a drying tube filled with Drierite® and self–indicating silica gel (not molecular sieves, as it has been indicated that molecular sieves produce oxygen over time)[20]. Two silicon oil bubblers were placed after the manifold, on the Ar line. The purpose of the bubblers is two–fold; firstly, they provide an indication of gas flow from the inert gas source and secondly, the second bubbler allows the equalization of pressure in the system during evacuation and flushing of glassware, without allowing air to enter from the environment. Two solvent traps were placed between the vacuum pump and the manifold, with one of the traps being immersed in liquid N_2 during evacuation to avoid solvent entering the vacuum pump.

Liquids were transferred using Ar–flushed disposable Norm–ject® syringes (without rubber plunger insert) and stainless steel needles and all solvents used were dried by the procedures described in Section 6.1.

General Procedure for the Filtration of Suspended Solids under Inert Gas

Filtration via *sintered funnel*

A Schlenk tube was connected to a sinter funnel (complete with Quickfit© joint below the sintered glass) and the system flushed with Ar. The reaction mixture was transferred to the sintered funnel, either by connecting the reaction Schlenk tube to the Quickfit© joint above the sintered glass or simply by transfer with a syringe and needle.

Filtration using Millipore syringe filter

The solution to be filtered was taken up in a syringe, the needle removed and replaced with a millipore filter (Millex–HV 0.45 μm) and a clean, dry needle. The solution was then transferred through the filter into a clean Ar–flushed Schlenk tube and the filter containing precipitate was discarded.

General procedure for the removal of solvents under vacuum

Reaction mixtures were concentrated *in vacuo* by removing solvents *via* condensation into one of the solvent traps, which was immersed in liquid N_2. Care needs to be taken to avoid liquid entering the tubing and manifold. Thus the Schlenk was evacuated under vigorous stirring and the tap was opened very slowly and carefully to avoid bumping. The tap was never opened fully until the liquid showed signs of cooling or convectional streams could be seen.

General procedure for 'pump freezing' solvents

Due to the possible sensitivity of the metal complexes to oxygen and/or moisture, deuterated solvents were degassed to avoid decomposition during NMR experiments. Activated molecular sieves (4Å) were added to a Schlenk tube/flask (no more than a quarter–filled) and deuterated solvent added to *ca* 2/3 above the level of the sieves. The flask was stoppered and connected to the manifold, then immersed to above the solvent line in liquid nitrogen. When the solvent was completely frozen, the flask was removed and placed under vacuum until the solvent started to thaw. The flask was then flushed with Ar until all of the solvent had thawed. The procedure was repeated twice before the solvent was stored under Ar in the dark.

6.4.2. Preparation of metal–NHC complexes

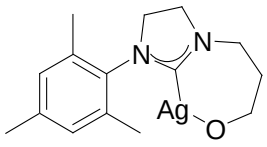

[1–(3–Oxidopropyl)–3–mesitylimidazolin–2–ylidene]silver **115**

1–(3–Hydroxypropyl)–3–mesitylimidazol–2–inium chloride **76** (500 mg, 1.77 mmol), Ag_2O (820 mg, 3.5 mmol) and type 4Å molecular sieves (1 g) were charged to a Schlenk flask and flushed with Ar. CH_2Cl_2 (5 mL) was added and the reaction mixture was stirred for 4 h, after which the suspension was passed through a column of Celite® on sintered glass (5 cm length) and rinsed with CH_2Cl_2 (5 mL). The filtrate was concentrated *in vacuo* to give a brown solid which was dissolved in a minimal volume of CH_2Cl_2, and pentane was added until a precipitate emerged. The supernatant was removed and the residue was dried *in vacuo* to give *[1–(3–oxidopropyl)–3–mesitylimidazolin–2–ylidene]silver* **115** as a black solid (260 mg, 52%); δ_H (400 MHz; $CDCl_3$) 1.66 (2H, quintet, *J* 5.4, CH_2), 2.20 (6H, s, 2 x *o*–CH_3), 2.30 (3H, s, *p*–CH_3), 2.81 (2H, q, *J* 7.1, CH_2), 2.87 (2H, t, *J* 5.4, CH_2), 3.67 (2H, t, *J* 7.0, CH_2), 3.77 (2H, q, *J* 5.1, CH_2) and 6.95 (2H, s, 2 x ArH); δ_C (100 MHz; $CDCl_3$) 18.2, 20.9, 31.1, 45.9, 47.7, 49.5, 63.9, 129.7, 136.3 and 164.0.

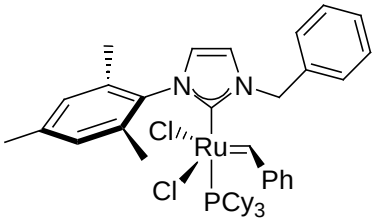

Benzylidene–(1–benzyl–3–mesitylimidazol–2–ylidene)dichloro(tricyclohexylphosphine) ruthenium **118**

1–Benzyl–3–mesitylimidazol–2–ium bromide **109** (100 mg, 0.28 mmol) and KHMDS (67 mg, 0.34 mmol) were placed in a dry Schlenk flask and flushed with Ar. Toluene (10 mL) was added and the reaction mixture was stirred for 30 min. before being transferred *via* a syringe through a millipore filter into a second Schlenk flask containing Grubbs I complex **25** (231 mg, 0.28 mmol) under Ar. The resultant mixture was stirred for 4 h (monitoring by TLC) before the solvent volume was reduced to *ca* 1 mL. Pentane (20 mL) was added and the suspension was agitated in an ultrasonic bath for 10 min. before the precipitate was allowed to settle. The supernatant was removed and the precipitate was washed with pentane (4 x 20 mL) before being dried *in vacuo* to give *benzylidene–(1–benzyl–3–mesitylimidazol–2–ylidene)dichloro(tricyclohexylphosphine)ruthenium* **118** as a pink solid (120 mg, 52%); ν_{max}/cm^{-1} 2935, 2924, 2852, 1441, 1229, 847, 714 and 691; *m/z* 819.3 ([M+H], 63 %), 820 ([M + 2H], 100 %); δ_H (600 MHz; $CDCl_3$) 1.13 – 1.23 (1H, m, CH), 1.55 (2H, q, *J* 11.9, CH_2), 1.35 (2H, q, *J* 12.2, CH_2), 1.75 – 1.84 (1H, m, CH), 2.18 (6H, s, 2 x *o*–CH_3), 2.60 (3H, s, *p*–CH_3), 6.17 (2H, s, $PhCH_2$), 7.02 (1H, s, NCH), 7.12 (1H, s, NCH), 7.38 (3H, t, *J* 7.5, 3 x ArH), 7.50 (s, 2H, 2 x ArH), 7.65 (2H, t, *J* 6.6, 2 x ArH), 7.69 (3H, t, *J* 7.5, 3 x ArH), 7.93 (2H, d, *J* 7.2, 2 x ArH) and 19.44 (1H, s, Ru=CH); δ_P (600 MHz; $CDCl_3$) 36.20; δ_C (120 MHz; $CDCl_3$) 18.2 (q, 2 x *o*–CH_3), 20.8 (q, *p*–CH_3), 26.4 (t, CH_2), 27.6 (t, CH_2), 29.4 (t, CH_2), 31.3 (d, PCH), 54.8 (t, Ph–CH_2), 120.7 (d, NCH), 123.6 (d, NCH), 127.8 (d, 3 x ArCH), 127.9 (d, 2 x ArCH), 128.5 (d, 3 x ArCH), 128.8 (s, ArC), 128.9 (d, 2 x ArCH), 129.5 (d, 2 x ArCH), 135.4 (s, ArC), 136.4 (s, ArC), 138.6 (s, ArC), 151.4 (s, ArC), 188.0 (s, Ru–C) and 294 (d, Ru=CH).

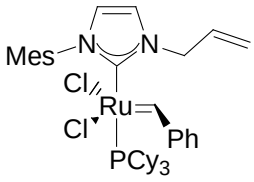

Benzylidenedichloro–[1–(prop–2–enyl)–3–mesitylimidazol–2–ylidene]–(tricyclohexylphosphine)ruthenium **121**

1–(Prop–2–enyl)–3–mesitylimidazol–2–ium iodide **108** (50 mg, 0.14 mmol) and KHMDS (34 mg, 0.17 mmol) were placed in a dry Schlenk flask under Ar. Toluene (10 mL) was added and the solution was stirred for 30 min. Since the starting material did not seem to dissolve, the suspension was transferred to a second Schlenk tube, containing Grubbs I complex **25** (116 mg, 0.141 mmol) under Ar. The resultant reaction mixture was stirred for 5 h (with monitoring by TLC) before the solvent volume was reduced to *ca* 1 mL. The solution was transferred to a clean Schlenk tube *via* a millipore filter and pentane (20 mL) was added and the suspension was agitated in an ultrasonic bath for 10 min. before the precipitate settled. The supernatant was removed and the residue was washed with pentane (4 x 20 mL) before being dried *in vacuo* to give a dark solid, indicated by ^{1}H NMR analysis to contain b*enzylidenedichloro–[1–(prop–2–enyl)–3–mesitylimidazole–2–ylidene]–(tricyclohexylphosphine)ruthenium*; δ_H (400 MHz; $CDCl_3$) 19.97 (1H, s, Ru=CH).

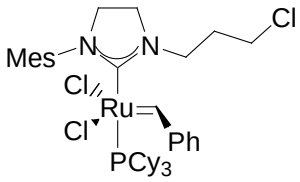

Benzylidene–[1–(3–chloropropyl)–3–mesitylimidazolin–2–ylidene]dichloro–(tricyclohexylphosphine)ruthenium **120**

1–(3–Chloropropyl)–3–mesitylimidazol–2–ium chloride **81** (100 mg, 0.33 mmol) and KHMDS (79mg, 0.4mmol) were placed in a dry Schlenk flask under Ar. Toluene (10 mL) was added and the mixture was stirred for 30 min. Since the starting material did not dissolve, the suspension was transferred to a second Schlenk tube containing Grubbs I complex **25** (100 mg, 0.12 mmol) under Ar. The resultant mixture was stirred for 4 h (with monitoring by

TLC) before the solvent volume was reduced *in vacuo* to *ca* 1 mL. The mixture was transferred to a clean Schlenk tube *via* a millipore filter and pentane (20 mL) was added. The suspension was agitated in an ultrasonic bath for 10 min. before the precipitate was allowed to settle. The supernatant was removed and the residue was washed with pentane (4 x 20 mL) before being dried *in vacuo* to give a dark solid, indicated by ^{1}H NMR analysis to contain *benzylidene–[1–(3–chloropropyl)–3–mesitylimidazolin–2–ylidene]dichloro–(tricyclohexylphosphine)ruthenium*; δ_H (400 MHz; $CDCl_3$) 20.0 (1H, s, Ru=CH).

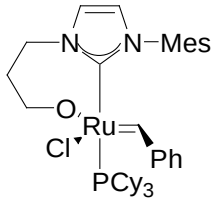

Benzylidenechloro–[1–(3–propoxy)–3–mesitylimidazol–2–ylidene)(tricyclohexylphosphine) ruthenium **119**

Method 1.

1–(3–Hydroxypropyl)–3–mesitylimidazol–2–ium chloride **100** (100mg, 0.36 mmol) and BuLi (46 mg, 0.71 mmol) were placed in a dry Schlenk under Ar. Toluene (5 mL) was added and the suspension was stirred for 2 h. Since the starting material did not dissolve, the suspension was transferred to a second Schlenk tube containing Grubbs I complex **25** (293 mg, 0.36 mmol) under Ar. The resultant suspension was stirred overnight before the solvent volume was reduced *in vacuo* to *ca* 1 mL. The reaction mixture was transferred to a clean Schlenk tube *via* a millipore filter and pentane (20 mL) was added. The suspension was agitated in an ultrasonic bath for 10 min. before the precipitate was allowed to settle. The supernatant was removed and the residue was washed with pentane (4 x 20 mL) before being dried *in vacuo* to give a brown solid, indicated by ^{1}H NMR analysis to contain b*enzylidenechloro–[1–(3–propoxy)–3–mesitylimidazol–2–ylidene)(tricyclohexylphosphine) ruthenium*; δ_H (400 MHz; $CDCl_3$) 19.96 (1H, s, Ru=CH).

Method 2.

The reaction was performed as before using 1–(3–hydroxypropyl)–3–mesitylimidazol–2–ium chloride, **100** (100 mg, 0.36 mmol), Grubbs I complex **25** (293mg, 0.36mmol) and KHMDS (142 mg, 0.71 mmol). The resultant mixture was stirred for 12 h (with monitoring by TLC) before the solvent volume was reduced *in vacuo* to *ca* 1 mL. The suspension was transferred to a clean Schlenk tube *via* a millipore filter and agitated and washed with pentane before being concentrated *in vacuo* to give a dark solid. The crude product did not contain the desired product and isolation was not pursued.

Method 3.

The reaction was performed as before using 1–(3–hydroxypropyl)–3–mesitylimidazol–2–ium chloride, **100** (100 mg, 0.36 mmol), Grubbs I complex **25** (293mg, 0.36mmol) and KHMDS (142 mg, 0.71 mmol). The resultant reaction mixture was stirred for 5 h (with monitoring by TLC) before the temperature was raised to 35 ºC and the reaction was stirred overnight. TLC analysis revealed decomposition of the catalyst and purification was not pursued.

6.4.3. Attempted Syntheses

*Chloro(*o*–isopropoxybenzylidene)–[1–mesityl–3–(3–oxidopropyl)imidazol–2–ylidene) ruthenium* **116**

[1–(3–Oxidopropyl)–3–mesitylimidazolin–2–ylidene]silver **115** (100 mg, 0.283 mmol) and Hoveyda–Grubbs I complex **35** (0.153 mg, 0.255 mmol) were charged to a Schlenk tube and flushed with Ar. THF (2.5 mL) and toluene (2.5 mL) were added and the resultant reaction mixture was stirred at 55 ^{o}C for 5 h. The reaction mixture was filtered through a millipore filter into a clean Schlenk tube to remove AgCl and the solution was concentrated *in vacuo* to give a black solid which was chromatographed [flash on oven–dried silica gel; elution with CH_2Cl_2 under Ar]. An orange fraction was collected and dried *in vacuo* to afford an orange solid which was left at –10 ºC in the dark under Ar overnight, the material turned from orange to brown and upon NMR analysis was revealed as starting material **35**.

[1–(3–oxidopropyl)–3–mesitylimidazol–2–ylidene]silver **131**

1–(3–Hydroxypropyl)–3–mesitylimidazol–2–ium chloride **100** (250 mg, 0.890 mmol), Ag_2O (413 mg, 1.78 mmol) and type 4 Å molecular sieves (1 g) were charged to a Schlenk flask and flushed with Ar. CH_2Cl_2 (5 mL) was added and the reaction mixture was stirred overnight, after which the suspension was passed through a column of Celite® on sintered glass (5 cm length) and rinsed with CH_2Cl_2 (5 mL). The filtrate was concentrated *in vacuo* to give a brown solid; ^{1}H NMR spectroscopic analysis of which did not indicate the presence of the desired product and isolation was not pursued.

7. MOLECULAR MODELLING

Molecular modelling calculations were performed using the Accelrys Materials Studio 4.4 package with geometry optimization being effected using the DMol^3 Density Functional Theory (DFT) method. All calculations were performed using the non–local generalized gradient approximation (GGA) functional PW91 with the following specifications:– a double numeric polarized (DNP) basis set and a medium self–consistent field (SCF) of 1 x 10^{-5} Ha with a maximum of 1000 SCF cycles and octupole multipolar expansion. Convergence criteria were of medium quality with threshold values of:– 2 x 10^{-5} Ha (energy), 0.004 Ha/Å (max. force) and 0.005 Å (max. displacement).

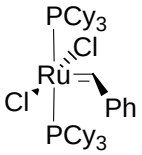

25

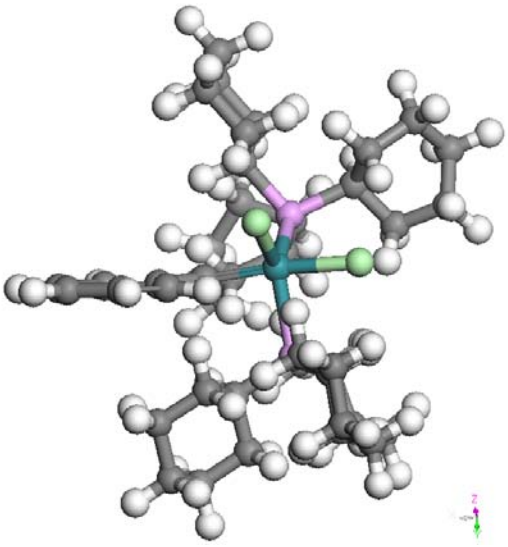

Figure 7.1 DFT geometry–optimized model of complex **25**.

Table 7.1 Calculated bond–lengths and bond–angles for complex **25**.

Bond	**Bond–length (Å)**	**Bond**	**Bond–angle (°)**
Ru–P^1	2.472	P^1–Ru–P^2	162.00
Ru=C	1.879	P^1–Ru=C	94.50
Ru–Cl^1	2.455	P^1–Ru–Cl^1	91.20
Ru–Cl^2	2.453	P^1–Ru–Cl^2	89.70
Ru–P^2	2.490	P^2–Ru=C	103.00
		Cl^1–Ru–Cl^2	174.70
		P^2–Ru–Cl^1	83.60
		P^2–Ru–Cl^2	83.60
		Cl^1–Ru=C	93.60
		Cl^2–Ru=C	106.60

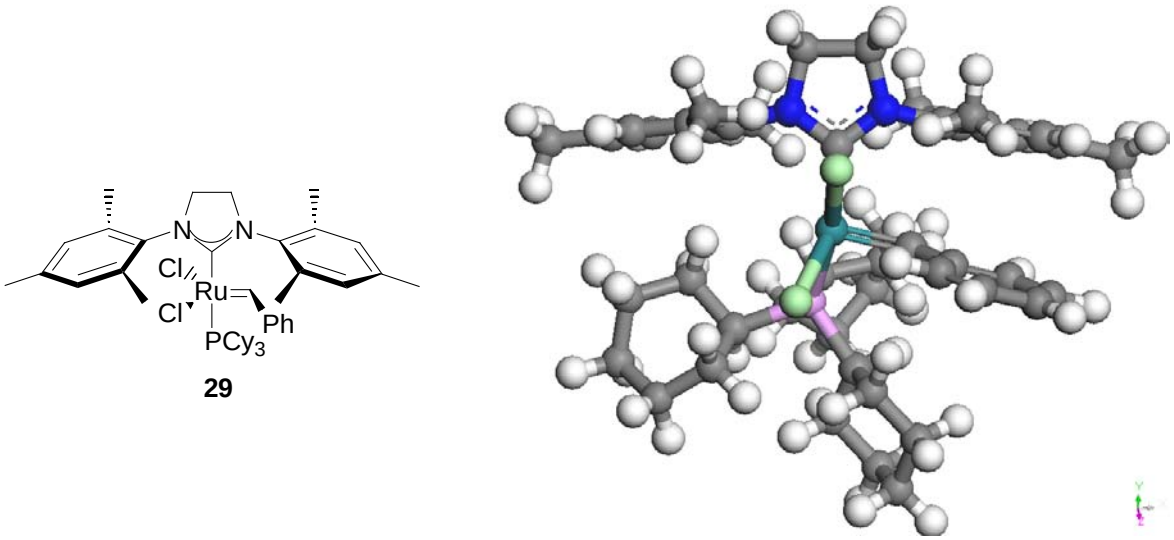

29

Figure 7.2 DFT geometry–optimized model of complex **29**.

Table 7.2 Calculated bond–lengths and bond–angles for complex **29**.

Bond	**Bond–length (Å)**	**Bond**	**Bond–angle (°)**
Ru–C	2.068	C–Ru–P	95.11
Ru=C	2.056	C–Ru=C	110.38
Ru–Cl^1	2.274	C–Ru–Cl^1	98.62
Ru–Cl^2	2.278	C=Ru–Cl^2	118.18
Ru–P	2.394	P–Ru=C	103.00
		Cl–Ru–Cl	81.55
		P–Ru–Cl^1	86.28
		P–Ru–Cl^2	164.82

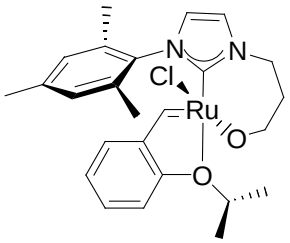

116

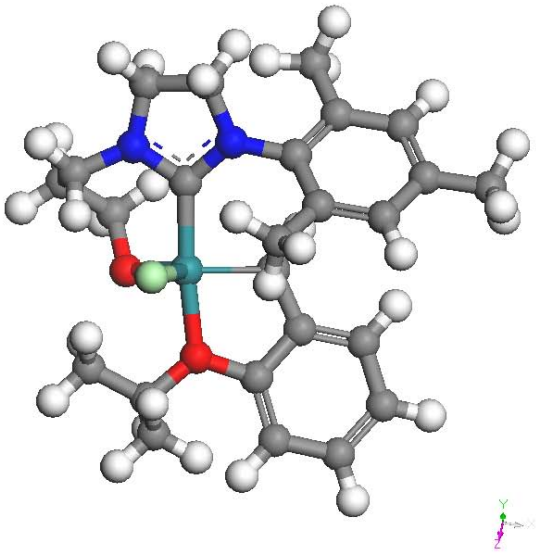

Figure 7.3 DFT geometry–optimized model of complex **116**.

Table 7.3 Calculated bond–lengths and bond–angles for complex **116**.

Bond	**Bond–length (Å)**	**Bond**	**Bond–angle (°)**
Ru–C	2.019	C–Ru–O*i*Pr	176.56
Ru–CH	1.873	C–RuCH	98.70
Ru–Cl	2.384	C–Ru–O	95.20
Ru–O	1.992	C–Ru–Cl	90.57
Ru–O*i*Pr	2.384	O–Ru–CH	110.04
		O–Ru–Cl	137.40

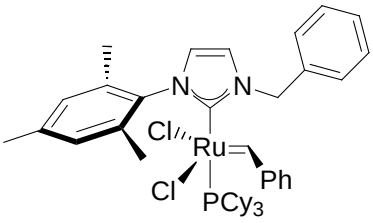

118

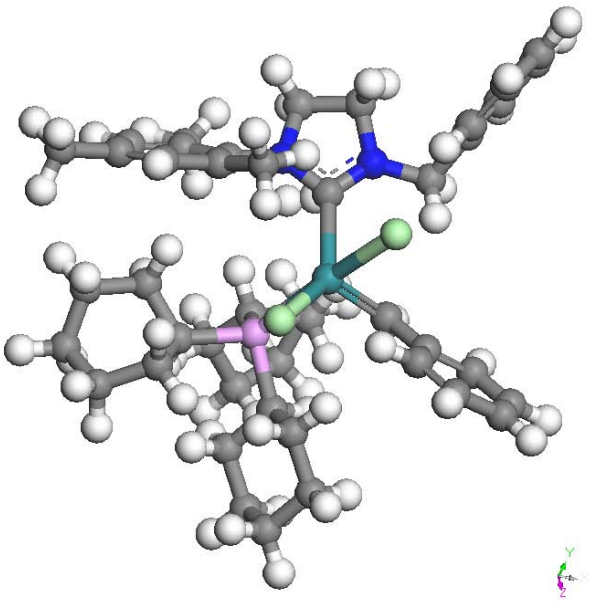

Figure 7.4 DFT geometry–optimized model of complex **118**.

Table 7.4 Calculated bond–lengths and bond–angles for complex **118**.

Bond	Bond–length (Å)	Bond	Bond–angle (°)
Ru–C	2.225	C–Ru–P	107.49
Ru=C	1.881	C–Ru=C	108.89
Ru–Cl^1	2.492	C–Ru–Cl^1	79.33
Ru–Cl^2	2.446	C–Ru–Cl^2	131.73
Ru–P	2.594	Cl^1–Ru–Cl^2	91.57
		C=Ru–P	93.16
		C=Ru–Cl^1	118.18
		C=Ru–Cl^2	88.14

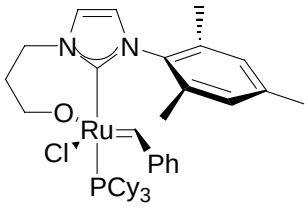

119

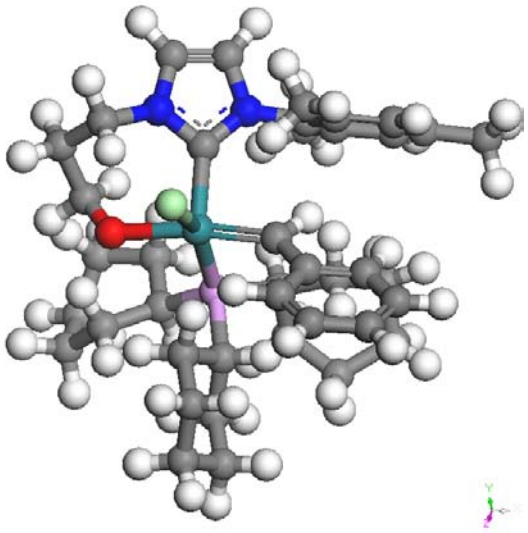

Figure 7.5 DFT geometry–optimized model of complex **119**.

Table 7.5 Calculated bond–lengths and bond–angles for complex **119**.

Bond	Bond–length (Å)	Bond	Bond–angle (°)
Ru–C	2.044	C–Ru–P	111.08
Ru=C	1.954	C–Ru=C	95.67
Ru–Cl	2.432	C–Ru–O	92.90
Ru–O	2.121	C–Ru–Cl	90.86
Ru–P	2.537	C=Ru–O	171.25
		C=Ru–P	88.52
		P–Ru–O	86.57
		P–Ru–Cl	157.90

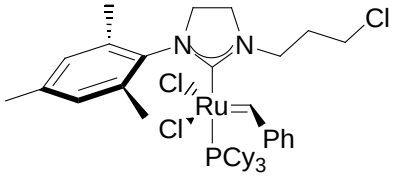

120

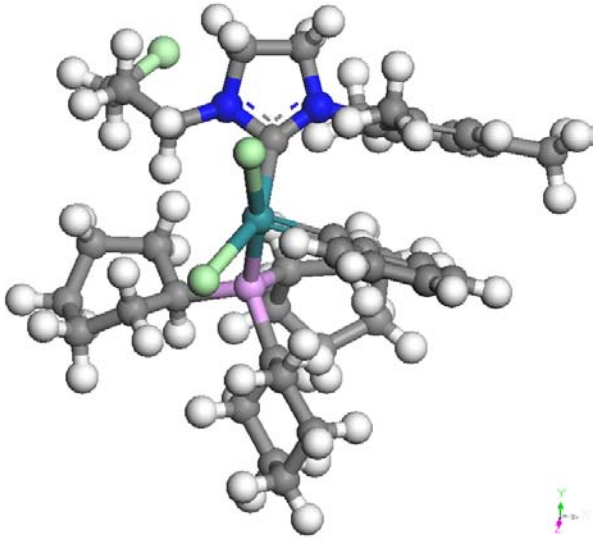

Figure 7.6 DFT geometry–optimized model of complex **120**.

Table 7.6 Calculated bond–lengths and bond–angles for complex **120**.

Bond	**Bond–length (Å)**	**Bond**	**Bond–angle (°)**
Ru–C	2.110	C–Ru–P	105.73
Ru=C	1.887	C–Ru=C	98.13
Ru–Cl^1	2.468	Cl^1–Ru–Cl^2	84.60
Ru–Cl^2	2.404	C–Ru–Cl^1	78.14
Ru–P	2.458	C–Ru–Cl^2	151.78

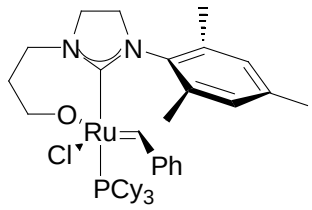

132

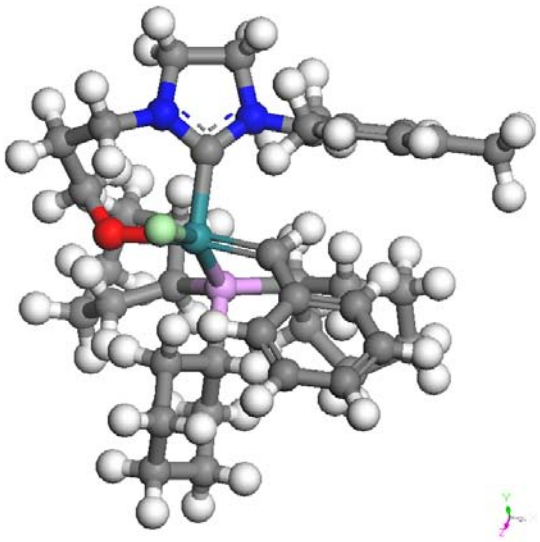

Figure 7.7 DFT geometry–optimized model of complex **132**.

Table 7.7 Calculated bond–lengths and bond–angles for complex **132.**

Bond	**Bond–length (Å)**	**Bond**	**Bond–angle (°)**
Ru–C	2.037	C–Ru–P	108.18
Ru=C	1.954	C–Ru=C	97.41
Ru–Cl	2.444	C–Ru–O	92.19
Ru–O	2.123	C–Ru–Cl	95.31
Ru–P	2.505	O–Ru=C	170.37
		C=Ru–P	89.11
		P–Ru–O	86.75
		P–Ru–Cl	157.90

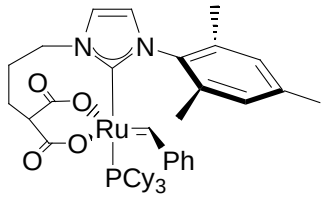

133

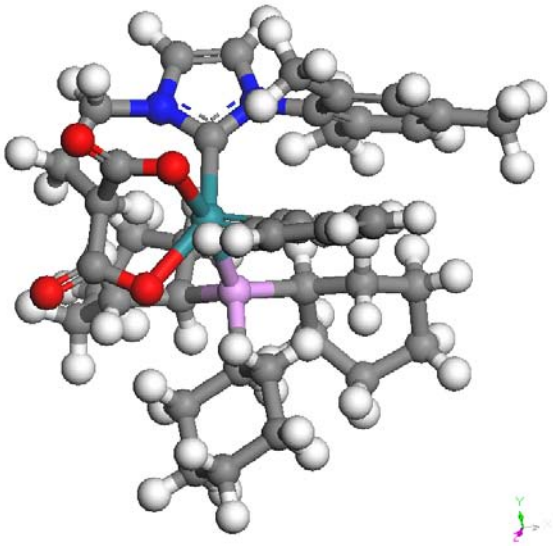

Figure 7.8 DFT geometry–optimized model of complex **133**.

Table 7.8 Calculated bond–lengths and bond–angles for complex **133**.

Bond	Bond–length (Å)	Bond	Bond–angle (°)
Ru–C	2.135	C–Ru–P	101.98
Ru=C	1.917	C–Ru=C	104.97
Ru–P	2.458	C–Ru–O^1	85.76
Ru–O^1	2.140	C–Ru–O^2	141.93
Ru–O^2	2.218	O^1–Ru–O^2	85.35
		C=Ru–P	91.32
		C=Ru–O^1	112.53
		C=Ru–O^2	93.94
		P–Ru–O^1	83.93
		P–Ru–O^2	169.21

References

1. F. Cavani and F. Trifiro, *Catal. Today,* 1997, **34**, 269–279.

2. E. Davy, *Philos. Trans. R. Soc.,* 1820, **110**, 108.

3. J. W. Doebereiner, *Ann. Chim. Phys.,* 1823, **24**, 91.

4. P. L. Dulong and L. G. Thenard, *Ann. Chim. Phys.,* 1823, **23**, 440.

5. M. Faraday, *Philos. Trans. R. Soc.,* 1834, **124**, 55.

6. G. A. Somorjai and K. McCrea, *Appl. Catal. A: Gen.,* 2001, **222**, 3–18.

7. A. Frennet and C. Hubert, *J. Mol. Catal. A: Chem.,* 2000, **163**, 163–188.

8. C. Marcilly, *J. Catal.,* 2003, **216**, 47–62.

9. J. A. Widegren and R. G. Finke, *J. Mol. Catal. A: Chem.,* 2003, **198**, 317–341.

10. E. L. V. Goetheer, A. W. Verkerk, L. J. P. van den Broeke, E. de Wolf, B. Deelman, G. van Koten and J. T. F. Keurentjies, *J. Catal.,* 2003, **219**, 126 – 133.

11. F. S. Stone, *J. Catal.,* 2003, **216**, 2–11.

12. R. V. Chaudhari, A. Seayad and S. Jayasree, *Catal. Today,* 2001, **66**, 371–380.

13. K. C. Nicolaou, P. G. Bulger and D. Sarlah, *Angew. Chem., Int. Ed.,* 2005, **44**, 4490–4527.

14. Y. Schrodi and R. L. Pederson, *Aldrichim ACTA,* 2007, **40**, 45–52.

15. A. H. Hoveyda and A. R. Zhugralin, *Nature,* 2007, **450**, 243–251.

16. D. Astruc, *New J. Chem.,* 2005, **29**, 42–56.

17. J. L. Herisson and Y. Chauvin, *Makromol. Chem.,* 1971, **141**, 161–176.

18. A. Fürstner, *Angew. Chem., Int. Ed.,* 2000, **39**, 3012–3043.

19. R. R. Schrock, *J. Am. Chem. Soc.,* 1974, **96**, 6796–6797.

20. M. Jordaan, *PhD Thesis, North–West University,* 2007.

21. D. Meng, P. Bertinato, A. Balog, D. Su, T. Kamenecka, E. J. Sorensen and S. J. Danishefsky, *J. Am. Chem. Soc.,* 1997, **119**, 10073–10092.

22. K. C. Nicolaou, N. Winssinger, J. Pastor, S. Ninkovic, F. Sarabia, Y. He, D. Vourloumis, Z. Yang, T. Li, P. Giannakakou and E. Hamel, *Nature*, 1997, **387**, 268–272.

23. K. A. Scheidt and W. R. Roush, *Chemtracts*, 1998, **11**, 522–530.

24. A. V. Statsuk, D. Liu and S. A. Kozmin, *J. Am. Chem. Soc.*, 2004, **126**, 9546–9547.

25. D. G. Gillingham and A. H. Hoveyda, *Angew. Chem., Int. Ed.*, 2007, **46**, 3860–3864.

26. T. Nicola, M. Brenner, K. Donsbach and P. Kreye, *Org. Process. Res. Dev.*, 2005, **9**, 513–515.

27. A. B. Smith III, C. M. Adams, S. A. Kozmin and D. V. Paone, *J. Am. Chem. Soc.*, 2001, **123**, 5925–5937.

28. J. C. Mol, *J. Mol. Catal. A: Chem.*, 2004, **213**, 39–45.

29. K. A. Burdett, L. D. Harris, P. Margl, B. R. Maughon, T. Mokhtar–Zadeh, P. C. Saucier and E. P. Wasserman, *Organometallics*, 2004, **23**, 2027–2047.

30. R. Schrock, S. Rocklage, J. Wengrovius, G. Rupprecht and J. Fellmann, *J. Mol. Catal.*, 1980, **8**, 73–83.

31. J. H. Wengrovius, R. R. Schrock, M. R. Churchill, J. R. Missert and W. J. Youngs, *J. Am. Chem. Soc.*, 1980, **102**, 4515–4516.

32. R. R. Schrock, J. S. Murdzek, G. C. Bazan, J. Robbins, M. DiMare and M. O'Regan, *J. Am. Chem. Soc.*, 1990, **112**, 3875–3886.

33. B. M. Novak and R. H. Grubbs, *J. Am. Chem. Soc.*, 1988, **110**, 7542–7543.

34. S. T. Nguyen, L. K. Johnson, R. H. Grubbs and J. W. Ziller, *J. Am. Chem. Soc.*, 1992, **114**, 3974–3975.

35. M. B. France, R. H. Grubbs, D. V. McGrath and R. A. Paciello, *Macromolecules*, 1993, **26**, 4742–4747.

36. Z. Wu, S. T. Nguyen, R. H. Grubbs and J. W. Ziller, *J. Am. Chem. Soc.*, 1995, **117**, 5503–5511.

37. G. C. Fu, S. T. Nguyen and R. H. Grubbs, *J. Am. Chem. Soc.*, 1993, **115**, 9856.

38. R. B. Andrade, O. J. Plante, L. G. Melean and P. H. Seeberger, *Org. Lett.*, 1999, **1**, 1811–1814.

39. H. E. Blackwell, D. J. O'Leary, A. K. Chatterjee, R. A. Washenfelder, D. A. Bussmann and R. H. Grubbs, *J. Am Chem. Soc.*, 2000, **122**, 58.

40. S. T. Diver and A. Giessert, *Chem. Rev.*, 2004, **104**, 1317–1382.

41. T. Weskamp, F. J. Kohl, W. Hieringer, D. Gleich and W. A. Herrmann, *Angew. Chem., Int. Ed.,* 1999, **38**, 2416–2419.

42. M. Scholl, T. M. Trnka, J. P. Morgan and R. H. Grubbs, *Tetrahedron Lett.,* 1999, **40**, 2247–2250.

43. M. Scholl, S. Ding, C. W. Lee and R. H. Grubbs, *Org. Lett.,* 1999, **1**, 953–956.

44. J. Huang, E. D. Stevens, S. P. Nolan and J. L. Petersen, *J. Am. Chem. Soc.,* 1999, **121**, 2674–2678.

45. M. Scholl, T. M. Trnka, J. P. Morgan and R. H. Grubbs, *Tetrahedron Lett.,* 1999, **40**, 2247–2250.

46. P. Van de Weghe, P. Bisseret, N. Blanchard and J. Eustache, *J. Organometal. Chem.,* 2006, **691**, 5078–5108.

47. R. M. Garbaccio, S. J. Stachel, D. K. Baeschlin and S. J. Danishefsky, *J. Am. Chem. Soc.,* 2001, **123**, 10903–10908.

48. A. K. Chatterjee, J. P. Morgan, M. Scholl and R. H. Grubbs, *J. Am. Chem. Soc.,* 2000, **122**, 3783–3784.

49. Y. Chauvin, *Angew. Chem., Int. Ed.,* 2006, **45**, 3740–3747.

50. R. H. Grubbs, *Angew. Chem., Int. Ed.,* 2006, **45**, 3760–3765.

51. R. H. Grubbs, *Angew. Chem., Int. Ed.,* 2006, **45**, 3760–3765.

52. J. Herisson and Y. Chauvin, *Makromol. Chem.,* 1971, **141**, 161–176.

53. S. T. Nguyen, R. H. Grubbs and J. W. Ziller, *J. Am. Chem. Soc.,* 1993, **115**, 9858.

54. A. G. Wenzel and R. H. Grubbs, *J. Am. Chem. Soc.,* 2006, **128**, 16048–16049.

55. M. S. Sanford, M. Ulman and R. H. Grubbs, *J. Am. Chem. Soc.,* 2001, **123**, 749–750.

56. J. S. Kingsbury, J. P. A. Harrity, P. J. J. Bonitatebus and A. H. Hoveyda, *J. Am. Chem. Soc.,* 1999, **121**, 791–799.

57. S. B. Garber, J. S. Kingsbury, B. L. Gray and A. H. Hoveyda, *J. Am. Chem. Soc.,* 2000, **122**, 8168–8179.

58. D. Bourissou, O. Guerret, F. P. Gabbai and G. Bertrand, *Chem. Rev.,* 2000, **100**, 39–91.

59. S. T. Liddle, I. S. Edworthy and P. L. Arnold, *Chem. Soc. Rev.,* 2007, **36**, 1732–1744.

60. S. T. Liddle, I. S. Edworthy and P. L. Arnold, *Chem. Soc. Rev.,* 2007, **36**, 1732–1744.

61. J. Mieusset and U. H. Brinker, *J. Org. Chem.*, 2008, **73**, 1553–1558.

62. R. S. Bon, F. J. J. De Kanter, M. Lutz, A. L. Spek, M. C. Jahnke, F. E. Hahn, M. B. Groen and R. V. A. Orru, *Organometallics*, 2007, **26**, 3639–3650.

63. H. W. Wanzlick, *Angew. Chem., Int. Ed.*, 1962, **1**, 75–80.

64. K. Oefele, *J. Organometal. Chem.*, 1968, **12**, 42–43.

65. H. W. Wanzlick and H. J. Schoenherr, *Angew. Chem., Int. Ed.*, 1968, **7**, 141–142.

66. A. P. T. Neveling, *PhD Thesis, Nelson Mandela Metropolitan University*, 2003.

67. K. M. Hindi, M. J. Panzner, C. L. Cannon and W. J. Youngs, *Chem. Rev.*, 2009, **109**, 3859–3884.

68. D. J. Cardin, B. Cetinkaya and M. F. Lappert, *Chem. Rev.*, 1972, **72**, 545–574.

69. A. J. Arduengo, R. L. Harlow and M. Kline, *J. Am. Chem. Soc.*, 1991, **113**, 361–363.

70. A. J. Arduengo, H. V. R. Dias, R. L. Harlow and M. Kline, *J. Am. Chem. Soc.*, 1992, **114**, 5530–5534.

71. A. J. Arduengo, *Acc. Chem. Res.*, 1999, **32**, 913–921.

72. L. Ray, M. M. Shaikh and P. Ghosh, *Dalton Trans.*, 2007, 4546–4555.

73. W. A. Herrmann and C. Kocher, *Angew. Chem., Int. Ed.*, 1997, **36**, 2162–2187.

74. T. Weskamp, V. P. W. Bohm and W. A. Herrmann, *J. Organomet. Chem.*, 2000, **600**, 12–22.

75. A. W. Waltman and R. H. Grubbs, *Organometallics*, 2004, **23**, 3105–3107.

76. M. S. Viciu, R. M. Kissling, E. D. Stevens and S. P. Nolan, *Org. Lett.*, 2002, **4**, 2229–2231.

77. M. Scholl, S. Ding, C. W. Lee and R. H. Grubbs, *Org. Lett.*, 1999, **1**, 953–956.

78. H. Clavier, L. Coutable, L. Toupet, J. Guillemin and M. Mauduit, *J. Organomet. Chem.*, 2005, **690**, 5237–5254.

79. B. F. Straub, *Adv. Synth. Catal.*, 2007, **349**, 204–214.

80. M. S. Sanford, J. A. Love and R. H. Grubbs, *Organometallics*, 2001, **20**, 5314–5318.

81. J. P. Morgan and R. H. Grubbs, *Org. Lett.*, 2000, **2**, 3153–3155.

82. S. T. Nguyen, L. K. Johnson, R. H. Grubbs and J. W. Ziller, *J. Am. Chem. Soc.*, 1992, **114**, 3974–3975.

83. A. M. Maj, L. Delaude, A. Demonceau and A. F. Noels, *J. Organomet. Chem.*, 2007, **692**, 3048–3056.

84. N. Stylianides, A. A. Danopoulos, D. Pugh, F. Hancock and A. Zanotti–Gerosa, *Organometallics*, 2007, **26**, 5627–5635.

85. I. C. Stewart, T. Ung, A. A. Pletnev, J. M. Berlin, R. H. Grubbs and Y. Schrodi, *Org. Lett.*, 2007, **9**, 1589–1592.

86. T. Ritter, M. W. Day and R. H. Grubbs, *J. Am. Chem. Soc.*, 2006, **128**, 11768–11769.

87. M. B. Dinger, P. Nieczypor and J. C. Mol, *Organometallics*, 2003, **22**, 5291–5296.

88. K. Vehlow, S. Maechling and S. Blechert, *Organometallics*, 2006, **25**, 25–28.

89. O. Kuhl, *Chem. Soc. Rev.*, 2007, **36**, 592–607.

90. C. C. Bickford, T. J. Johnson, E. R. Davidson and K. G. Caulton, *Inorg. Chem.*, 1994, **33**, 1080–1086.

91. T. J. Johnson, J. C. Huffman and K. G. Caulton, *J. Am. Chem. Soc.*, 1992, **114**, 2725–2726.

92. P. L. Arnold, M. Rodden, K. M. Davis, A. C. Scarisbrick, A. J. Blake and C. Wilson, *Chem. Commun.*, 2004, 1612–1613.

93. D. Patel, S. T. Liddle, S. A. Mungur, M. Rodden, A. J. Blake and P. L. Arnold, *Chem. Commun.*, 2006, 1124–1126.

94. G. Occhipinti, V. R. Jensen, K. W. Törnroos, N. Å. Frøystein and H. Bjørsvik, *Tetrahedron*, 2009, **65**, 7186–7194.

95. G. Occhipinti, H. Bjørsvik, K. W. Törnroos, A. Furstner and V. R. Jensen, *Organometallics*, 2007, **26**, 4383–4385.

96. J. J. Van Veldhuizen, J. E. Campbell, R. E. Giudici and A. H. Hoveyda, *J. Am. Chem. Soc.*, 2005, **127**, 6877–6882.

97. J. J. Van Veldhuizen, S. B. Garber, J. S. Kingsbury and A. H. Hoveyda, *J. Am. Chem. Soc.*, 2002, **124**, 4954–4955.

98. J. J. Van Veldhuizen, S. B. Garber, J. S. Kingsbury and A. H. Hoveyda, *J. Am. Chem. Soc.*, 2003, **125**, 12666.

99. S. Pruhs, C. W. Lehmann and A. Fürstner, *Organometallics*, 2004, **23**, 280–287.

100. I. T. Sabbagh, *Ph.D. Thesis, Rhodes University,* 2005.

101. N. Magqi, *MSc Thesis, Rhodes University,* 2007.

102. T. Millward, *MSc Thesis, Rhodes University,* 2008.

103. M. Ulman and R. H. Grubbs, *J. Org. Chem.,* 1999, **64**, 7202–7207.

104. G. C. Vougioukalakis and R. H. Grubbs, *Organometallics,* 2007, **26**, 2469–2472.

105. J. J. Eisch, C. A. Kovacs, P. Chobe and M. P. Boleslawski, *J. Org. Chem.*, 1987, **52**, 4427–4437.

106. Y. Fu, H. Li, W. Hu and D. Zhu, *Chem. Commun.,* 2005, 3189 – 3191.

107. J. Wolf, A. Labande, M. Natella, J. Daran and R. Poli, *J. Mol. Cat. A: Chem.*, 2006, **259**, 205–212.

108. F. Ameer, *PhD Thesis, University of Natal,*1985.

109. S. K. Jain, *J. Biol. Chem.,* 1984, **259**, 3391–3394.

110. D. Lee, J. Kim, B. Jun, H. Kang, J. Park and Y. Lee, *Org. Lett.*, 2008, **10**, 1609–1612.

111. A. J. Arduengo III, F. P. Gentry Jr., P. K. Taverkere and H. E. Simmons, US Patent C07D233, 2001, **58**.

112. A. Flahaut, S. Roland and P. Mangeney, *J. Organomet. Chem.,* 2007, **692**, 5754–5762.

113. A. T. Normand, S. K. Yen, H. V. Huynh, T. S. A. Hor and K. J. Cavell, *Organometallics,* 2008, **27**, 3153–3160.

114. M. S. Viciu, G. A. Grasa and S. P. Nolan, *Organometallics,* 2001, **20**, 3607–3612.

115. A. J. Boydston, Y. Xia, J. A. Kornfield, I. A. Gorodetskaya and R. H. Grubbs, *J. Am. Chem. Soc.,* 2008, **130**, 12775–12782.

116. Alois Fürstner, Helga Krause, Lutz Ackermann and Christian W. Lehmann, *Chem. Commun.,* 2001, 2240–2241.

117. M. C. Perry, X. Cui, M. T. Powell, D. Hou, J. H. Reibenspies and K. Burgess, *J. Am. Chem. Soc.,* 2003, **125**, 113–123.

118. H. M. Peng, R. D. Webster and X. Li, *Organometallics*, 2008, **27**, 4484–4493.

119. B. U. W. Maes, K. T. J. Loones, S. Hostyn, G. Diels and G. Rombouts, *Tetrahedron,* 2004, **60**, 11559–11564.

120. H. M. Peng, G. Song, Y. Li, X. Li, *Inorg. Chem.,* 2008, **47**, 8031–8043.

121. E. Alcalde, I. Dinarès, s. Rodríguez and C. D. de Miguel, *Eur. J. Org. Chem*, 2005, 1637 –1643.

122. R. J. Giguere, T. L. Bray, S. M. Duncan and G. Majetich, *Tetrahedron Lett.,* 1986, **27**, 4945–4948.

123. R. Gedye, F. Smith, K. Westaway, H. Ali, L. Baldisera, L. Laberge and J. Rousell, *Tetrahedron Lett.,* 1986, **26**, 279–282.

124. C. O. Kappe, *Angew. Chem., Int. Ed.,* 2004, **43**, 6250–6284.

125. K. T. J. Loones, B. U. W. Maes, G. Rombouts, S. Hostyn and G. Diels, *Tetrahedron,* 2005, **61**, 10338–10348.

126. S. Narayan, T. Seelhammer and R. E. Gawley, *Tetrahedron Lett.,* 2004, **45**, 757–759.

127. B. Hayes L., *Microwave Synthesis: Chemistry at the Speed of Light*, CEM Publishing, Matthews N. C. U.S.A., 2002.

128. D. M. P. Mingos and D. R. Baghurst, *Chem. Soc. Rev.,* 1991, **20,** 1–47.

129. M. Abid, B. Toeroek and X. Huang, *Aust. J. Chem,* 2009, **62**, 208–222.

130. F. Wiesbrock, R. Hoogenboom and U. S. Schubert, *Macromol. Rapid Commun.,* 2004, **25**, 1739–1764 .

131. P. L. Arnold, A. C. Scarisbrick, A. J. Blake and C. Wilson, *Chem. Commun.,* 2001, 2340–2341.

132. M. K. Samantaray, K. Pang, M. M. Shaikh and P. Ghosh, *Inorg. Chem.,* 2008, **47**, 4153–4165.

133. L. Ray, M. M. Shaikh and P. Ghosh, *Inorg. Chem,* 2008, **47**, 230–240.

134. L. Ray, S. Barman, M. M. Shaikh and P. Ghosh, *Chem. Eur. J.,* 2008, **14**, 6646–6655.

135. M. K. Samantaray, D. Roy, A. Patra, R. Stephen, M. Saikh, R. B. Sunoj and P. Ghosh, *J. Organomet. Chem.,* 2006, **691**, 3797–3805.

136. M. K. Samantaray, V. Katiyar, D. Roy, K. Pang, H. Nanavati, R. Stephen, R. B. Sunoj and P. Ghosh, *Eur. J. Inorg. Chem.,* 2006, **15**, 2975–2984.

137. G. Frenking and U. Pidun, *J. Chem. Soc., Dalton Trans.,* 1997, **10**, 1653–1662.

138. S. F. Vyboishchikov and G. Frenking, *Chem. Eur. J.,* 1998, **4**, 1439–1448.

139. A. A. D. Tulloch, A. A. Danopoulos, S. Winston, S. Kleinhenz and G. Eastham, *Dalton Trans.,* 2000, **24**, 4499–4506.

140. T. K. Maishal, B. Mondal, V. G. Puranik, P. P. Wadgaonkar, G. K. Lahiri and A. Sarkar, *J. Organomet. Chem.*, 2005, **690**, 1018–1027.

141. C. A. A. Huijsmans, *MSc Thesis, North–West University*, 2009.

142. S. H. Hong, A. G. Wenzel, T. T. Salguero, M. W. Day and R. H. Grubbs, *J. Am. Chem. Soc.*, 2007, **129**, 7961–7968.

143. D. D. Perrin and W. L. F. Armarego, *Purification of Laboratory Chemicals*, Pergamon Press, Oxford, 1988.

144. O. J. Nicaise, D. M. Mans, A. D. Morrow, E. V. Hefti, E. M. Palkovacs, R. K. Singh, M. A. Zukowska and M. D. Morin, *Tetrahedron*, 2003, **59**, 6433–6443.

145. S. Adimurthy, G. Ramachandraiah, A. V. Bedekar, S. Ghosh, B. C. Ranu and P. K. Ghosh, *Green Chem.*, 2006, **8**, 916–922.

146. K. Morita, F. Irreverre, F. Sakiyama and B. Witkop, *J. Am. Chem. Soc.*, 1963, **85**, 2832–2834.

147. W. Hu, J. Wang, CN Patent 1422847, 8, 2003, *Chem. Abstr.* 2003**, 143**, 172688.

148. J. Novotny, V. Dalecky, I. Zavodna, F. Kiss, A. Mikuskova, P. Jonas, M. Macka, L. Marcikova, R. Kozisek, CS Patent 277196, 9, 1992; *Chem. Abstr.* 1992, **120**, 322819.

149. L. Song, X. Luo, Y. Wang, B. Gai and Q. Hu, *J. Organomet. Chem.*, 2009, **694**, 103–112.

150. A. Kermagoret and P. Braunstein, *Organometallics*, 2008, **27**, 88–99.